YAEC-1233

METHODS FOR THE ANALYSIS OF BOILING WATER REACTORS A SYSTEMS TRANSIENT ANALYSIS MODEL (RETRAN)

Prepared By A. A. Farooq Ansari — A.F. Ansari — 4-15-81 (Date)

Prepared By James T. Cronin — J.T. Cronin — 4/15/81 (Date)

Reviewed By Stephen P. Schultz — S.P. Schultz — 4/15/81 (Date)

Approved By Bruce C. Slifer — B.C. Slifer — 4/15/81 (Date)

Yankee Atomic Electric Company
Nuclear Services Division
1671 Worcester Road
Framingham, Massachusetts 01701

DISCLAIMER OF RESPONSIBILITY

This document was prepared by Yankee Atomic Electric Company on behalf of Vermont Yankee Nuclear Power Corporation. This document is believed to be completely true and accurate to the best of our knowledge and information. It is authorized for use specifically by Yankee Atomic Electric Company, Vermont Yankee Nuclear Power Corporation and/or the appropriate subdivisions within the Nuclear Regulatory Commission only.

With regard to any unauthorized use whatsoever, Yankee Atomic Electric Company, Vermont Yankee Nuclear Power Corporation and their officers, directors, agents and employees assume no liability nor make any warranty or representation with respect to the contents of this document or to its accuracy or completeness.

ABSTRACT

A transient systems analysis model of the Vermont Yankee Nuclear Power Station's Nuclear Steam Supply System is described. The model is based on the RETRAN computer code. The ability of the model to accurately predict the course of reactor transients is shown by comparisons to experimental results. Qualification includes simulation of the Peach Bottom turbine trip tests using modeling techniques developed for Vermont Yankee. Analyses of typical licensing transients are also presented.

ACKNOWLEDGEMENTS

The authors wish to acknowledge Joe Holzer, Dr. Edward Pilat, Michelle Kmetz, Richard Woehlke, and Dave VerPlanck for providing their help and many valuable suggestions in developing the core reactivity modeling methodology. The contributions of Stan Jefferson, Pat Donnelly, and Bernie Buteau of Vermont Yankee Nuclear Power Station, in terms of providing the plant startup test data and information concerning plant control systems, is gratefully acknowledged. We wish to thank Kevin Burns for his help during Peach Bottom transient simulations. Our thanks also goes to Edwin Vidito, James Pattulo, and Bijan Baharynejad for their work in preparing the figures for this report. Finally, we thank the staff of the Word Processing Center and the Computer Operations staff at YAEC who gave prompt assistance and remained patient while handling considerable workloads under this project.

TABLE OF CONTENTS

TABLE OF CONTENTS (Continued)

LIST OF FIGURES

LIST OF FIGURES (Continued)

LIST OF FIGURES (Continued)

LIST OF FIGURES (Continued)

LIST OF TABLES

1.0 INTRODUCTION

1.1 Purpose

This report will describe a system analysis model of the Vermont Yankee Nuclear Power Station's Nuclear Steam Supply System (NSSS), which is a General Electric designed BWR [1]. The model is based on the RETRAN computer code [2]. This model will be used to evaluate the transient response of the NSSS to operational transients, normal or abnormal. The model will be used for operational and licensing support of the Vermont Yankee Nuclear Power Station.

1.2 Brief Description

RETRAN contains the same fluid differential and state equations as RELAP4 for describing homogeneous equilibrium flow in one dimension. Improvements have been made to describe moving interphase fronts. The representations used in previous RELAP codes for control volumes and junctions are used in RETRAN also. The system of equations which govern the state of the thermal-hydraulic system of interest are based on the spatially integrated fluid conservation equation. In this manner, the volume and junction representation can be utilized to represent the fluid transient conditions in any part of the components which comprise the overall reactor system and to any level of detail which the analyst so chooses within the basic constraints of one-dimensional homogeneous equilibrium flow.

The reactor kinetics capabilities in RETRAN are based on the commonly used point kinetics model. Power can also be specified as a function of time by the user.

The system component models utilized in RETRAN include a pump model which describes the interaction between the centrifugal pump and the primary system fluid, valve models which range in capabilities from simple valves to check valves to inertial valves which can all be signaled open or closed subject to user specified conditions. The model flexibility for valves and their configuration is very important in allowing a wide variety of options to the user for modeling plant response. Several representations for heat exchangers can be modeled by the code. The most realistic method is by the utilization of two-sided heat transfer where the fluid volumes on both the primary side and secondary side of the system are used for determining local conditions. Several more simplistic representations of the heat exchangers take the form of the special boundary condition used in conjunction with a heat conduction model. A variety of trip controls, control system models and trip logic models have been included in RETRAN which can specify control functions typical of a reactor system and the sequence in which they are operated.

The development of the input to RETRAN to represent Vermont Yankee was based on as-built drawings and vendor specifications. The fluid volume nodalization scheme used to describe the system was based on sensitivity studies and comparisons of model predictions to experimental data.

1.3 Model Qualification

RETRAN has been extensively exercised by the utility and consulting communities on a wide variety of transient problems. The base RETRAN documentation [2] contains reports on comparisons of RETRAN results to separate effects tests, system effects tests, and power reactor startup

and special tests. Vermont Yankee has built upon this base level of qualification data through application of Vermont Yankee methods to the analysis of:

1) Vermont Yankee startup tests;

2) The Peach Bottom series of turbine trip tests using Vermont Yankee methods to define the input to RETRAN; and

3) Sensitivity studies on various types of transients to provide assurance that a converged solution was arrived at by the modeling technique selected.

The results of these evaluations are presented in Section 3 and Appendix A. These results show that the Vermont Yankee RETRAN model can predict the course of a wide variety of transients with a high degree of accuracy, and can be applied with a high degree of confidence to the evaluation of normal and abnormal operational transients.

1.4 Model Application

The Vermont Yankee RETRAN model is designed as a general purpose, best-estimate, systems analysis tool, which can be used for a variety of purposes. These will include evaluations of operational transients, special tests, and design changes. By using appropriately conservative evaluation techniques, the model can also be used to analyze limiting transients for core reload licensing purposes.

2.0 DESCRIPTION

The principal inputs to the code are described in the following sections. These descriptions should be viewed as "typical" for the Vermont Yankee model. The actual inputs used to model any particular transient may vary from the following description, based on the nature of the transient and the previous experience gained in modeling it. Such variations will be noted in the sections described in Appendix A.

2.1 Fluid Volumes and Junctions

The fluid volumes used in RETRAN are based on Vermont Yankee as-built drawings. Comment statements on the input listing identify the source of the information for each of the volumes. For the most part, fluid volumes are defined by the distinct regions of the primary system (e.g., lower plenum, upper plenum, etc.). Certain regions are divided into subregions (such as the downcomer) when the assumption of homogeneous properties within the region is not valid, or when the transient situation to be modeled requires further nodalization.

The junctions connecting the volumes are based on RELAP/RETRAN coding practice for connecting fluid volumes. The junction loss coefficients are based on measured and predicted steady-state pressure distributions between various regions in the reactor. The predicted pressure drops were obtained from either the vendor's component performance reports or calculated using standard engineering practice. Core pressure drop was determined using steady-state core flow distribution code FIBWR [8].

A list of the key parameters for the volumes and junctions are

presented in Tables 2.1 and 2.2. Figure 2.1 shows how the junctions and volumes are grouped to represent the entire system.

2.1.1 Steam Dome and Downcomer Region

The steam dome and downcomer region is defined here to be the area within the reactor vessel and outside the core shroud - exclusive of the jet pumps. This region influences the system response primarily through three effects: pressure, water level, and temperature. The relative importance of these effects varies with the particular type of transient.

The steam dome and downcomer region is split into two volumes, with the boundary being one foot above the feedwater inlet nozzle. The upper volume represents the steam dome and the two-phase mixture outside of the steam separators. The formulation of the RETRAN non-equilibrium pressurizer model [2] is well suited for modeling this region and hence, it is employed. The model allows for phase separation and predicts a mixture level. In addition, the model allows for thermal non-equilibrium between the steam and liquid regions while enforcing mechanical equilibrium. This feature is particularly important in simulations of pressurization transients.

The lower volume represents the lower downcomer region where the mixing of the subcooled feedwater and the return flow from the steam separators takes place. A homogeneous equilibrium assumption is normally used in this volume. For simulations where temperature transport is of primary interest, this volume may be further subdivided and the transport delay option [2] used.

In summary, the use of the non-equilibrium pressurizer model combined

with the transport delay option, when temperature transport is of interest, accounts for the important physics of this region.

2.1.2 Steam Lines

Referring to Figure 2.1, all four steam lines are represented by a single line which is broken up into six volumes. Two volumes are used to model the steam piping inside the containment. Volume 55 is a small volume which provides the pressure signal to the electrical pressure regulator of the turbine control system.

2.2 Heat Conductors

Table 2.3 contains a description of each of the 24 heat conductors used in the model. A total of twelve heat conductors represent the fuel rods. These conductors have internal heat generation. A non-conducting heat exchanger was used to account for direct heat deposition into the core bypass region.

Twelve heat conductors were used to represent the reactor vessel, reactor vessel internals, steam line piping and the recirculation loops. These heat conductors were modeled as passive heat conductors interacting with adjacent fluid volumes. The heat conductors representing the reactor vessel, steam line piping, and the recirculation loop piping were insulated from the atmosphere and were allowed to interact only with the adjacent fluid volumes.

2.3 Core Model

2.3.1 Core Fluid Volumes

The core region is modeled with thirteen volumes: twelve axial volumes representing the active core and a single volume for the bypass region. The steady-state flow split between the active core and bypass region along with the initial overall pressure drop from the core lower to upper plenum is based on FIBWR predictions [8]. The Baroczy two-phase friction multiplier is used to calculate volume wall friction losses. Junction loss coefficients for the average core are forced to be consistent with the specified pressure drop and known inlet orifice loss coefficient.

2.3.2 Core Heat Conductors

The reactor fuel is modeled with twelve heat conductors, one per volume. The standard cylindrical, three region representation of the fuel pin is used with six nodes in the fuel, one node in the gap, and eight nodes in the cladding. The gap thermal conductivity is set to yield a given heat transfer coefficient value.

2.3.3 Core Power Calculation

The aim of this section is to describe the neutron power calculation utilized in the Vermont Yankee RETRAN model. The methodology used in generating kinetics parameters, scram reactivity, and feedback reactivity functions is not described here, but is addressed in our transient core physics report [10].

For the purposes of understanding the transient nature of the

calculation, the total power associated with the core at any given point in time may be viewed as being due to two coupled but distinct processes: (1) fission, and (2) radioactive decay. The contribution of the former in the model is based on the solution of the classical point kinetics equation with six delayed neutron groups. This component of core power is referred to as prompt in RETRAN [2] and should not be confused with the concept of prompt and delayed neutrons. The contribution of the radioactive decay process, referred to as delayed in RETRAN [2], is based on a fission product decay model consisting of eleven groups. The decay constants of the eleven fission product groups are provided in Table V.1-1, Vol. 1 of Reference 2.

The two processes are coupled because the production of fission products is proportional to the fission rate and because the energy release due to radioactive decay affects the fuel temperature and moderator density. The model accounts for this coupling; the production term in the radioactive decay balance equation is proportional to the amplitude function; and the radioactive decay component implicitly enters the point kinetics solution through the moderator and fuel feedback reactivity components.

For the point kinetics equation to accurately predict the fission power component, it is necessary to have the correct functional relations between reactivity components and their associated state variables, as predicted by the system model, and to have a system model which accurately predicts the above state variables.

The methodology developed for generating the feedback reactivity function is consistent with the RETRAN field equations [10]. The reactivity

calculation itself is described below.

The reactivity function comprises three components: control rod, moderator and Doppler. The control rod reactivity is generally specified as a function of time after some initiating event (e.g., turbine stop valve 10% close trip). The method used in the model for calculating the moderator and Doppler components differs from the standard approach. The standard approach is to provide a single table of reactivity versus the associated independent variable for each component. The single appropriate table is entered for each core region and a weighted sum is calculated, yielding the component reactivity. This standard approach is bypassed in the model, and the control system option of the code is used to calculate the moderator and Doppler reactivity components. The approach used here is to provide each core region with at least one separate table for each component. This allows for more detailed and diverse functional relations between the core thermal-hydraulic variables and feedback reactivity components.

The model accounts for the direct deposition of prompt energy (fission related) into regions outside the fuel pellet region. Separate fractions of the fission power component are directly deposited into the coolant present in the active core and bypass region. The remainder is deposited into the pellet region of the fuel. The direct moderator heating of the active core region is a standard feature of RETRAN [2]. The direct moderator heating of the bypass region is not. This phenomena is simulated by including a non-conducting heat exchanger in the bypass region. The heat transfer rate of the heat exchanger is set proportional to the amplitude function of the point kinetics solution via the control system modeling feature.

The predictive capabilities of the above calculational scheme are demonstrated in Section 3 of this report by comparison to test data. It is seen that even for very fast transients (e.g., turbine trip), the model yields good agreement with the test data.

2.4 Component Models

The steady-state and transient performance of a BWR is controlled or determined by the response characteristics of various components of the system, such as the recirculation pumps and motor-generator sets, the jet pumps, and steam separators. The following sections describe the major components of the Vermont Yankee RETRAN model.

2.4.1 Jet Pumps

There are ten jet pumps in each of the two recirculation loops. The ten jet pumps per loop are modeled as a single jet pump. This jet pump has one volume, representing both the throat section and the diffuser. The loss coefficients for the junctions are specified. This model has been compared to manufacturer's out-of-core hydraulic test data for a single jet pump. The comparisons were accomplished by setting up a small RETRAN model of the jet pump and the test stand. Pressure distribution data were used to determine suitable values for the suction and drive nozzle loss coefficients. All other junction data and volume geometry data were calculated. Jet pump M-ratio and N-ratio characteristics were calculated and compared to the test data. The results of this comparison are shown in Figure 2.2. The comparison shows that this modeling technique provides an acceptable representation of the performance characteristics of the

Vermont Yankee jet pumps.

2.4.2 Recirculation Pumps

The centrifugal pump model in RETRAN is used to represent the VY recirculation pumps. This is done by input of the actual pump performance data, which are available for the normal (or positive) head vs. flow quadrant. The characteristics of a similar pump (N_s = 4200) are overlayed to provide data in the other three quadrants. For the anticipated range of model application, pump operation significantly outside of the normal quadrant is not expected. Rated values for the mass moment of inertia of the pump and its drive motor are used. The pump motor electrical torque is simulated along with the M-G sets which supply power to the pump motor. This modeling is discussed in the following section.

2.4.3 M-G Sets and Recirculation Pump Motor Electrical Torque

The M-G sets are modeled using the control theory option of RETRAN. Figures 2.3a and b show the control inputs and control blocks for the simulation of a single M-G set and recirculation pump motor.

The simulation of the M-G set is concerned with two rotating systems: (1) the M-G set drive motor and input shaft portion of the hydraulic coupler and (2) the output shaft portion of the hydraulic coupler and the generator. The governing differential equation for the rotational dynamics of each system is solved. The torque transmitted by the hydraulic coupler to the generator is based on the algebraic model described in [4]. It is assumed that the coupler does not dissipate any energy. The position (x) of the coupler scoop tube is controlled by the M-G set speed control system which

is modeled as described in Section 2.5.2.

The model used for determining the recirculation pump motor electrical torque accounts for the variable supply frequency. The model is based on the following assumptions:

1) For a given frequency, the motor torque curve is linear.

2) At rated conditions the percent slip is constant for frequency variations.

3) Rated motor torque is inversely proportional to frequency squared.

4) Supply voltage is constant.

The same model is used for the M-G set drive motor electrical torque. In the case of the M-G set drive motor simulation, the electrical frequency is input explicitly as a function of time.

2.4.4 Steam Separators

The steam separators are an important component to the system simulation in that they physically couple two areas of primary interest, the core and the steam dome. The emphasis in modeling the separators has been placed on achieving the proper coupling between these two regions rather than on a detailed thermal-hydraulic calculation of the separators.

The 129 steam separators are modeled as a single component. An equilibrium volume is used with the standard RETRAN phase separation model [2]. Referring to Figure 2.1, the interior of the separators is represented by volume 3. The entering two-phase fluid flow path is represented by

junction 2. Separation takes place within volume 3; junctions 3 and 5 represent the steam and separated liquid flow paths.

The most important parameters of the separator model relative to the coupling between the steam dome and core region are the effective inlet inertia, the frictional pressure drop, the initial mass inventory, and the carry under fraction. The inlet inertia and initial mass inventory used in the model are based on manufacturer's data [4]. The steady-state value for this parameter is a function of quality, but the transient model here assumes a constant value. The inlet loss coefficient has been adjusted to agree with vendor overall pressure drop data from prototype testing [3]. The carry under fraction is initially set within the performance requirements of the component. All other parameters associated with the model are based on physical dimensions.

Although the above model is a crude approximation to the existing complex flow geometry and separation phenomena, the modeling techniques used have provided good agreement with data both in fast transients such as the Peach Bottom 2 turbine trip tests, Section 3, and slower transients such as the Vermont Yankee generator load rejection startup test, Appendix A.

2.5 Control Systems and Trip Logic

The feedwater, turbine, and M-G set speed control systems are modeled using the control system model option of RETRAN [2]. Controller settings and compensation element time constants are based on actual plant values. Sensor element time constants, position loop characteristics, and other parameters are based on either plant or manufacturer's supplied data. The

specific control systems are described below.

2.5.1 Turbine Control System

The reader is referred to Reference 1 for a general description of the turbine control system (TCS). The RETRAN model of the TCS is presented in Figure 2.4. The electrical pressure regulator (EPR) which is normally controlling control valve and bypass valve position is modeled explicitly. Time constants for the EPR used in this analysis are based on preoperational tests. The mechanical pressure regulator which serves as a backup to the EPR is not modeled. The speed control portion of the system is not modeled explicitly. The control signal received at the primary relay from either the acceleration or speed relay is explicitly input through the use of a function generator control block. Time constants for relays and valve servos are nominal values. The nonlinear turbine control valve characteristics have been modeled. The bypass valves are assumed to be linear.

2.5.2 M-G Set Speed Control System

The reader is referred to References 1 and 6 for descriptions of the M-G set speed control system. The RETRAN model of the system, presented in Figure 2.5, is based on the master manual control mode of the system. This is the normal operating mode for the Vermont Yankee Nuclear Power Station. Separate speed controllers are modeled for each of the two M-G sets. Speed controller proportional band and reset rate reflect the current plant settings. The scoop tube actuator logic is based on frequency response measurements taken during the plant startup tests [7].

2.5.3 Feedwater Flow Control System

The reader is referred to Reference 2 for a description of the feedwater flow control system. The RETRAN model of the flow control system is shown in Figure 2.6. Emphasis is placed on the transient prediction of feedwater flow. The enthalpy of the feedwater entering the vessel is specified explicitly as a function of time.

The three element control mode of the system is modeled. The simulated level signal takes into account the non-uniform cross-sectional area of the vessel and the steam dryer pressure drop. The two control valves and their positioners are assumed to be identical and are modeled as a single component. The feedwater flow is governed by an unsteady momentum equation. This equation takes into account the effects of time-varying steam dome pressure and control valve position, piping system frictional resistance and inertia, and system pumping mode. Augmentations have been made to allow the specification of controller output signal versus time or feedwater flow versus time. The latter, of course, overrides the unsteady momentum equation calculation.

2.5.4 Reactor Trips

The Vermont Yankee RETRAN model has the capability of simulating either directly or indirectly all Reactor Protection System (RPS) trips. This may be accomplished with the model via RETRAN trip cards in one of two ways: (1) by specifying the process variable reactor trip setpoint and monitoring the variable or (2) by specifying a priori the time at which the reactor trip occurs. In any simulation, consideration is given by the safety analyst as to what RPS trips are appropriate. Table 3.1.1 of Reference 5 provides a listing of all RPS instruments and their setpoints.

TABLE 2.1

Volume Descriptions

Vol. No.	Fluid Volume (ft^3)	Flow Area (ft^2)	Bottom Elev. (ft)	Volume Height (ft)	Enthalpy Transport (ET) or Transport Delay (TD) Model	Volume Description
1	728.61	116.187	29.292	6.271	None	Vessel Upper Plenum
2	137.09	25.88	35.563	4.438	None	Stand Pipes
3	566.30	114.40	38.375	7.7917	None	Steam Separators
4	2604.30	85.0	8.542	30.625	None	Lower Downcomer
5	216.63	3.90	-26.583	39.083	TD	Recirculation Loop 2 Suction Piping
6	315.73	2.31	-22.253	47.540	TD	Recirculation Loop 2 Discharge Piping
7	216.63	3.90	-26.583	39.083	TD	Recirculation Loop 1 Suction Piping
8	315.73	2.31	-22.253	47.540	TD	Recirculation Loop 1 Discharge Piping
9	2185.05	126.362	0.0	17.292	None	Vessel Lower Plenum
11	852.27	71.020	17.292	12.00	ET	Core Bypass
12	40.06	10E+6	-26.583	4.33	None	Recirculation Pump Loop 2
13	40.06	10E+6	-26.583	4.33	None	Recirculation Pump Loop 1
15	107.25	6.4	8.167	16.75	None	10 Jet Pumps Loop 2
16	107.25	6.4	8.167	16.75	None	10 Jet Pumps Loop 1
22	2327.40	85.00	39.1667	27.38	None	Steam Dome & Steam Dryers & Upper Downcomer
50	393.30	5.673	3.583	46.00	None	Main Steam Line Piping Upstream of MSIV's (inboard)
51	103.96	5.673	-13.417	17.00	None	Main Steam Line Piping Upstream of MSIV's (inboard)
52	432.516	5.673	-13.42	11.00	None	Main Steam Line piping Downstream of MSIV's (inboard)
53	395.351	5.673	-3.300	1.75	None	Main Steam Line piping Downstream of MSIV's (inboard)
54	389.139	5.673	-4.20	1.75	None	Main Steam Line Piping Downstream of MSIV's (inboard)
55	160.055	5.673	-7.50	3.30	None	Main Steam Line Piping Downstream of MSIV's (inboard)
100	10E+9	10E+9	-30.0	150.00	None	Primary Containment (Dummy Sink Volume)

TABLE 2.1 (Cont'd)

Volume Descriptions

Vol. No.	Fluid Volume (ft^3)	Flow Area (ft^2)	Bottom Elev. (ft)	Volume Height (ft)	Enthalpy Transport (ET) or Transport Delay (TD) Model	Volume Description
201	40.05	40.04	17.292	1.0	ET	1/12 Average Core
202	40.05	40.04	18.292	1.0	ET	1/12 Average Core
203	40.05	40.04	19.292	1.0	ET	1/12 Average Core
204	40.05	40.04	20.292	1.0	ET	1/12 Average Core
205	40.05	40.04	21.292	1.0	ET	1/12 Average Core
206	40.05	40.04	22.292	1.0	ET	1/12 Average Core
207	40.05	40.04	23.292	1.0	ET	1/12 Average Core
208	40.05	40.04	24.292	1.0	ET	1/12 Average Core
209	40.05	40.04	25.292	1.0	ET	1/12 Average Core
210	40.05	40.04	26.292	1.0	ET	1/12 Average Core
211	40.05	40.04	27.292	1.0	ET	1/12 Average Core
212	40.05	40.04	28.292	1.0	ET	1/12 Average Core

TABLE 2.2

Junction Descriptions

Junc. No.	Connects Volume From	To	Flow Area (ft^2)	Elev. (ft.)	Inertia (ft^{-1})	Form Loss Coefficients Forward	Reverse	Junction Description
1	1	2	25.877	35.563	0.129	0.423	0.716	Upper Plenum to Stand Pipes
2	2	3	25.877	40.00	0.4774	1.557	0.0	Stand Pipes to Steam Separators
3	3	22	36.98	46.1667	0.1827	-1.0	0.4193	Steam Separators to Upper Downcomer
4	4	15	1.482	24.917	4.27	0.1461882	1.5	Lower Downcomer to Jet Pumps
5	3	22	36.98	38.375	0.1827	-1.0	0.0	Steam Separators to Upper Downcomer
6	4	5	3.903	12.5	7.20	0.18	1.18	Lower Downcomer to Recirc. Pump Suction
7	5	12	3.903	-22.253	7.045	0.45	0.45	Suction Piping to Recirc. Pump
8	12	6	3.903	-22.253	14.50	-1.0	0.0	Recirc. Pump to Discharge Piping
9	6	15	0.5275	24.917	22.11	0.14524	0.0	Recirc. Pump Discharge to Jet Pumps
10	4	7	3.903	12.50	7.20	0.18	1.18	Lower Downcomer to Recirc. Pump Suction
11	7	13	3.903	-22.253	7.045	0.45	0.45	Suction Piping to Recirc. Pump
12	13	8	3.903	-22.253	14.50	-1.0	0.0	Recirc. Pump to Discharge Piping
13	8	16	0.5272	24.917	22.11	0.14524	0.0	Recirc. Pump Discharge to Jet Pumps
14	4	16	1.482	24.917	4.27	0.1461882	1.5	Lower Downcomer to Jet Pumps
15	9	201	9.0186	17.292	0.081	2.49	2.49	Lower Plenum to Bottom of Active Core
16	9	11	0.318	17.292	0.153	-1.0	0.0	Lower Plenum to Core Bypass
17	212	1	40.04	29.292	0.0395	-1.0	0.0	Top of Active Core to Upper Plenum
18	11	1	44.971	29.292	0.112	0.376	0.307	Core Bypass to Upper Plenum
19	15	9	11.08	8.167	0.74	1.75	1.114	Jet Pumps to Lower Plenum
20	16	9	11.08	8.167	0.74	1.75	1.114	Jet Pumps to Lower Plenum
21	22	4	85.0	39.1667	0.3413	0.177	0.211	Upper to Lower Downcomer

TABLE 2.2 (Cont'd)

Junction Descriptions

Junc. No.	Connects Volume From	To	Flow Area (ft^2)	Elev. (ft.)	Inertia (ft^{-1})	Form Loss Coefficients Forward	Reverse	Junction Description
50	22	50	5.673	49.583	6.271	1.11534	1.11534	Steam Dome to Steam Lines
51	50	100	0.1469	5.083	1.0	1.0	0.0	One Relief Valve
52	50	100	0.2938	5.083	1.0	1.0	0.0	Two Relief Valves
53	50	100	0.1469	5.083	1.0	1.0	0.0	One Relief Valve
54	50	100	0.2938	5.083	1.0	1.0	0.0	Two Safety Valves
55	50	51	5.673	3.583	7.726	0.50127	0.50127	Steam Line to MSIV (inboard)
56	51	52	5.673	-13.385	8.335	3.28577	3.28577	Steam Line Downstream of MSIV's
57	52	53	5.673	-2.420	12.862	0.3625	0.3625	Steam Line Downstream of MSIV's
58	0	53	1.0	-6.75	19.5	-1.0	0.0	Turbine Stop Valves
59	0	53	1.0	-6.23	27.37	1.0	0.0	Steam Bypass Valves
60	53	54	5.673	-3.292	12.862	0.201	0.201	Steam Line Downstream of MSIV's
61	54	55	5.673	-4.20	8.532	0.248	0.248	Steam Line Downstream of MSIV's
201	201	202	40.04	18.292	0.025	0.738	0.738	Junctions Connecting Core Volumes
202	202	203	40.04	19.292	0.025	0.738	0.738	Junctions Connecting Core Volumes
203	203	204	40.04	20.292	0.025	0.738	0.738	Junctions Connecting Core Volumes
204	204	205	40.04	21.292	0.025	0.738	0.738	Junctions Connecting Core Volumes
205	205	206	40.04	22.292	0.025	0.738	0.738	Junctions Connecting Core Volumes
206	206	207	40.04	23.292	0.025	0.738	0.738	Junctions Connecting Core Volumes
207	207	208	40.04	24.292	0.025	0.738	0.738	Junctions Connecting Core Volumes
208	208	209	40.04	25.292	0.025	0.738	0.378	Junctions Connecting Core Volumes
209	209	210	40.04	26.292	0.025	0.738	0.738	Junctions Connecting Core Volumes
210	210	211	40.04	27.292	0.025	0.738	0.738	Junctions Connecting Core Volumes
211	211	212	40.04	28.292	0.025	0.738	0.738	Junctions Connecting Core Volumes
999	0	4	1.0	38.833	0.0	0.0	0.0	Feedwater Fill Junction

NOTE: A -1.0 for forward form loss coefficient indicates that sufficient volume pressures were supplied to allow the code to calculate the form loss coefficients.

A 0.0 for the reverse form loss coefficient indicates that the reverse form loss coefficient is set equal to forward form loss coefficient.

TABLE 2.3

Description of Heat Conductors

Heat Cond. No.	Volume On: Left	Right	Geometry TYPE	Conductor Volume (ft^3)	Surface Area Left (ft^2)	Right (ft^2)	Heat Conductor Description
9	4	1	Rectangular	49.63	335.17	254.12	Core shroud head & core spray spargers & upper core grid
10	9	0	Rectangular	328.98	6155.29	0.0	Vessel lower plenum & guide tubes
13	2	4	Cylindrical	138.30	4914.51	2950.09	Stand pipes & steam separators
50	16	4	Rectangular	13.98	595.22	595.22	10 Jet pumps & risers for recirc. Loop #1
51	15	4	Rectangular	13.98	595.22	595.22	10 Jet pumps & risers for recirc. Loop #2
100	8	0	Cylindrical	61.942	1070.433	0.0	Recirculation Loop #1 piping
101	6	0	Cylindrical	61.942	1070.433	0.0	Recirculation Loop #2 piping
201	0	201	Cylindrical	31.1737*	0.0	2657.7915	Fuel rods, 1/12 core
202	0	202	Cylindrical	31.1737*	0.0	2657.7915	Fuel rods, 1/12 core
203	0	203	Cylindrical	31.1737*	0.0	2657.7915	Fuel rods, 1/12 core
204	0	204	Cylindrical	31.1737*	0.0	2657.7915	Fuel rods, 1/12 core
205	0	205	Cylindrical	31.1737*	0.0	2657.7915	Fuel rods, 1/12 core
206	0	206	Cylindrical	31.1737*	0.0	2657.7915	Fuel rods, 1/12 core
207	0	207	Cylindrical	31.1737*	0.0	2657.7915	Fuel rods, 1/12 core
208	0	208	Cylindrical	31.1737*	0.0	2657.7915	Fuel rods, 1/12 core
209	0	209	Cylindrical	31.1737*	0.0	2657.7915	Fuel rods, 1/12 core
210	0	210	Cylindrical	31.1737*	0.0	2657.7915	Fuel rods, 1/12 core
211	0	211	Cylindrical	31.1737*	0.0	2657.7915	Fuel rods, 1/12 core
212	0	212	Cylindrical	31.1737*	0.0	2657.7915	Fuel rods, 1/12 core

TABLE 2.3 (Cont'd)

Description of Heat Conductors

Heat Cond. No.	Volume On: Left	Volume On: Right	Geometry TYPE	Conductor Volume (ft^3)	Surface Area Left (ft^2)	Surface Area Right (ft^2)	Heat Conductor Description
500	50	0	Cylindrical	96.75	1170.75	0.0	Steam line piping upstream of MSIV's (inboard)
501	51	0	Cylindrical	25.57	309.45	0.0	Steam line piping upstream of MSIV's (inboard)
502	52	0	Cylindrical	334.29	4045.12	0.0	Steam line piping downstream of MSIV's (inboard)
503	4	0	Cylindrical	755.50	1643.61	0.0	Vessel barrel around lower downcomer
999	11	4	Cylindrical	248.26	951.80	983.15	Core shroud barrel

*Cycle dependent, based on type of fuel present in the core.

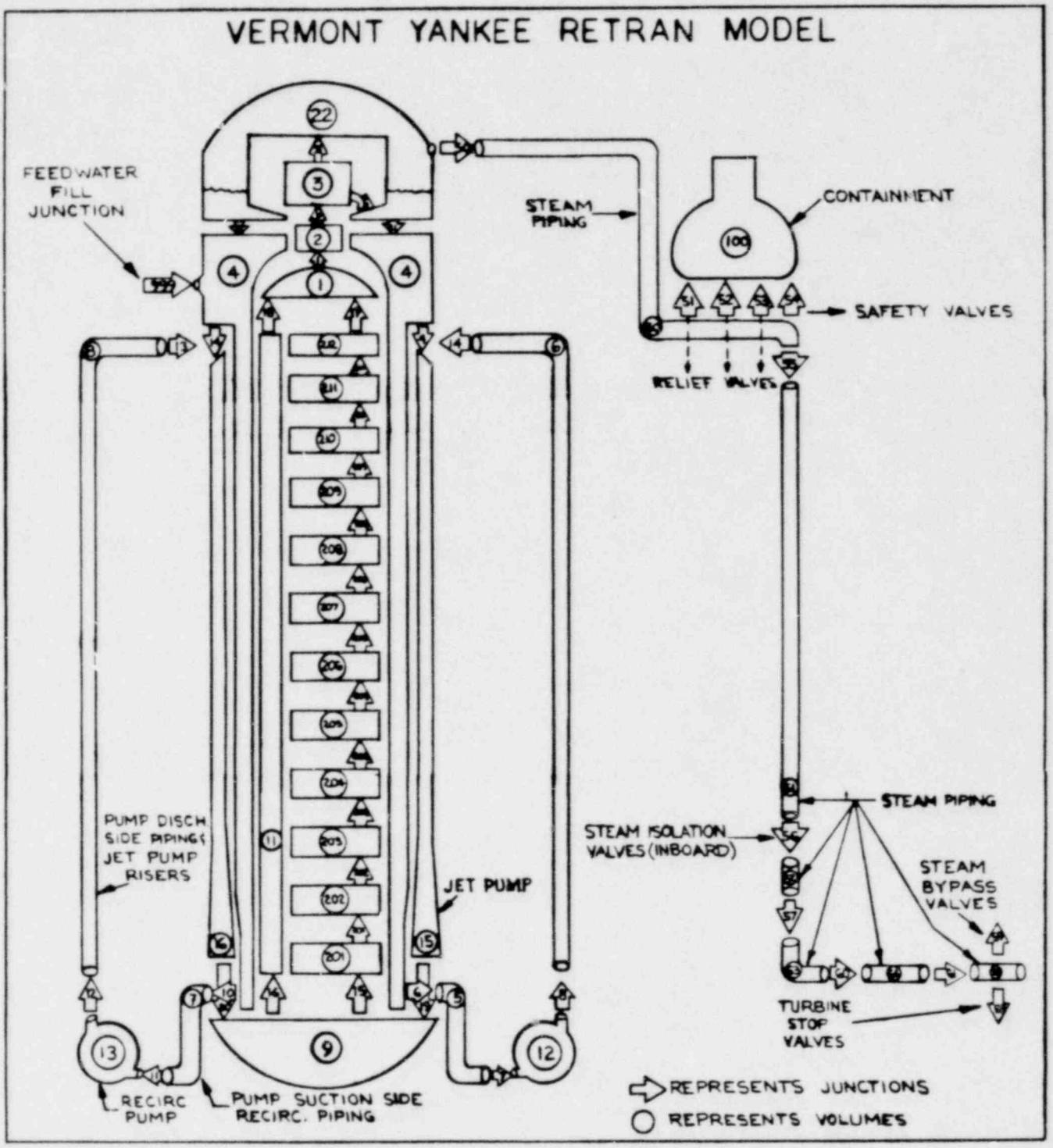

Figure 2.1 Vermont Yankee RETRAN Model

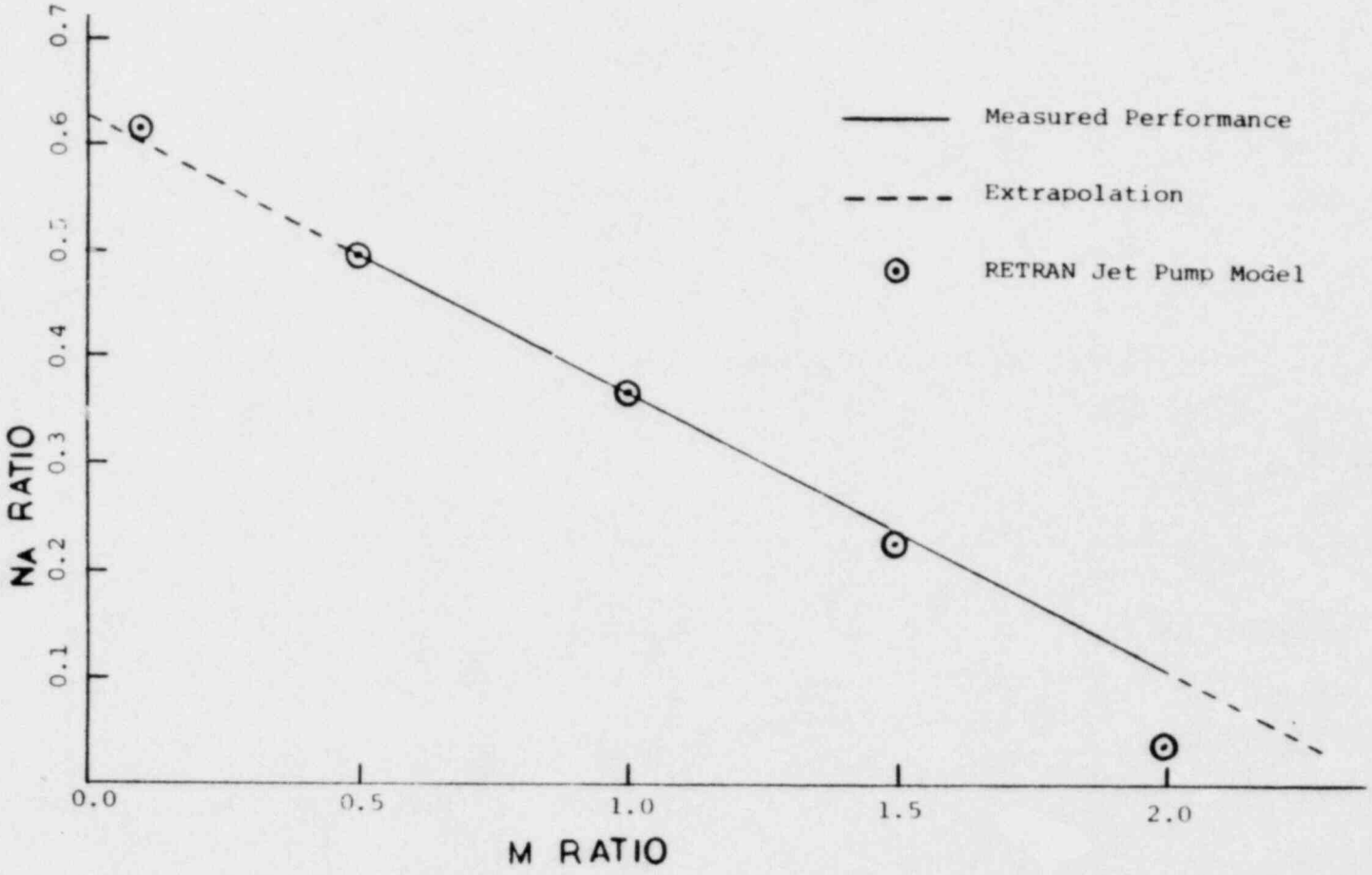

Figure 2.2 Comparison of RETRAN Jet Pump Model to Measured Performance Data

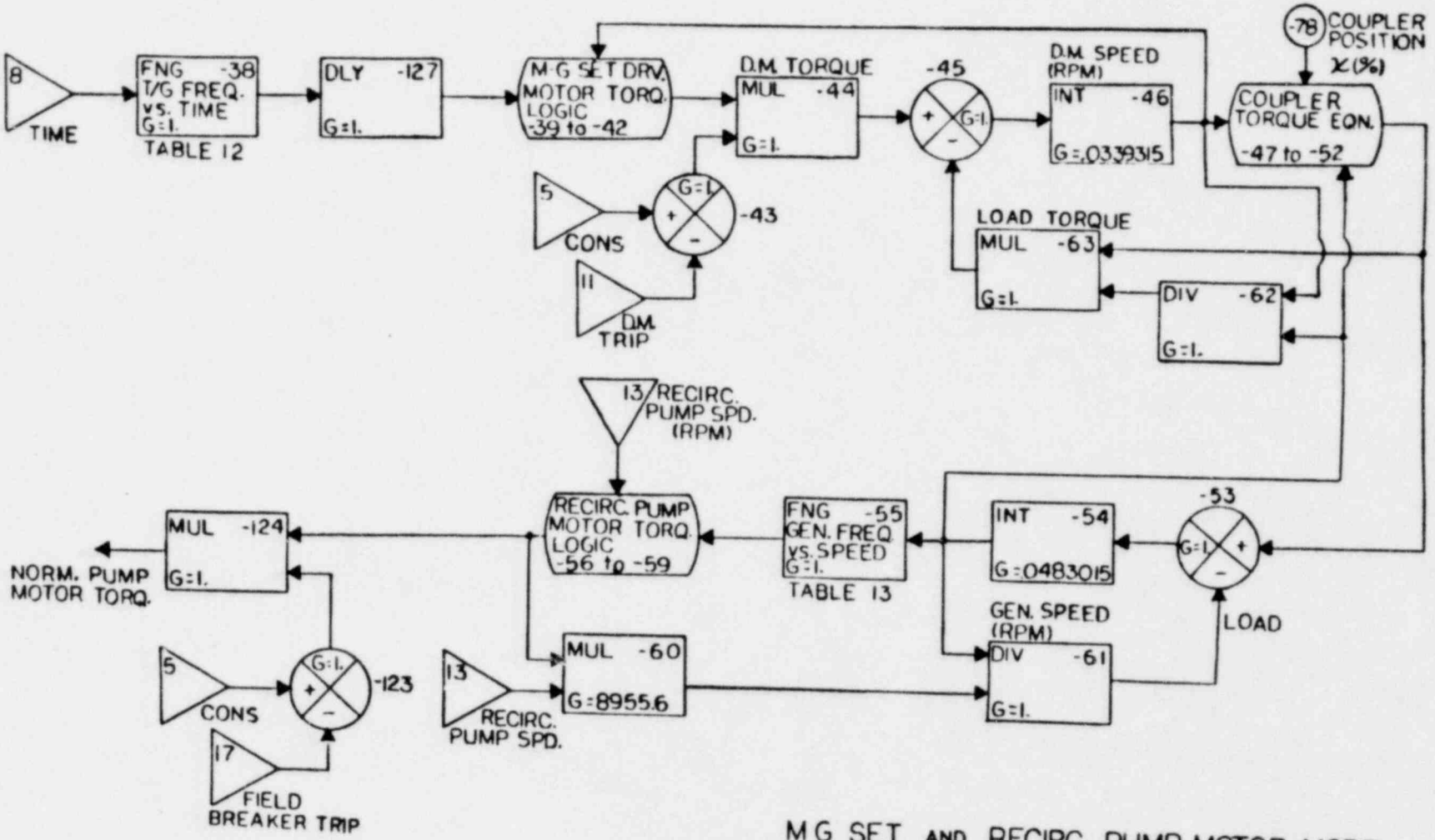

M G SET AND RECIRC PUMP MOTOR MODEL

NOTE: THE ABOVE CORRESPONDS TO EQUIPMENT ASSOIATED WITH A SINGLE RECIRC. LOOP. THE OTHER LOOP IS SIMILARLY MODELED.

Figure 2.3a MG Set and Recirculation Pump Motor Model

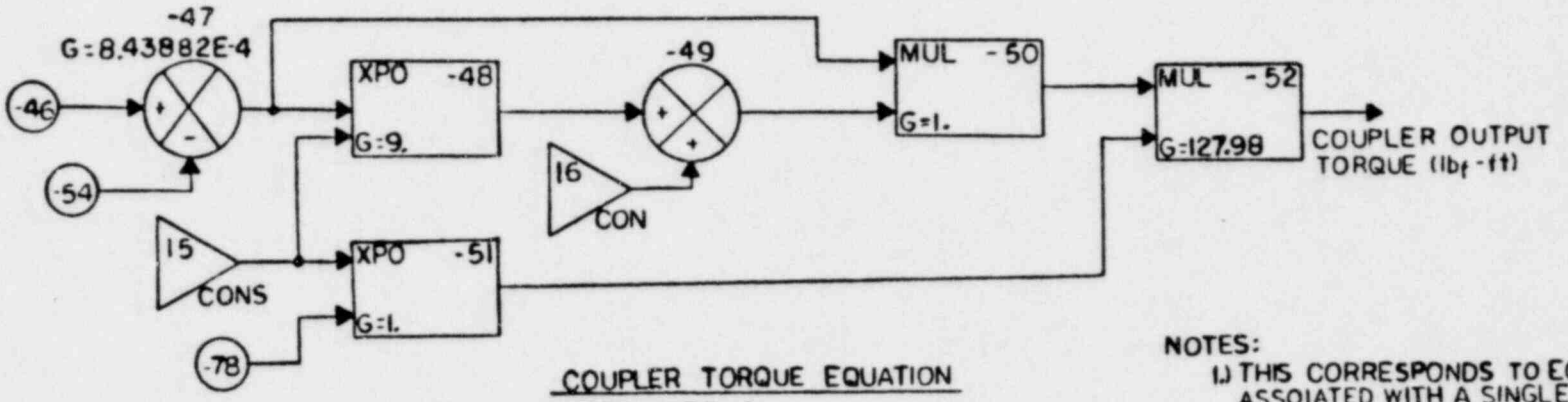

COUPLER TORQUE EQUATION
(SEE NOTE 1.)

NOTES:
1.) THIS CORRESPONDS TO EQUIPMENT ASSOIATED WITH A SINGLE RECIRC. LOOP. THE OTHER LOOP IS SIMILARLY MODELED.
2.) M-G SET DRIVE MOTORS SIMILARLY MODELED.

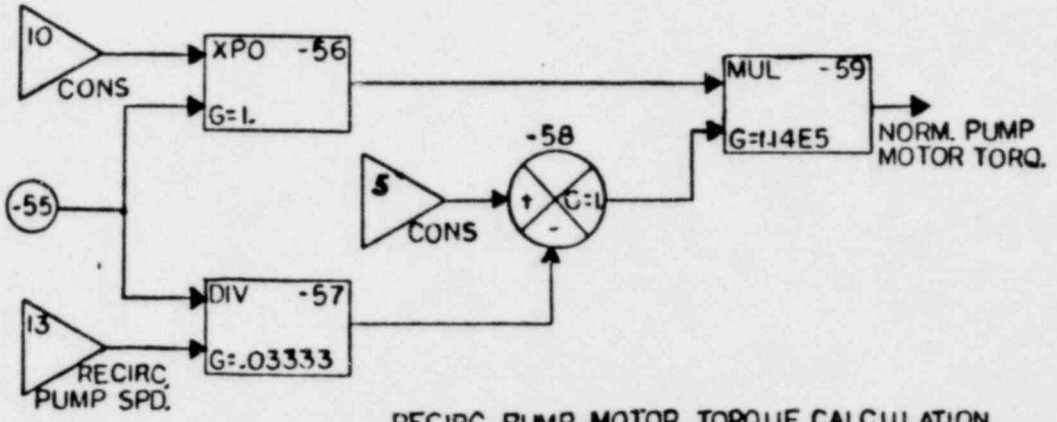

RECIRC PUMP MOTOR TORQUE CALCULATION
(SEE NOTES 1/2.)

Figure 2.3b MG Set and Recirculation Pump Motor Model

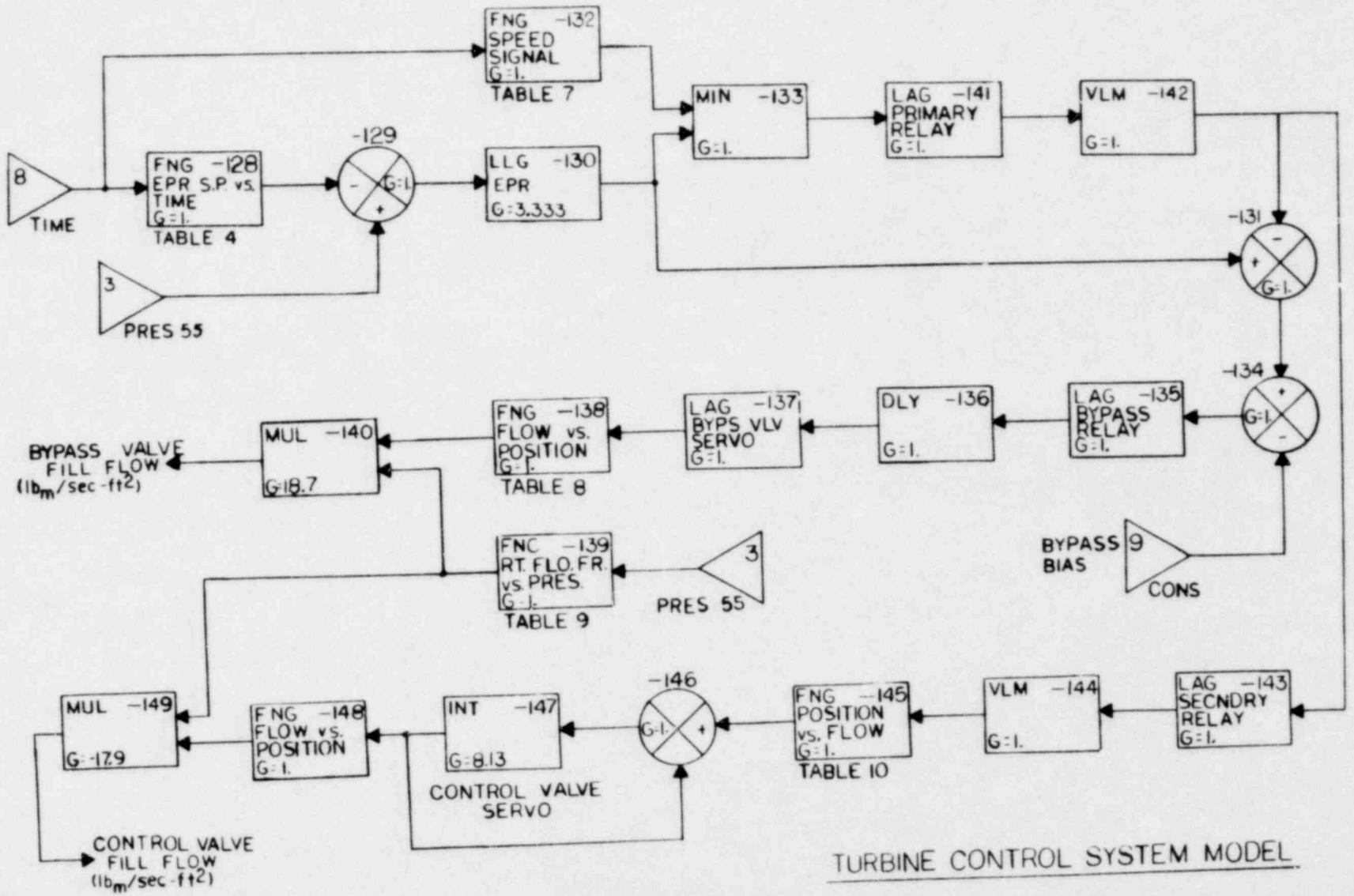

Figure 2.4 Turbine Control System Model

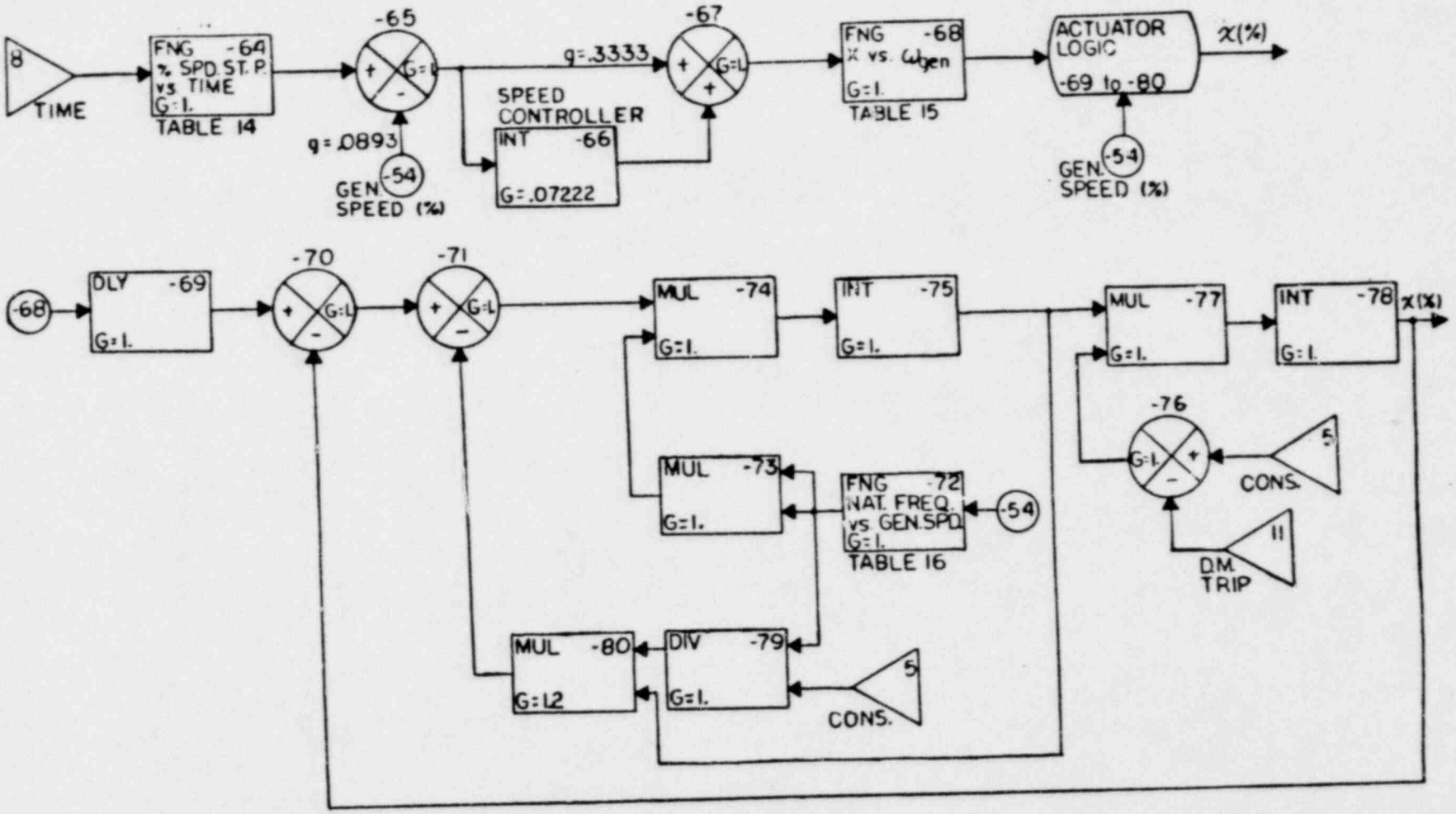

NOTE: THE ABOVE CORRESPONDS TO A SINGLE M-G SET. CONTROLS FOR THE OTHER M-G SET ARE FUNCTIONALLY IDENTICAL.

MG SET SPEED CONTROL SYSTEM

MASTER MANUAL MODE

Figure 2.5 MG Set Speed Control System

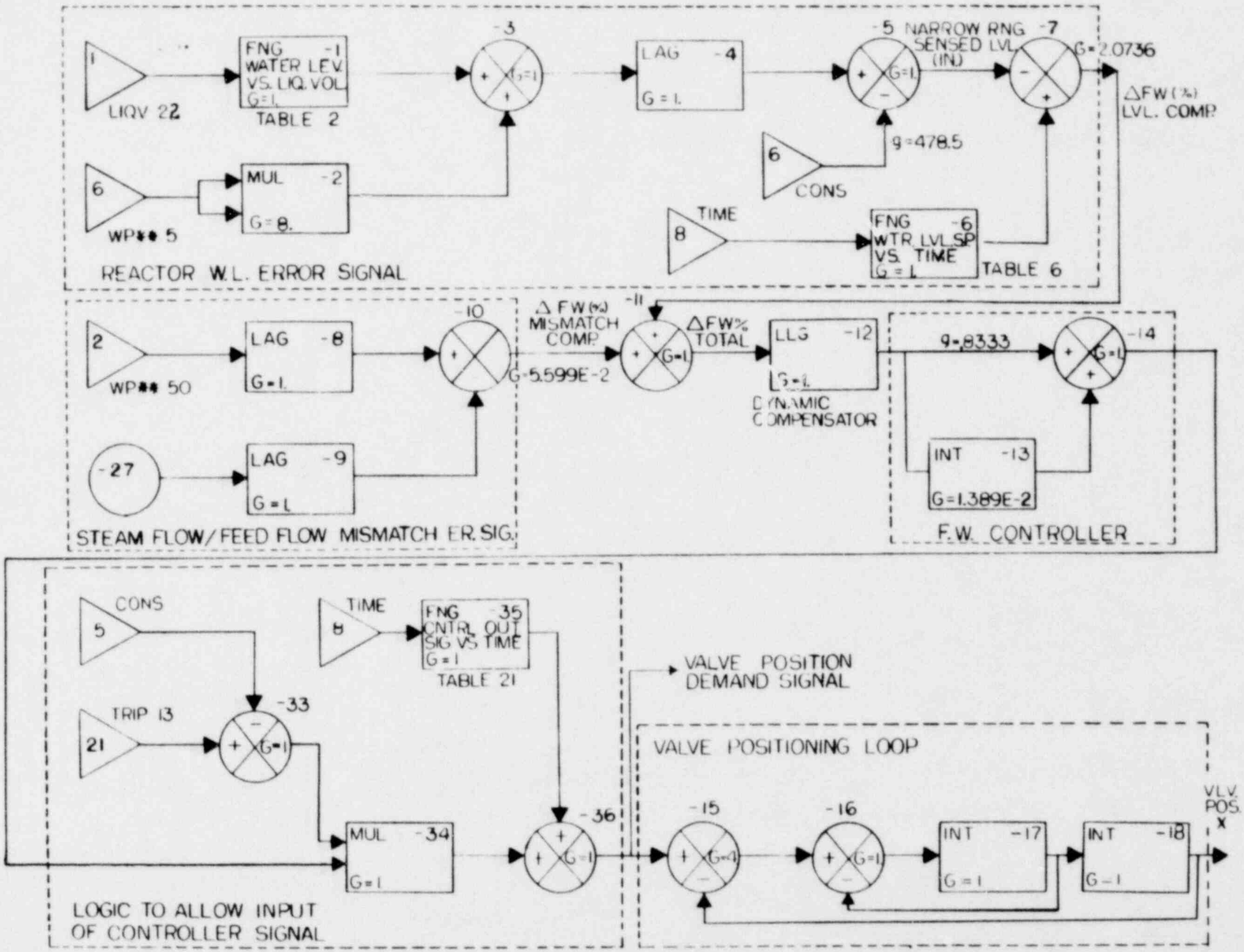

Figure 2.6a Feedwater Flow Control System

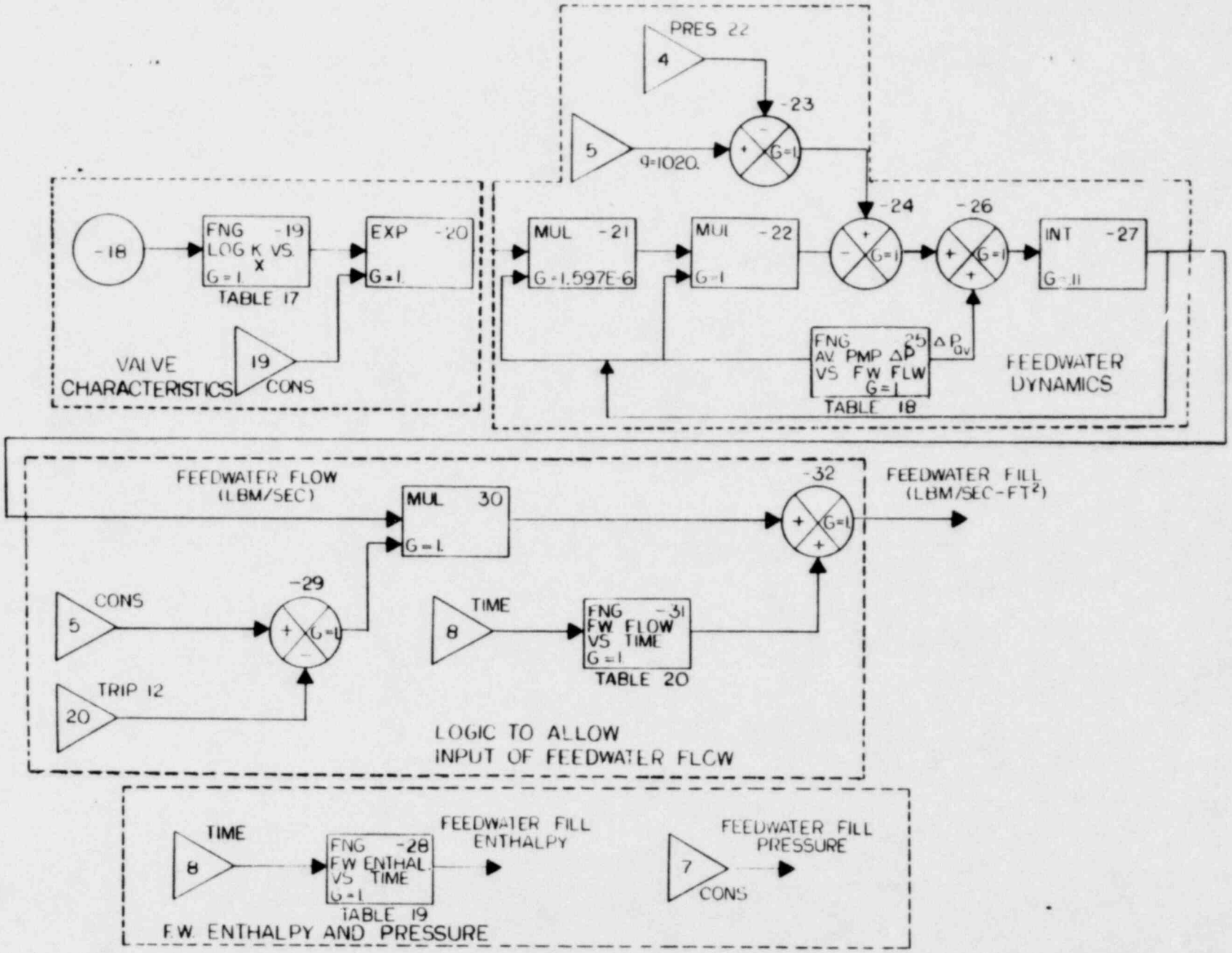

Figure 2.6b Feedwater Flow Control System

3.0 QUALIFICATION

RETRAN qualification entails comparison of predicted results to experimental data for a variety of transients. The information presented in this section should be viewed as supplemental to the large body of qualification results presented in the basic RETRAN documentation [2], where it can be seen that RETRAN has already demonstrated its ability to accurately predict the course of many types of transients. This section presents the RETRAN predictions of the turbine trip tests performed at the Peach Bottom Nuclear Power Plant. The RETRAN simulation of the Peach Bottom tests is intended as a qualification of Vermont Yankee modeling techniques, and, in particular, the techniques involved in developing the core kinetics model.

Results of two Vermont Yankee startup tests and four licensing type transients are presented in Appendix A. These analyses are also part of the model qualification. Indeed, the current form of the model was derived through the performance of these analyses. They are included in an appendix because parts of the modeling used in the analyses are different than those described in Section 2. In general, none of the analyses employed the non-equilibrium model in the steam dome region (Section 2.1.1), nor was the methodology used to generate the reactivity data or the reactivity calculation precisely the same as described (Section 2.3.3). The particular areas that are significantly different than those described in Section 2 are identified. Conclusions have been drawn only in areas that are essentially the same as the model.

Appendix A as a whole is a good example of the modeling process:

the iterative loop of formulation, analysis and validation. It is a collection of YAEC model development iterations and the insights gained over a three-year period. The latest iteration in this loop, the simulation of the Peach Bottom turbine trip tests, is presented below.

3.1 Simulation of the Peach Bottom Unit 2 Turbine Trip Tests

The three turbine trip tests simulated were performed at Peach Bottom Atomic Power Station Unit 2 prior to a refueling shutdown in April 1977. The equipment, initial conditions, results, and measurement error analysis for the test are reported in Reference 14.

The above tests are the best set of benchmark tests available in the area of BWR system transients for computer code and modeler qualification. Our purpose in simulating these tests is to demonstrate the adequacy of the modeling techniques used in the Vermont Yankee system analysis model (Section 2). The fact that these tests were performed at Peach Bottom rather than Vermont Yankee has little bearing on the ability of these tests to serve as a data base for the described models and modeling techniques. Indeed, most of the individual components of the Peach Bottom 2 reactor are identical to their Vermont Yankee counterparts and it is only the number of components which differ (e.g., separators and fuel assemblies).

For the simulation of fast pressurization type transients, such as the above tests, certain areas of the model are of more importance than others. The areas judged to be of most importance for the above class of transients are the following:

i. the reactor power calculation,

ii. the steam line model,

iii. the steam dome and downcomer region model,

iv. the separator model, and

v. the core thermal-hydraulics model.

The merit or deficiencies of the above modeling should be brought out by the test simulations.

A considerable amount of analysis for these tests has been performed with RETRAN by other workers [15]. This work was the starting point for the simulations presented here. The philosophy adopted was to incorporate the previously described models into the already developed RETRAN model [15]. This was done with particular emphasis placed on the modeling areas listed above. The net result is a model identical to the Vermont Yankee system transient analysis model in modeling philosophy. The model is described below.

3.1.1 Peach Bottom Unit 2 Model Description

A schematic of the model is shown in Figure 3.1. Comparing this figure with that of the Vermont Yankee model, Figure 2.1, it is seen that the nodalization within the reactor vessel and of the main steam lines are identical - except that the two recirculation loops are combined into one in the Peach Bottom model. The Peach Bottom model includes the entire bypass system. This model is the best estimate bypass system model of Hornyik and Naser [15], and is included to provide a realistic simulation of this component so as not to bias other portions of the model.

As previously stated, the starting point for the development of

the system model used in these simulations was the system model of Hornyik and Naser [15]. In modifying this model to be consistent with the Vermont Yankee system model, the changes indicated in Table 3.1 were made. The modeling area that required the most extensive changes was the core power calculation, discussed below.

The core power calculation performed in the simulations utilizes the methodology described in Section 2.3.3. The functional relation for moderator reactivity is characterized by two independent variables; these are local volume fluid density and the ratio of the local volume fluid density to the density of saturated liquid water at the local volume pressure, hereafter called relative density. This relation is realized in the model by having two moderator reactivity tables per local core region, one being reactivity versus density, and the other being reactivity versus relative density. The output of the two tables for a given local region is summed to yield the moderator reactivity component for that region.

The generation of these tables took into account the initial core state and the range of pressure and inlet enthalpy expected to be encountered in each simulation. If a region was predicted to remain single-phase within the constraints of the RETRAN homogeneous equilibrium assumption, all the moderator reactivity was associated with the relative density table. Likewise, all the moderator reactivity was associated with the density table for a region that was predicted to remain two-phase. Finally, for a region that was predicted to change phase, both tables had data, and care was taken to assure a piecewise smooth relation. The inclusion of the relative density representation enables the model to account for reactivity changes associated with subcooled boiling in an approximate manner.

The control rod and Doppler reactivity components were generated in the standard manner [10]. All rods were assumed to be inserted at the same rate which was based on the average rod speed presented in Figure 6-12 of Reference [14]. Prompt direct moderator heating fractions used for the active core coolant and the bypass coolant were estimated to be .014 and .012 by Monte Carlo calculations [16].

In summary, the Peach Bottom model used here incorporates in all areas of importance the modeling techniques presented in Section 2. The test simulations and comparisons to the data are discussed below.

3.1.2 Simulations and Comparisons to Test Data

An important step in any simulation is the initialization of the model. Defining the initial operating state for off-design conditions, such as encountered in these tests, is not a trivial task. The approach used here was to rely on key measured parameters and to use the steady-state initialization feature of RETRAN [2] to determine the initial conditions. A summary of the model's initial operating state is provided in Table 3.2.

All three tests were simulated in the same manner. The measured closing and opening rates for the turbine stop and bypass valves were input to the model. The control rod scram initiation was based on the calculated neutron power reaching the trip setpoint; a delay of 0.195 seconds was assumed to account for the circuit delay and rod acceleration.

A summary of results for all three tests along with the measured values is provided in Table 3.3. The average neutron flux and steam dome pressure are selected as the parameters of most interest. The model

overpredicts the peak neutron flux in each of the tests; agreement is best---38% higher than the measured value---for the third test, where the flux transient was turned over by the effect of control rod insertion. The time at which the peak occurs is accurately predicted for each test with the maximum error being 20 milliseconds. The area under the peak is a more important parameter than the peak itself, since the magnitude of the initial rise in fuel surface heat flux is approximately proportional to it. The model predictions are closer to the data for this parameter than for the peak neutron flux. The closest prediction, test point 3, is 12% higher than the measured value.

Steam dome pressure is accurately predicted by the model. The first peak pressure predictions agree with the measurements to within 0.5 psi. The second and third peaks are overpredicted with the maximum deviations being 5 psi and 9 psi. This is expected since the neutron flux and, thus, the total energy released to the coolant are overpredicted.

Comparisons of the model predictions to the test measurements for all three tests are made in Figures 3.2 through 3.25. The figures have been grouped into three sets, each associated with a test. Each set has been divided into two time regions: 0.0 - 1.5 seconds to evaluate the core power calculation, and 0.0 - 10.0 seconds to evaluate the reactor vessel pressurization. Before discussing the specific comparisons, a few comments about the measurements and comparison in general need to be made.

The test traces presented are the raw test data, as recorded by the test data acquisition system, with elevation corrections applied to the pressure measurements [14]. The dynamic response of the instrument

lines are inherent in the pressure measurements. No attempt has been made here to model the instrument lines. Regarding the comparisons, no translations of the curves with respect to either axis have been made. The point t = 0.0 on the time axis coincides with the initiation of the stop valve closure - this point had to be estimated for the first test because both stop valve measurements failed.

The neutron power predictions for the three tests are compared with the average of the LPRM signals in Figures 3.2, 3.10 and 3.18. In all three cases, the initial rise time, rate of rise, time of peak, and rate of decrease are in good agreement with the data.

The calculated reactivity components, total reactivity, and the reactivity implied by the data are presented in Figures 3.3, 3.11 and 3.19. The curve labeled RHOINV is the total reactivity implied by the data. It was calculated by solving the inverse point kinetics equation [10] using the kinetics parameters input to the model and the average of the LPRM signals as the amplitude function. The agreement between the predicted total reactivity and the RHOINV curve is good with the peaks being overpredicted by approximately 10 cents in all cases. The contrast in the magnitudes of the overpredictions in total reactivity relative to those of the neutron power demonstrates the sensitivity of the neutron power peak to small changes in reactivity close to the prompt critical condition. From examining the reactivity components, it is seen that the total reactivity is turned over before the effect of control rod insertion in the first and second tests, while the reverse is true for the third test. This is in agreement with the observed test data [14].

A comparison of steam dome and upper plenum pressure with the test measurements is shown in Figures 3.4, 3.5, 3.12, 3.13, 3.20 and 3.21. The overall agreement between the prediction and data is excellent, particularly in the rate of rise. The time delay of the measurement system associated with a pressure ramp input has been estimated by the experimenters to be 30 milliseconds [14]. The delay indicated by the figures for the initial rise in steam dome pressure is approximately 40 milliseconds. Hence, this agreement is even better than would appear at a first glance.

To provide a better perspective on the transient pressure predictions in the steam dome and upper plenum, Figures 3.6, 3.7, 3.14, 3.15, 3.22 and 3.23 have been included. It can be seen that the trends are well-matched out to and beyond the peak pressures. The pressure predictions decrease at a faster rate than the measurements further out on the time axis. The exact reason for this behavior has not been identified. Better information on the size of the bypass valve ports and pressure reducer orifice plates would be necessary before a detailed assessment could be made.

Comparisons of model predictions to the "A" steam line pressure measurements at both the steam flow element and turbine inlet are made in Figures 3.8, 3.9, 3.16, 3.17, 3.14 and 3.25. The dynamics of the steam lines is well simulated. Although not attempted here, other investigators have modeled the instrument sensor lines and matched the higher frequency component in the data [15].

The question of convergence must be addressed in any simulation. What is meant here by convergence is the effect on the numerical results of the number of discrete regions used to represent the distributed system

and the time step scheme chosen. The turbine trip without bypass work (Appendix A, Section 4) demonstrates the adequacy of the six volume steam line model and the fuel rod radial nodalization used for these simulations. The only nodalization question left is that of the core region.

To evaluate the twelve volume model of the active core region, the turbine trip two test was simulated with a twenty-four volume model, and the results compared. The figures of merit chosen in this comparison - and the one below - are the peak neutron flux and the peak rise in steam dome pressure. The twenty-four volume model results agreed with those of the twelve volume model to within 0.5%.

The adequacy of the time step scheme chosen was investigated by simulating the turbine trip two test with a scheme utilizing a maximum time step size of one half the original scheme. The results agreed to within 0.7%.

In summary, the nodalization and time step scheme used in the test simulations yield a converged solution.

3.1.3 Conclusions

The close agreement between the model predictions and the data provide a sound basis of confidence for modeling assumptions that are otherwise difficult to evaluate given the current state of the art. In the simulations performed, the following modeling areas exhibited sound predictive capabilities:

i. the reactor power calculation,

ii. the steam dome and upper downcomer model,

iii. the steam separator model, as it effects the neutron power through core exit flow rate,

iv. the steam line model, and

v. the core thermal-hydraulics modeling, as it affects the core power calculation.

The fact that all three test simulations successfully employed the same modeling techniques, but used different inputs (e.g., reactivity data, mass inventories in separator and steam dome region, separator L/A, etc.) to account for varying initial conditions increases the confidence in the overall methods, including the supporting codes.

TABLE 3.1

Summary of Modifications Made to Hornyik and Naser Peach Bottom Model [15]

Modeling Area	Description
Core Heat Conductors	Heat conductor geometry and material properties were made consistent with the Vermont Yankee model. The modeling of the gap region was such as to yield a constant gap conductance value of 1000 Btu/hr-ft^2-^{o}F.
Core Junctions	Loss coefficients and the flow split between the active core and bypass region were based on FIBWR [8] calculations.
Core Power Calculations	The methodology described in Section 2.3.3 was used. Separate sets of feedback reactivity data were generated for each test [10].
Feedwater Flow	The feedwater flow rate was modeled as a constant flow. Differences between Vermont Yankee and Peach Bottom in the hardware (e.g., steam driven versus electric motor driven feedwater pumps) and a lack of information concerning the Peach Bottom system precluded a more detailed modeling. The effect of the above model on the parameters compared to in Section 3.1.2 is judged to be nil.
Separators and Stand Pipes	This area was renodalized to incorporate the separator model described in Section 2.4.4.
Steam Dome and Downcomer Region	This area was renodalized and made consistent with the modeling techniques described in Section 2.1.1.
Steam Lines	All junction and volume data were recalculated and made consistent with the Vermont Yankee model.

TABLE 3.2

Summary of Peach Bottom Unit 2 Model Initial Conditions

Parameter	Turbine Trip Test		
	TT 1	TT 2	TT 3
Core Thermal Power*[1] (MWth)	1562.0	2030.0	2275.0
Total Core Flow* (lbm/sec)	28140.0	23027.8	28140.0
Core Plate Pressure Differential (psi)	16.2	11.3	16.9
Bypass Flow (lbm/sec)	1647.2	1400.4	1801.7
Steam Flow (lbm/sec)	1576.0	2183.0	2461.0
Core Inlet Enthalpy (Btu/lbm)	525.7	518.1	521.7
Steam Dome Pressure* (psia)	991.3	976.3	986.6
Turbine Inlet Pressure (psia)	983.5	960.1	966.1
Carryunder Fraction	.001	.001	.001
Recirculation Flow* (lbm/sec)	9090.0	7680.0	9441.0

[1]Parameters based on test data [14] are indicated with an asterisk.

TABLE 3.3

Summary of Results
Peach Bottom Turbine Trip Tests

Parameter	Turbine Trip Test		
	TT 1	TT 2	TT 3
Neutron Flux[1]	Data/Calc.	Data/Calc.	Data/Calc.
Peak Flux	4.85/8.17	4.53/6.66	4.93/6.80
Time of Peak (sec)	0.80/0.80	0.72/0.74	0.70/0.71
Area Under Peak[2]	0.898/1.297	0.738/0.903	0.675/0.756
Steam Dome Pressure (psia)			
First Peak at 1 sec.	1024./1024.	1018./1018.	1034./1034.
Second Peak at 2 sec.	1030./1032.	1035./1040.	1054./1058.
Third Peak at 3 sec.	1030./1034.	1041./1050.	1061./1070.

1. Regarding the data, the neutron flux is defined as the average of the LPRM signals.

2. The area under the peak is the positive area bounded by the line flux = 1.0 and the flux trace.

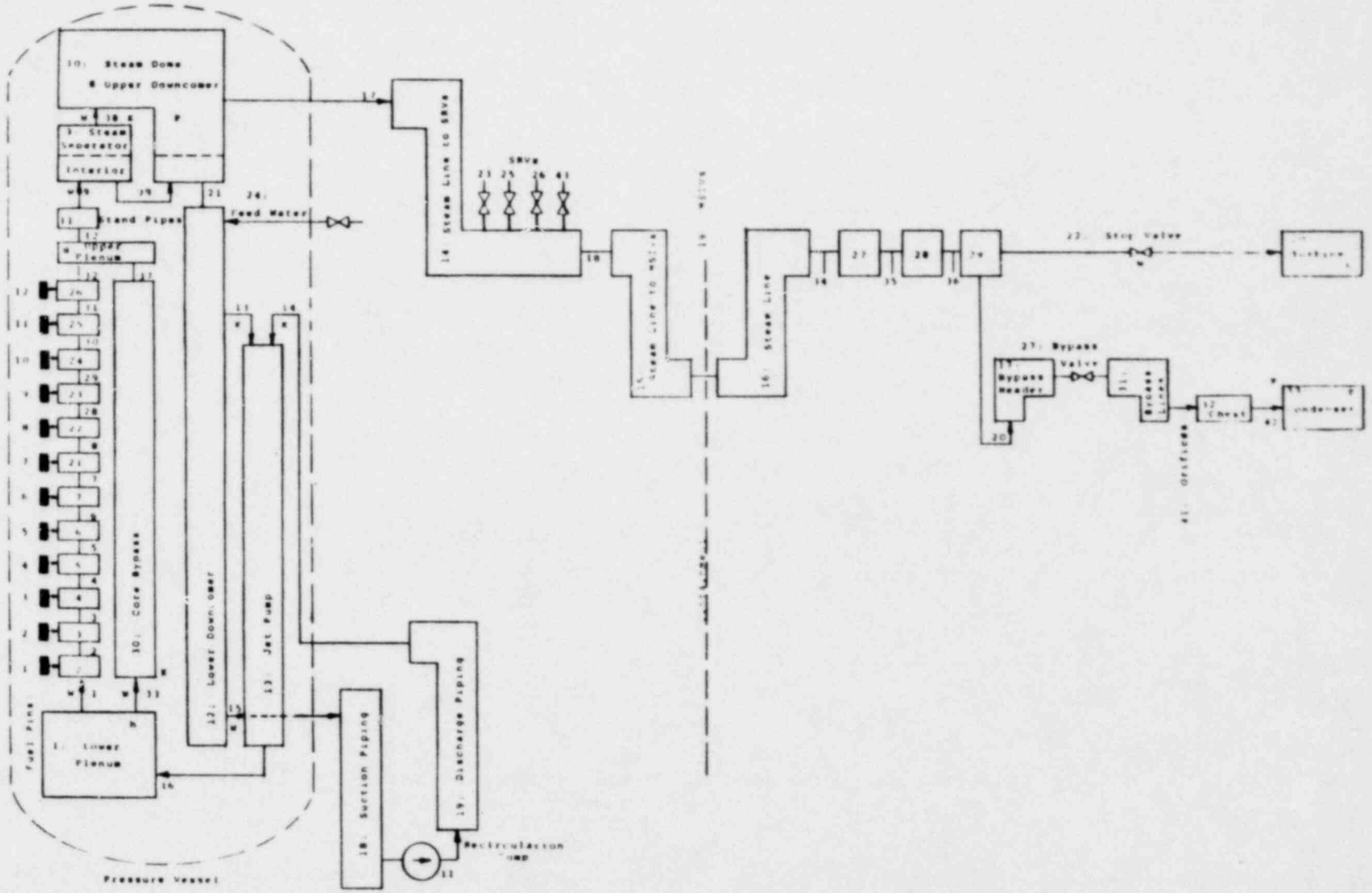

Figure 3.1 Peach Bottom - 2 RETRAN Model

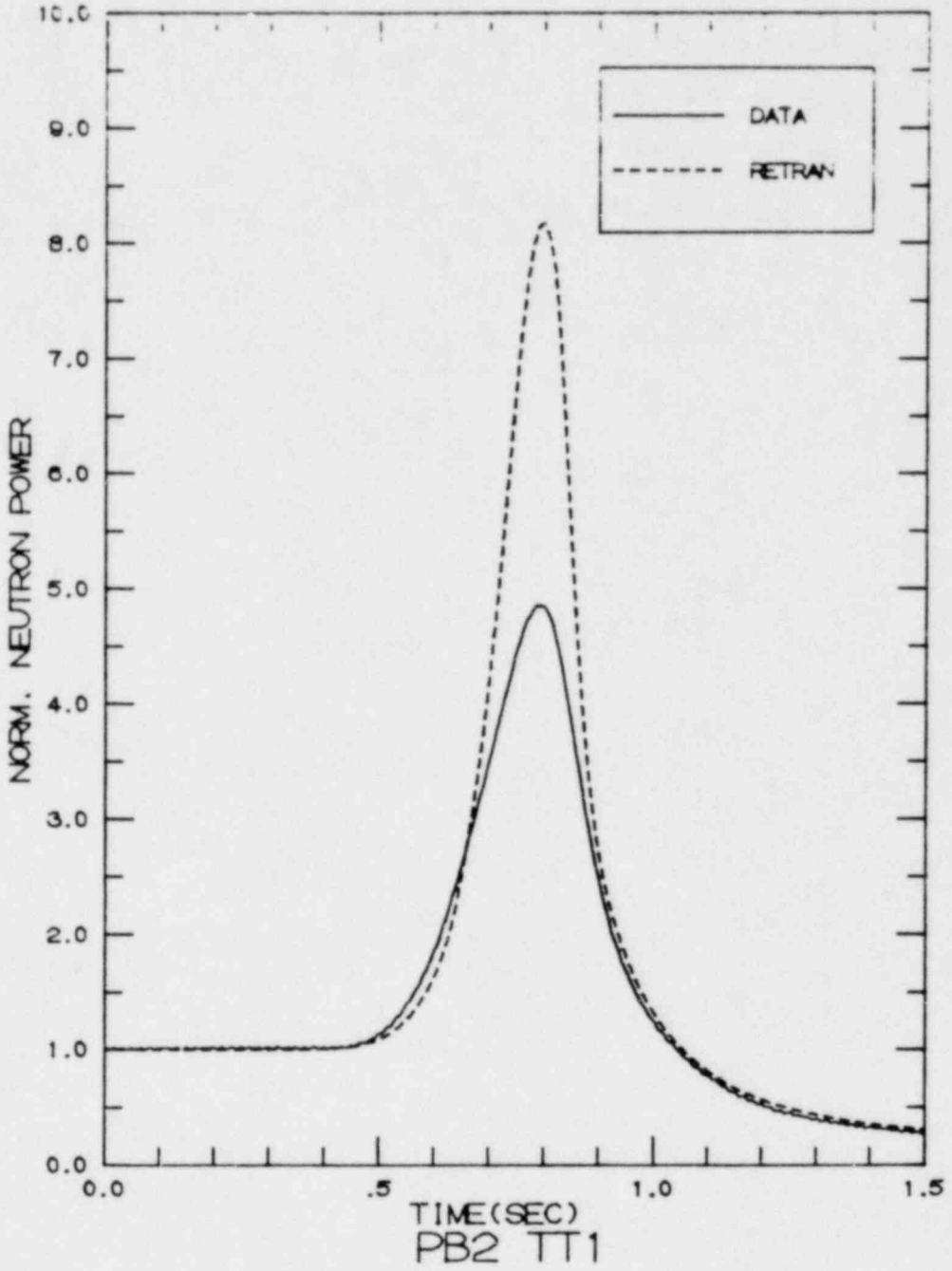

Figure 3.2 Peach Bottom-2 Turbine Trip Test 1
Neutron Power vs. Time

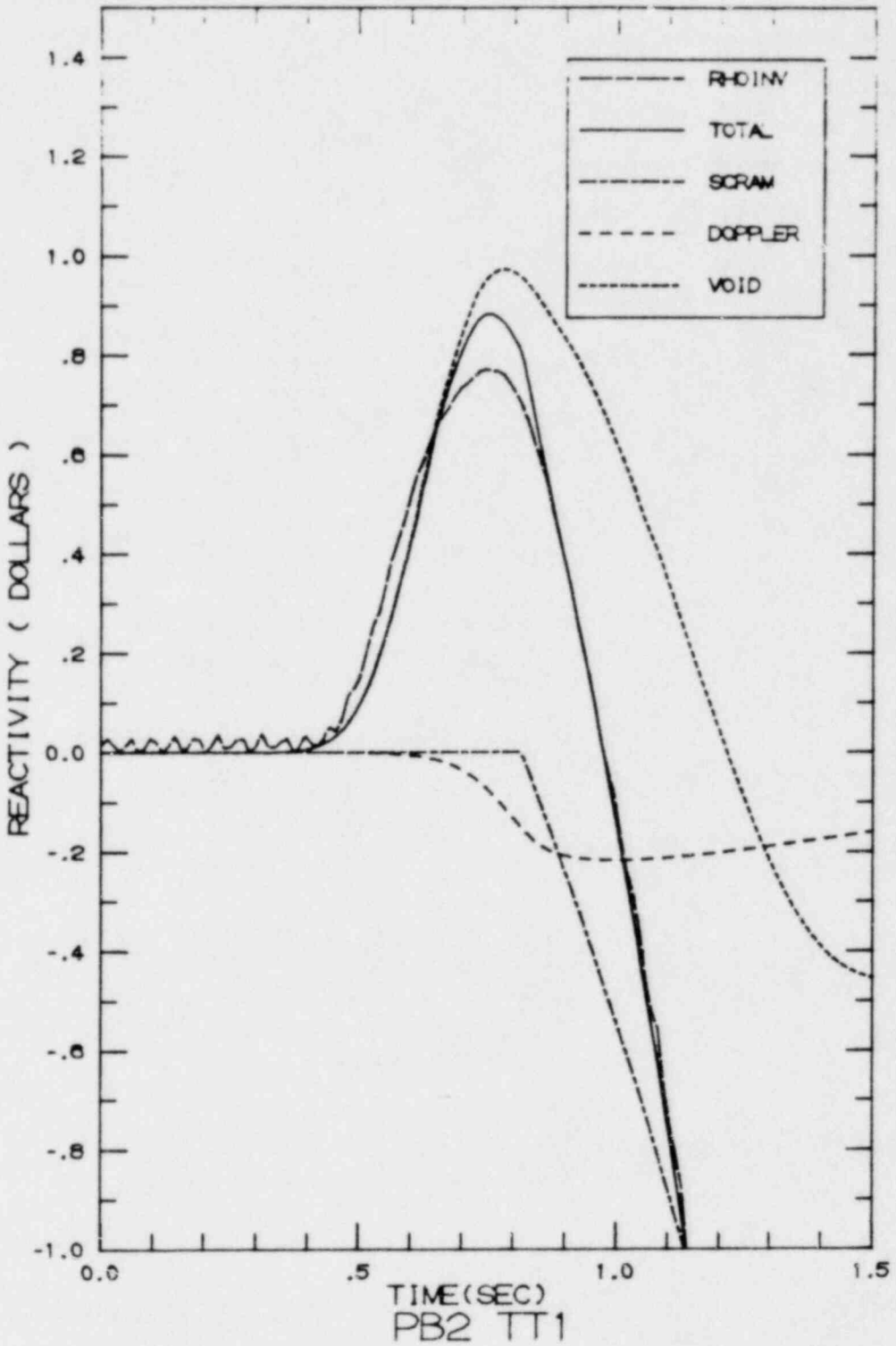

Figure 3.3 Peach Bottom-2 Turbine Trip Test 1
Total Reactivity and Reactivity Components vs. Time

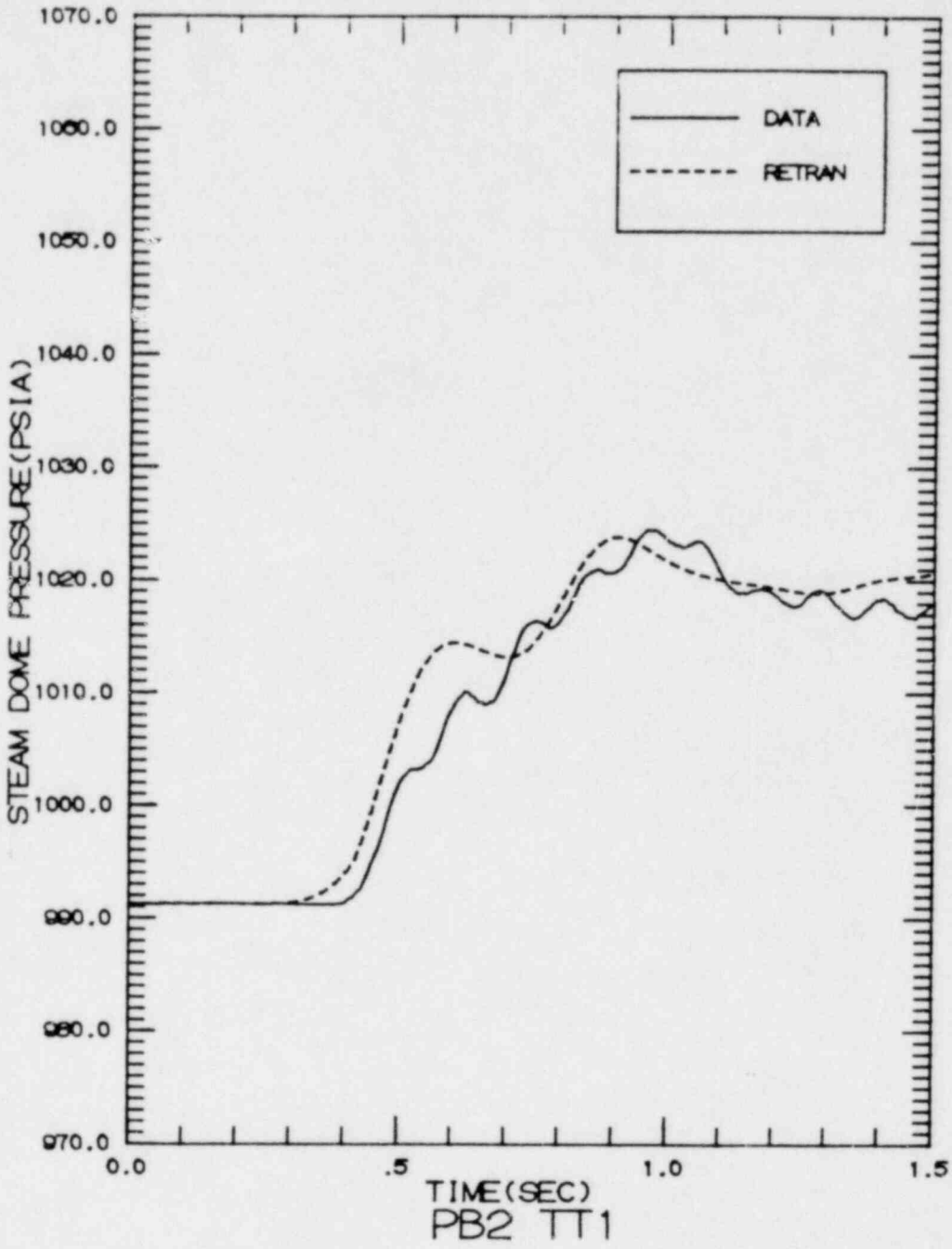

Figure 3.4 Peach Bottom-2 Turbine Trip Test 1
Steam Dome Pressure vs. Time (0.0-1.5 Sec.)

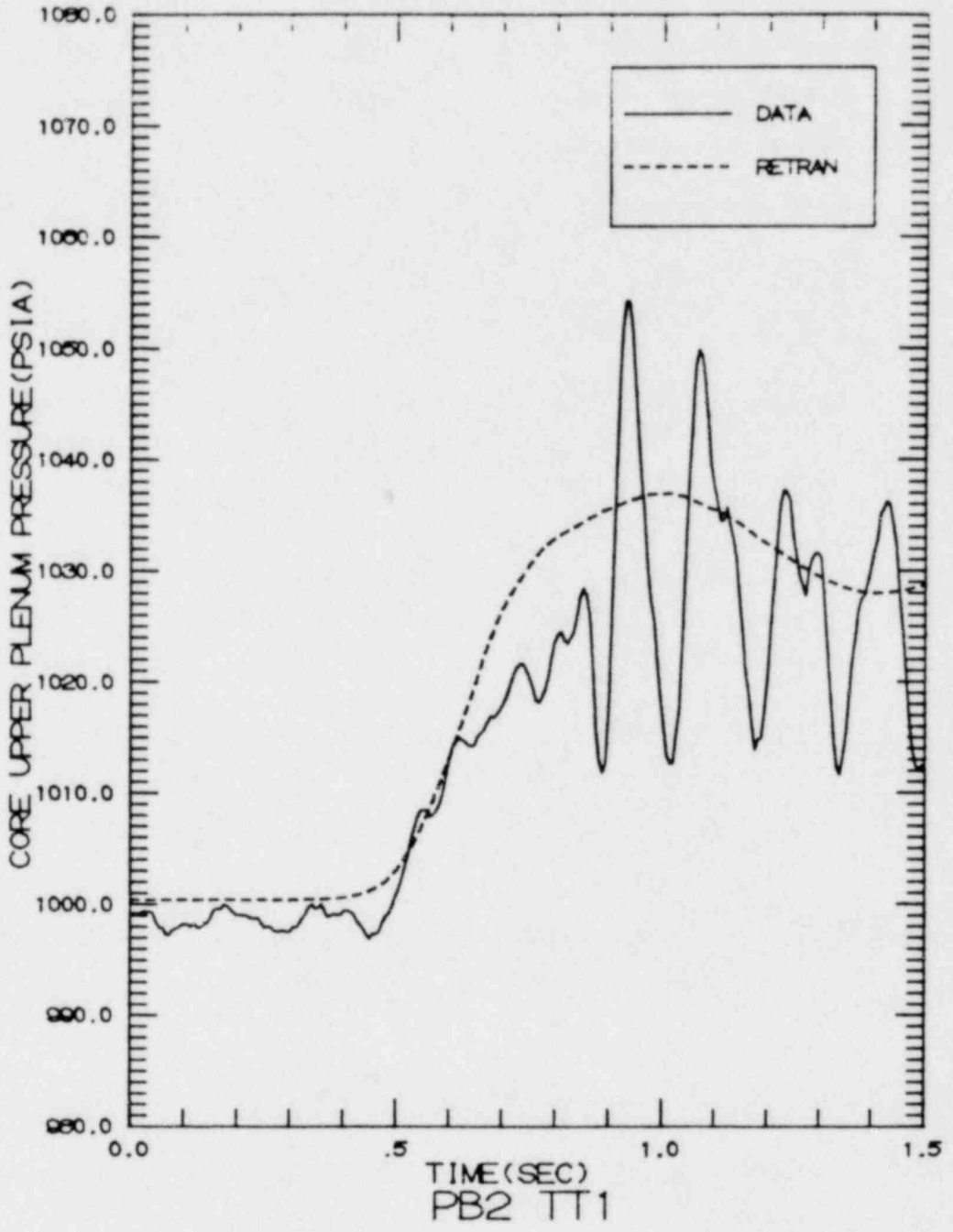

Figure 3.5 Peach Bottom-2 Turbine Trip Test 1
Core Upper Plenum Pressure vs. Time (0.0-1.5 Sec.)

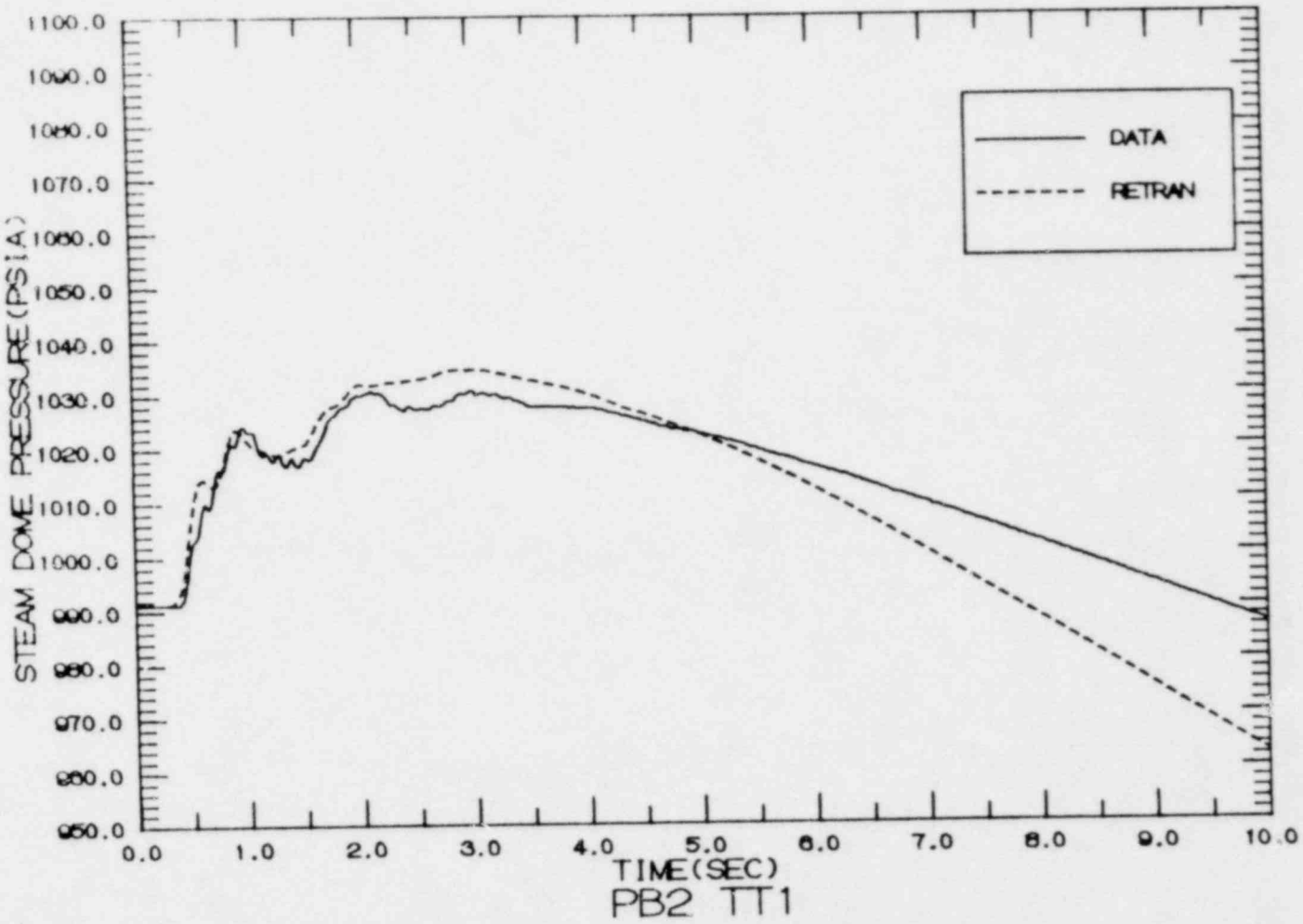

Figure 3.6 Peach Bottom-2 Turbine Trip Test 1
Steam Dome Pressure vs. Time (0.0-10.0 Sec.)

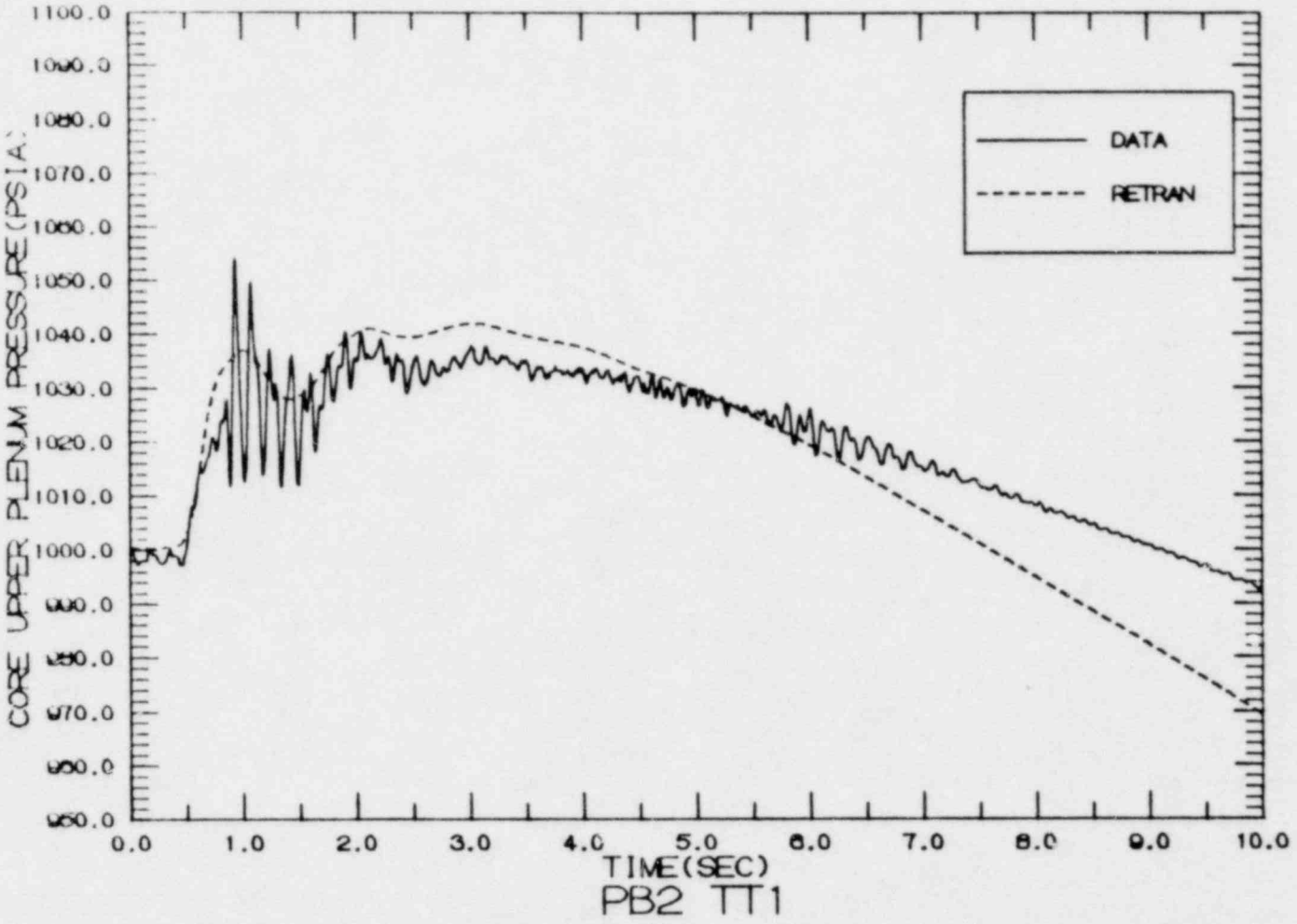

Figure 3.7 Peach Bottom-2 Turbine Trip Test 1
Core Upper Plenum Pressure vs. Time (0.0-10.0 Sec.)

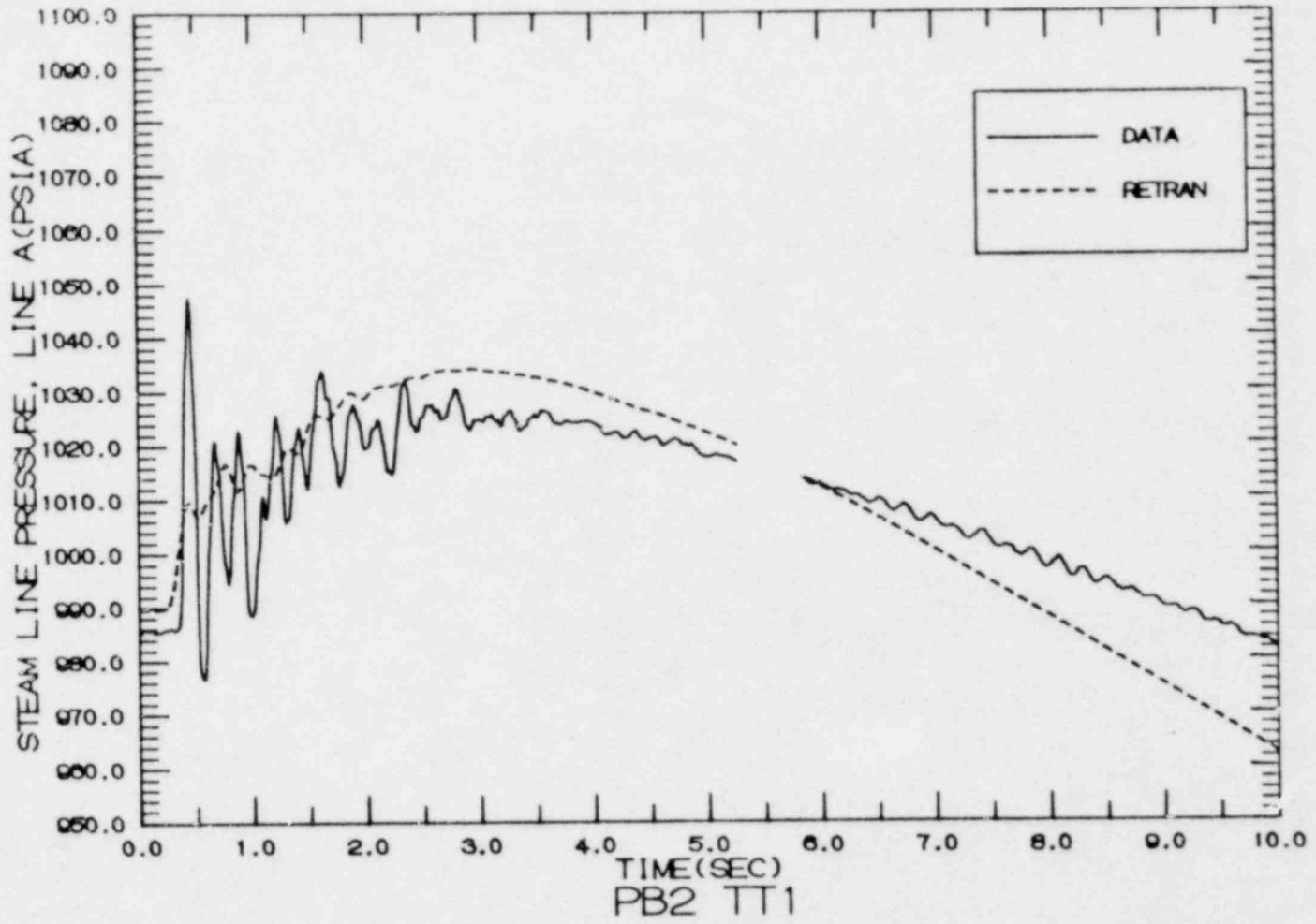

Figure 3.8 Peach Bottom-2 Turbine Trip Test 1
Steam Line A-Pressure at Flow Element vs. Time

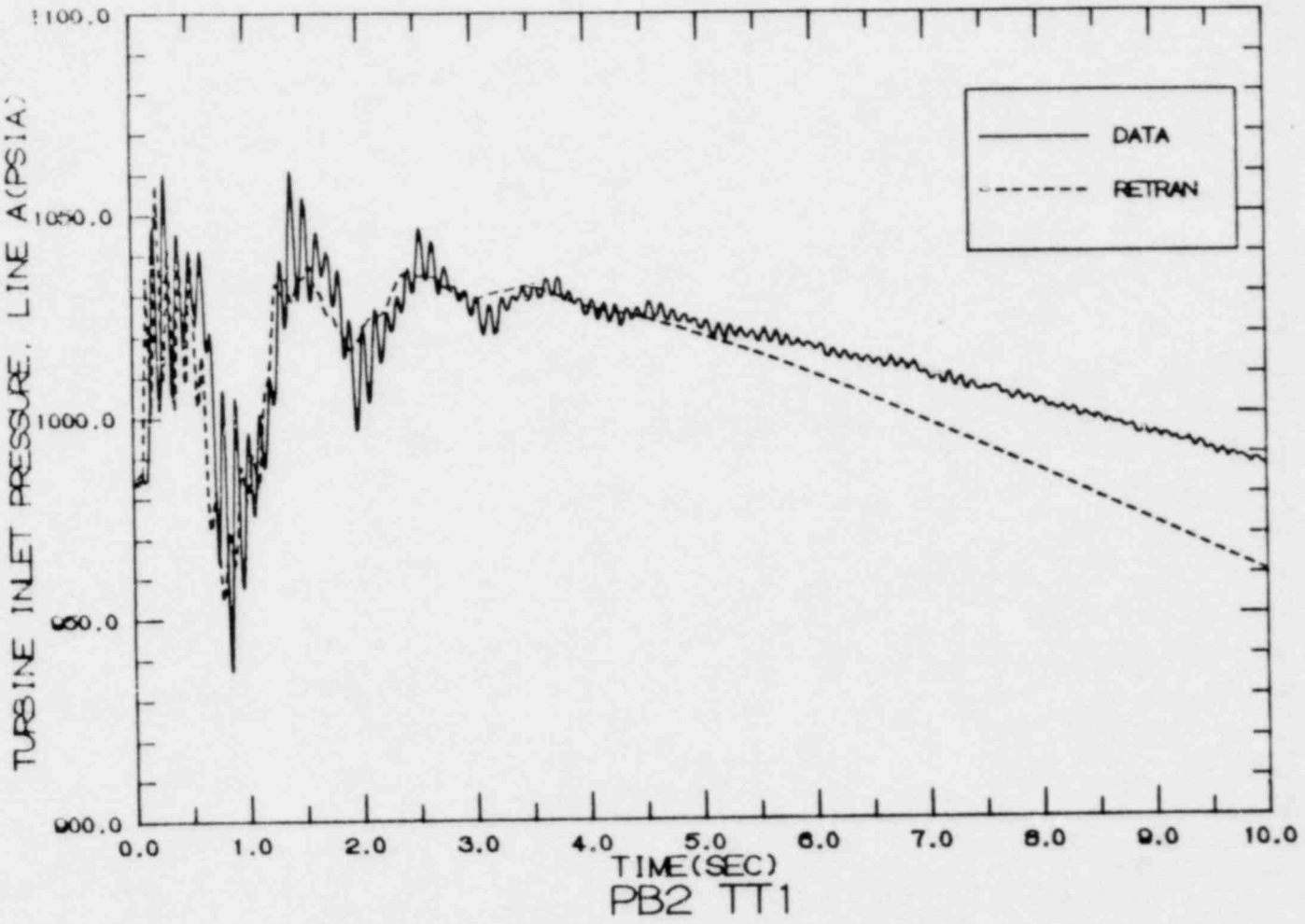

Figure 3.9 Peach Bottom-2 Turbine Trip Test 1
Steam Line A-Turbine Inlet Pressure vs. Time

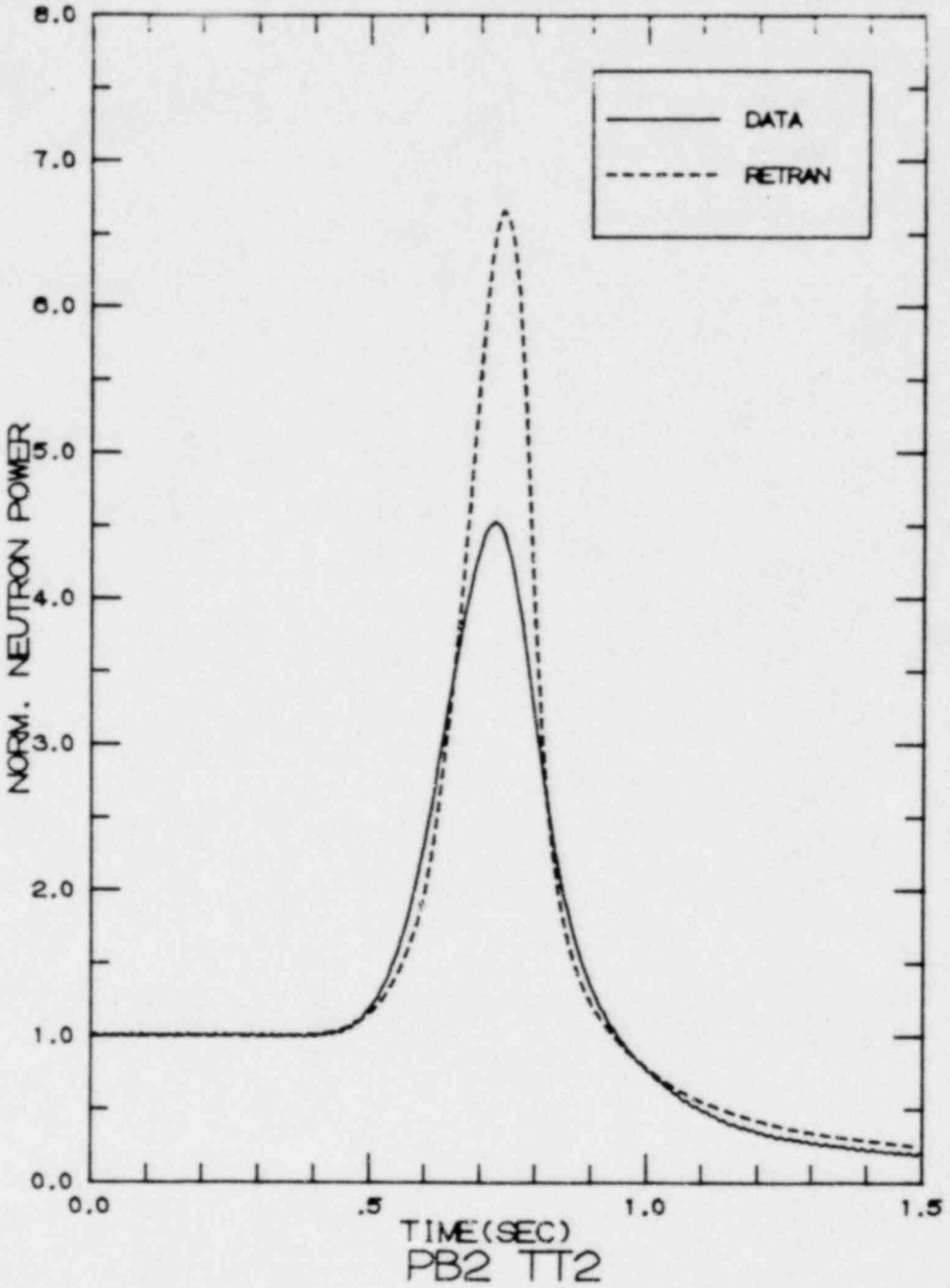

Figure 3.10 Peach Bottom-2 Turbine Trip Test 2
Neutron Power vs. Time

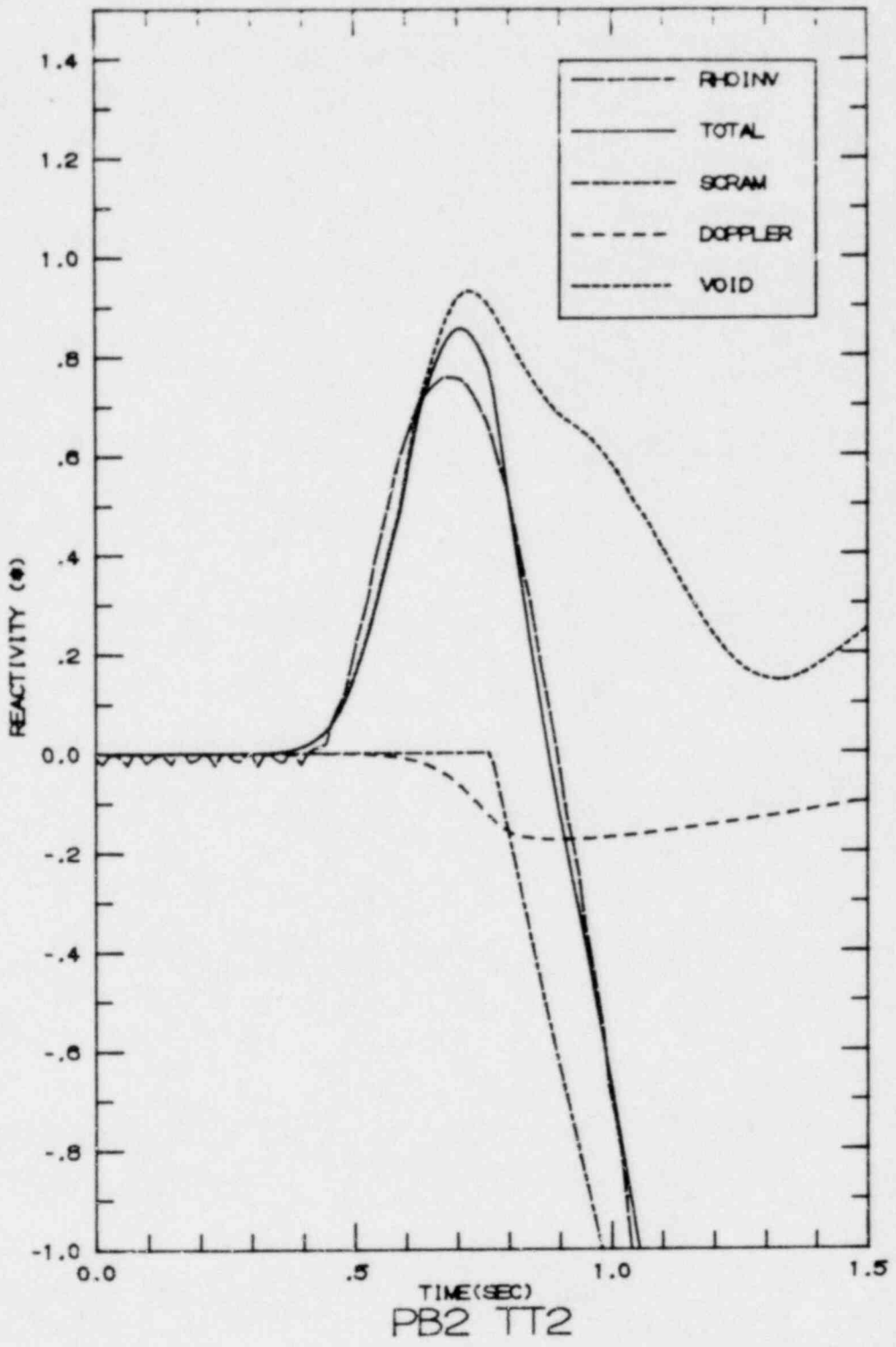

Figure 3.11 Peach Bottom-2 Turbine Trip Test 2
Total Reactivity and Reactivity Components vs. Time

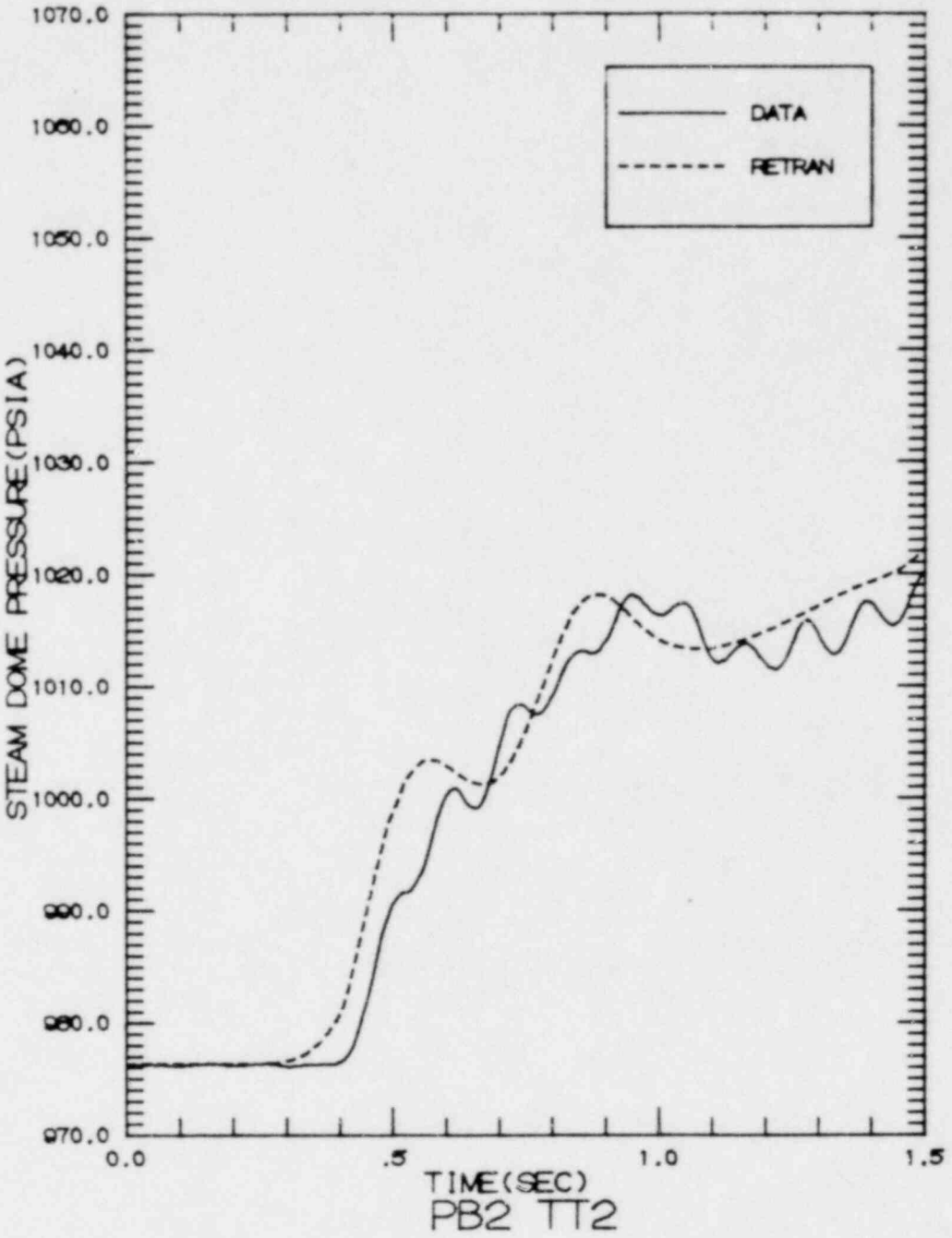

Figure 3.12 Peach Bottom-2 Turbine Trip Test 2
Steam Dome Pressure vs. Time (0.0-1.5 Sec.)

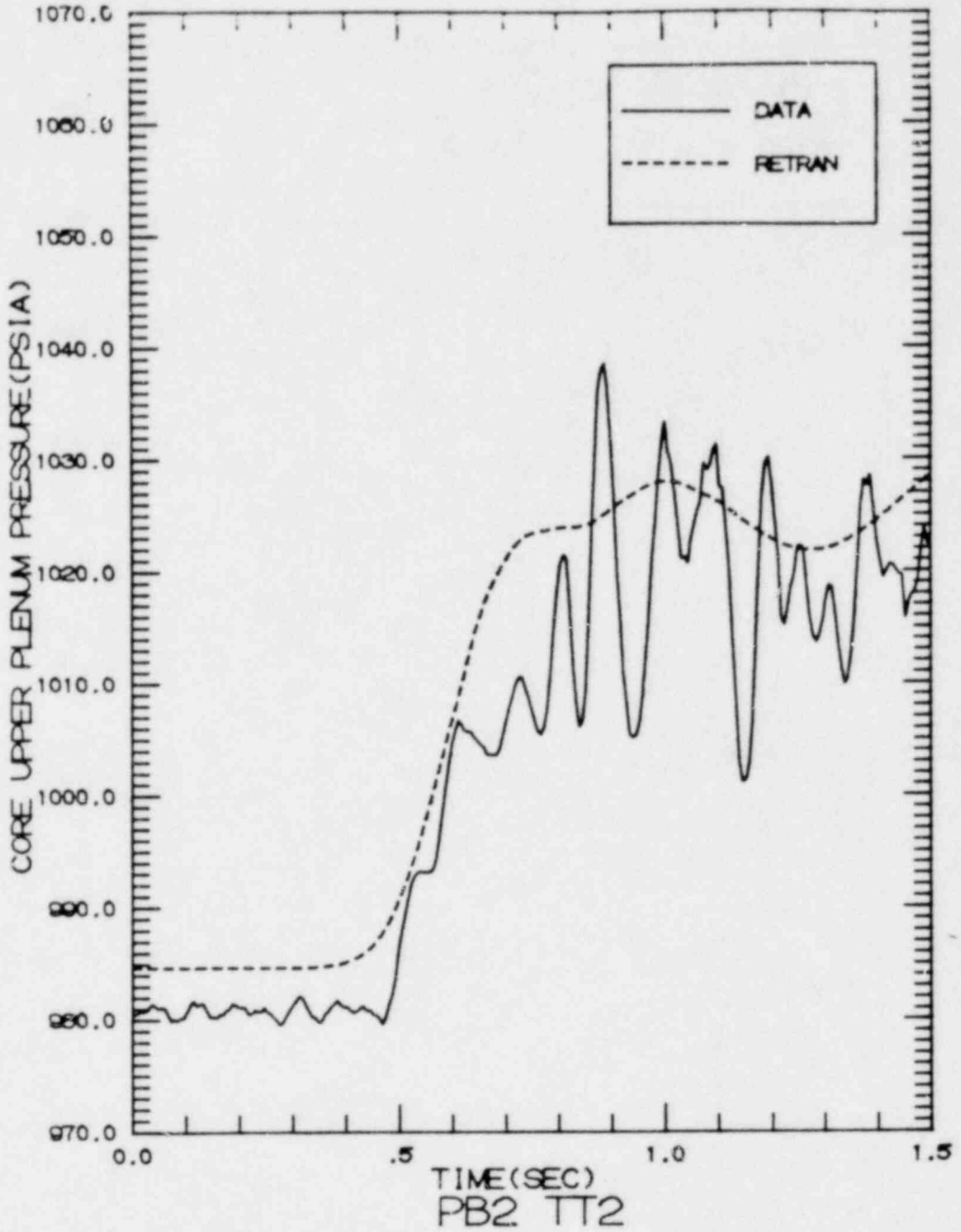

Figure 3.13 Peach Bottom-2 Turbine Trip Test 2
Core Upper Plenum Pressure vs. Time (0.0-1.5 Sec.)

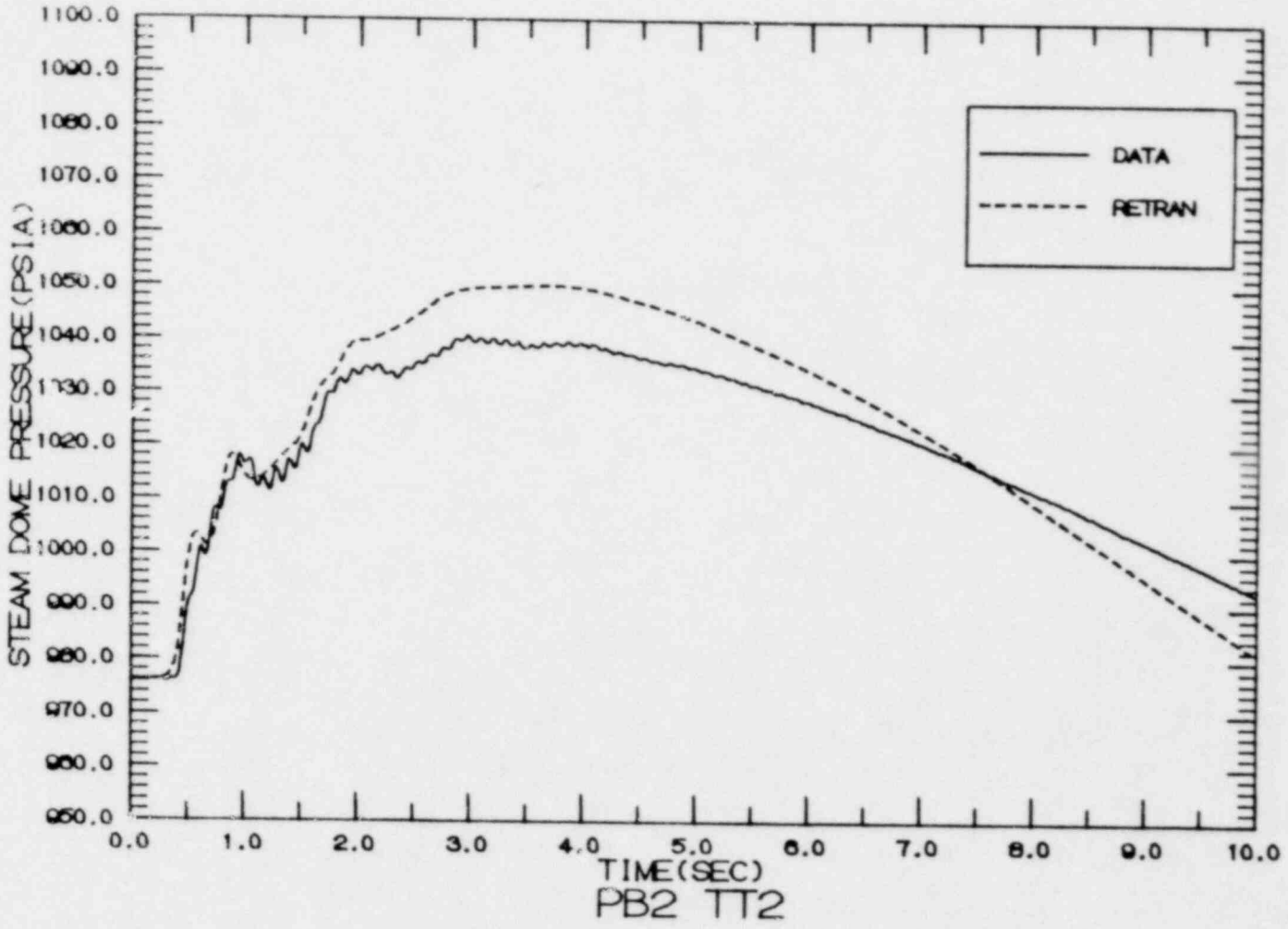

Figure 3.14 Peach Bottom-2 Turbine Trip Test 2
Steam Dome Pressure vs. Time (0.0-10.0 Sec.)

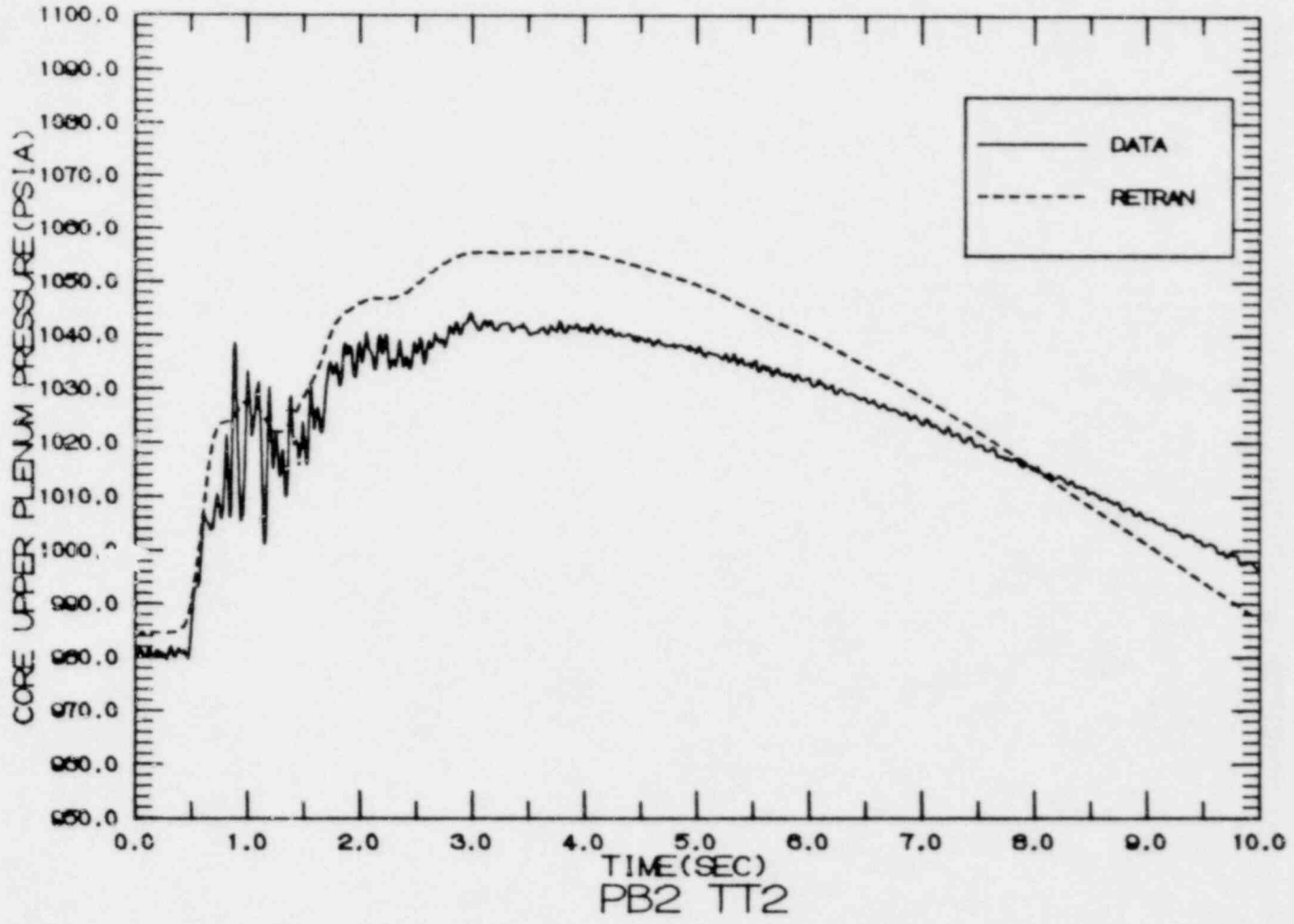

Figure 3.15 Peach Bottom-2 Turbine Trip Test 2
Core Upper Plenum Pressure vs. Time (0.0-10.0 Sec.)

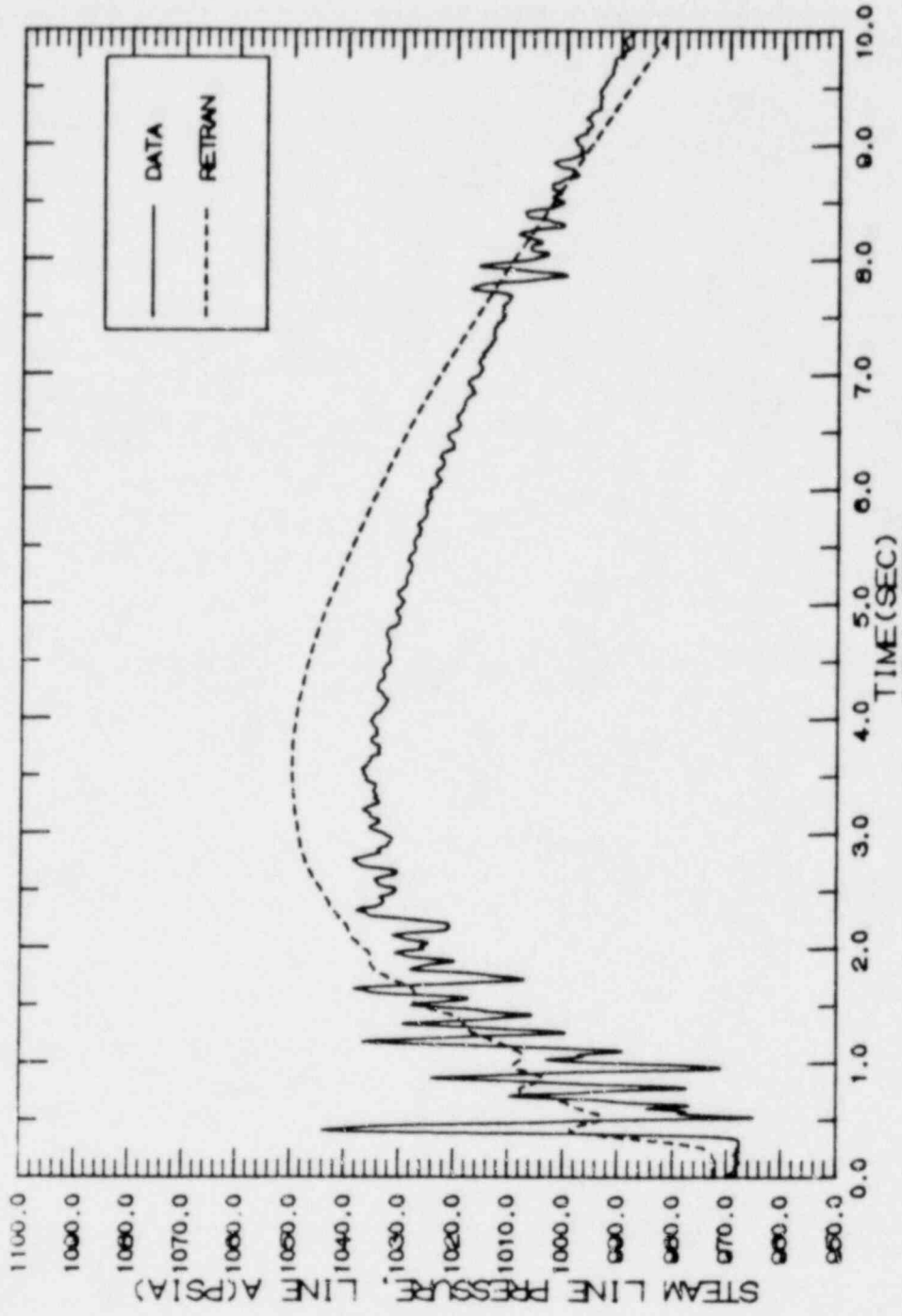

Figure 3.16 Peach Bottom-2 Turbine Trip Test 2
Steam Line A-Pressure at Flow Element vs. Time

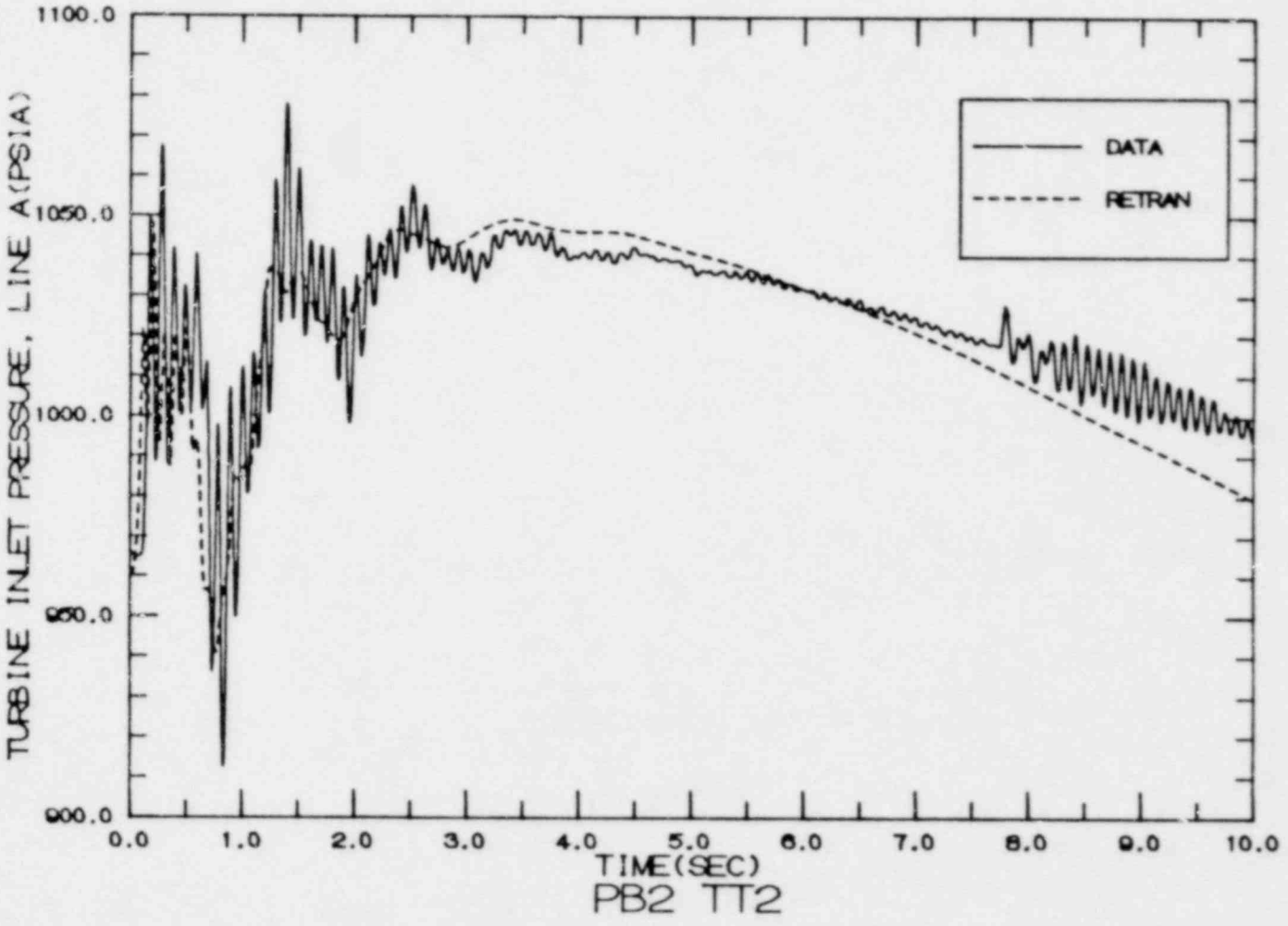

Figure 3.17 Peach Bottom-2 Turbine Trip Test 2
Steam Line A-Turbine Inlet Pressure vs. Time

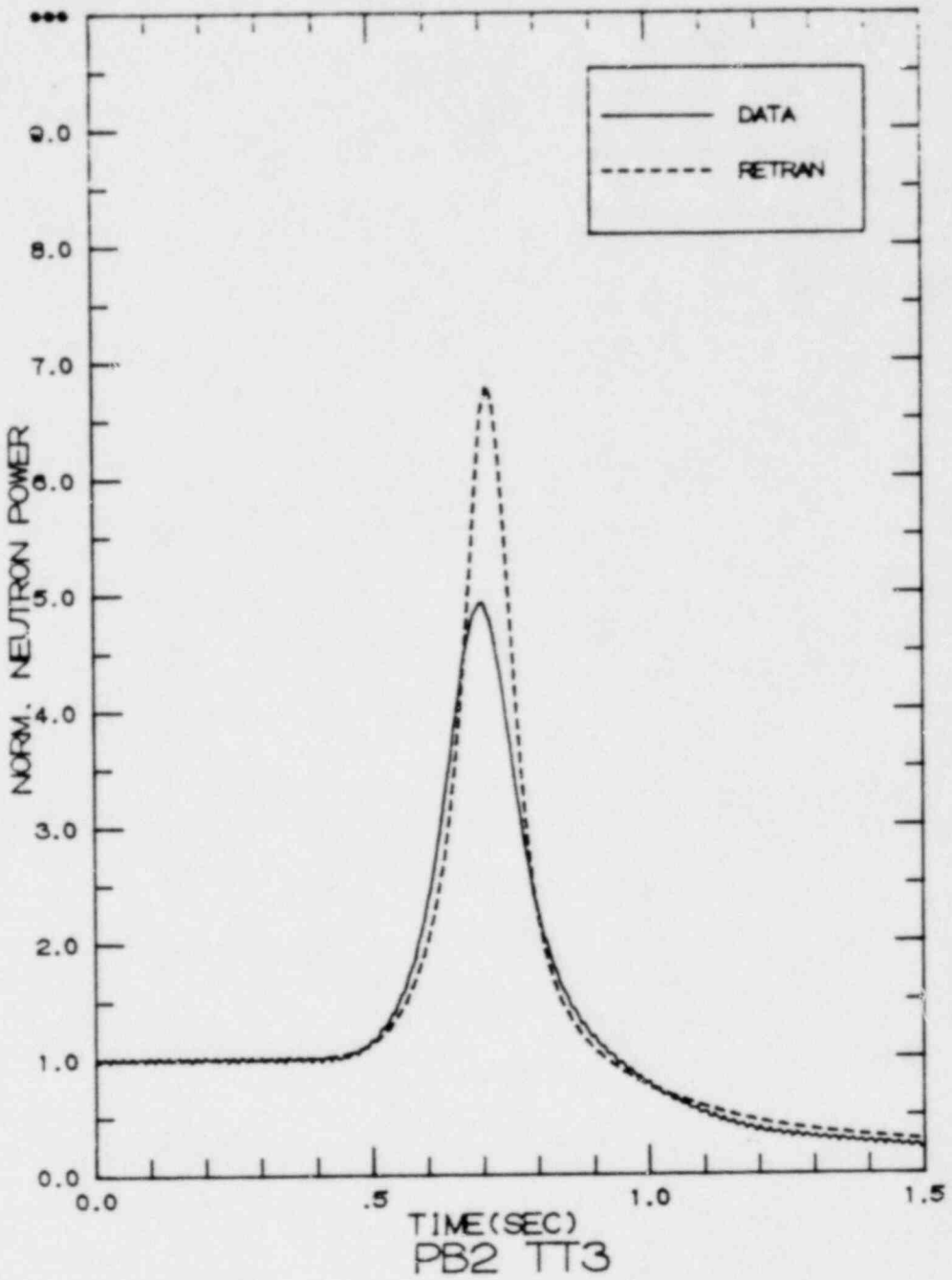

Figure 3.18 Peach Bottom-2 Turbine Trip Test 3
Neutron Power vs. Time

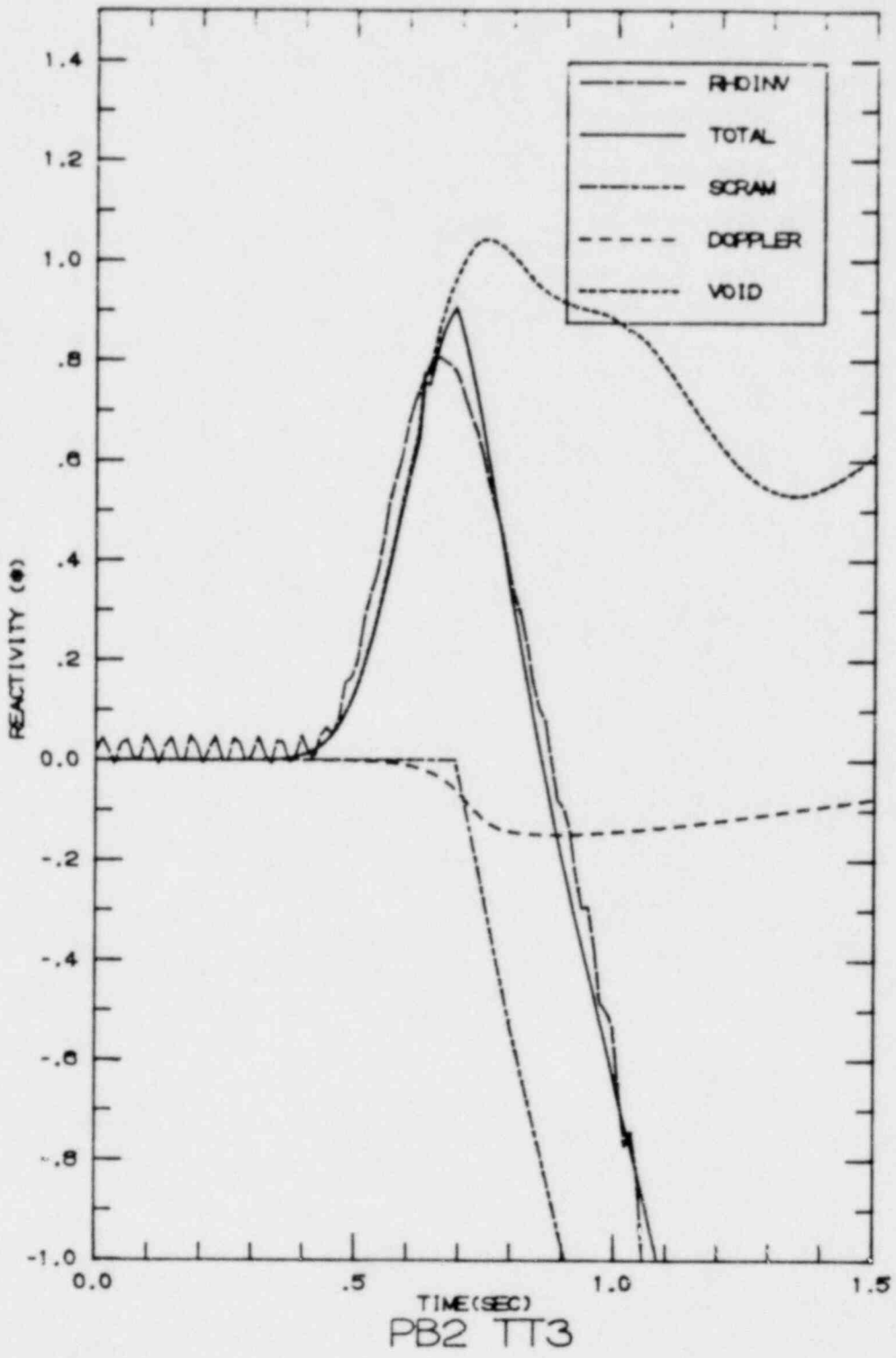

Figure 3.19 Peach Bottom-2 Turbine Trip Test 3
Total Reactivity and Reactivity Components vs. Time

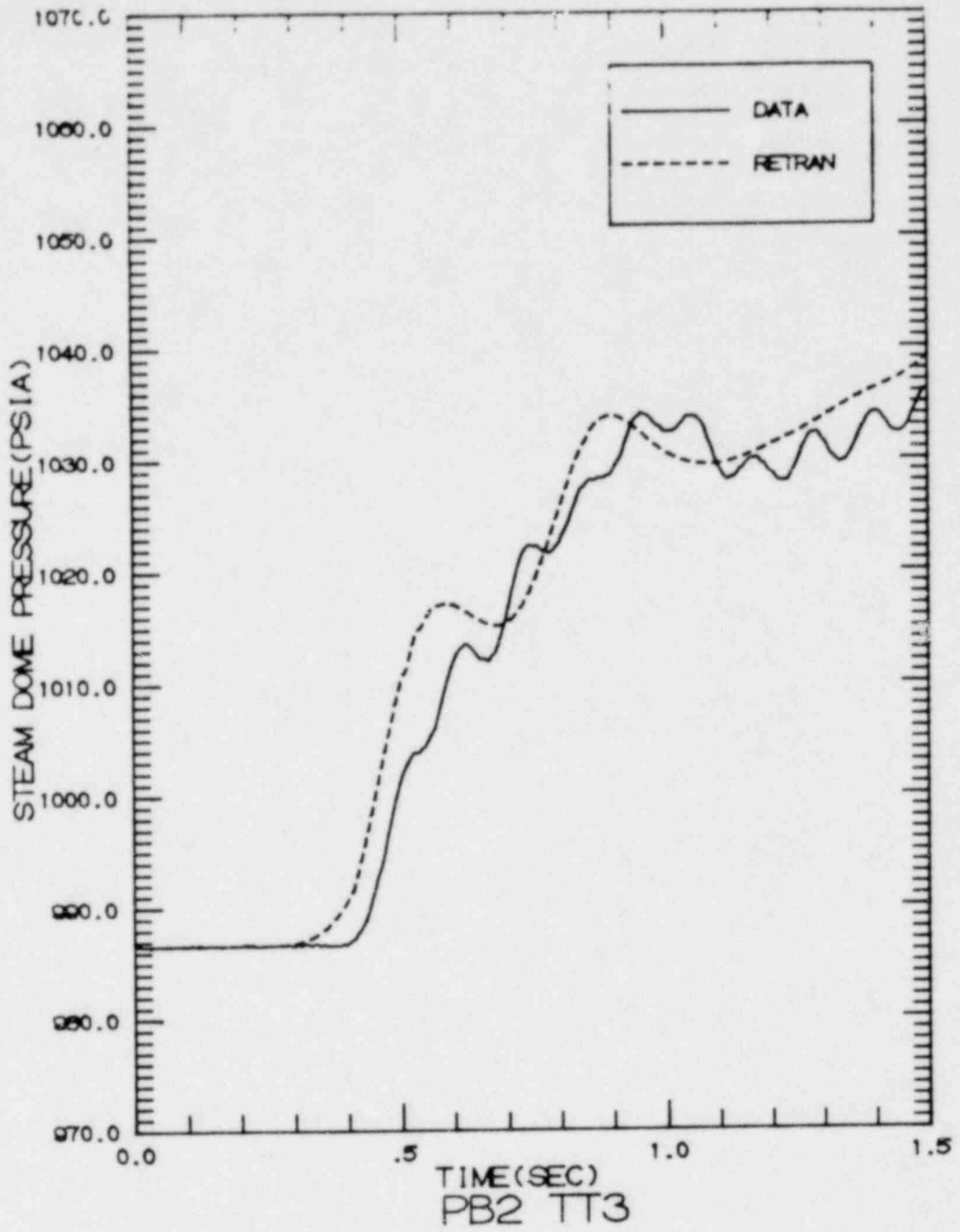

Figure 3.20 Peach Bottom-2 Turbine Trip Test 3
Steam Dome Pressure vs. Time (0.0-1.5 Sec.)

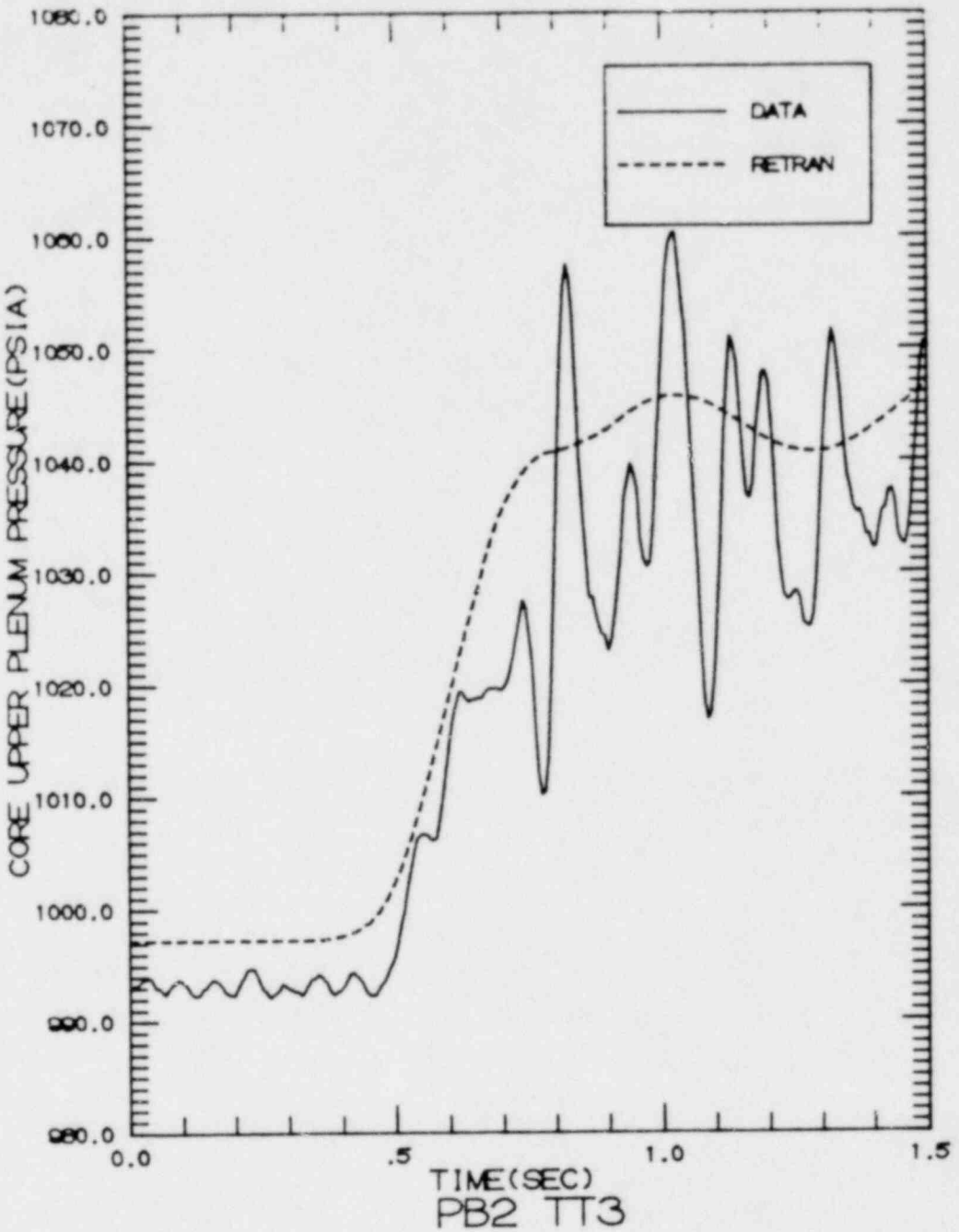

Figure 3.21 Peach Bottom-2 Turbine Trip Test 3
Core Upper Plenum Pressure vs. Time (0.0-1.5 Sec.)

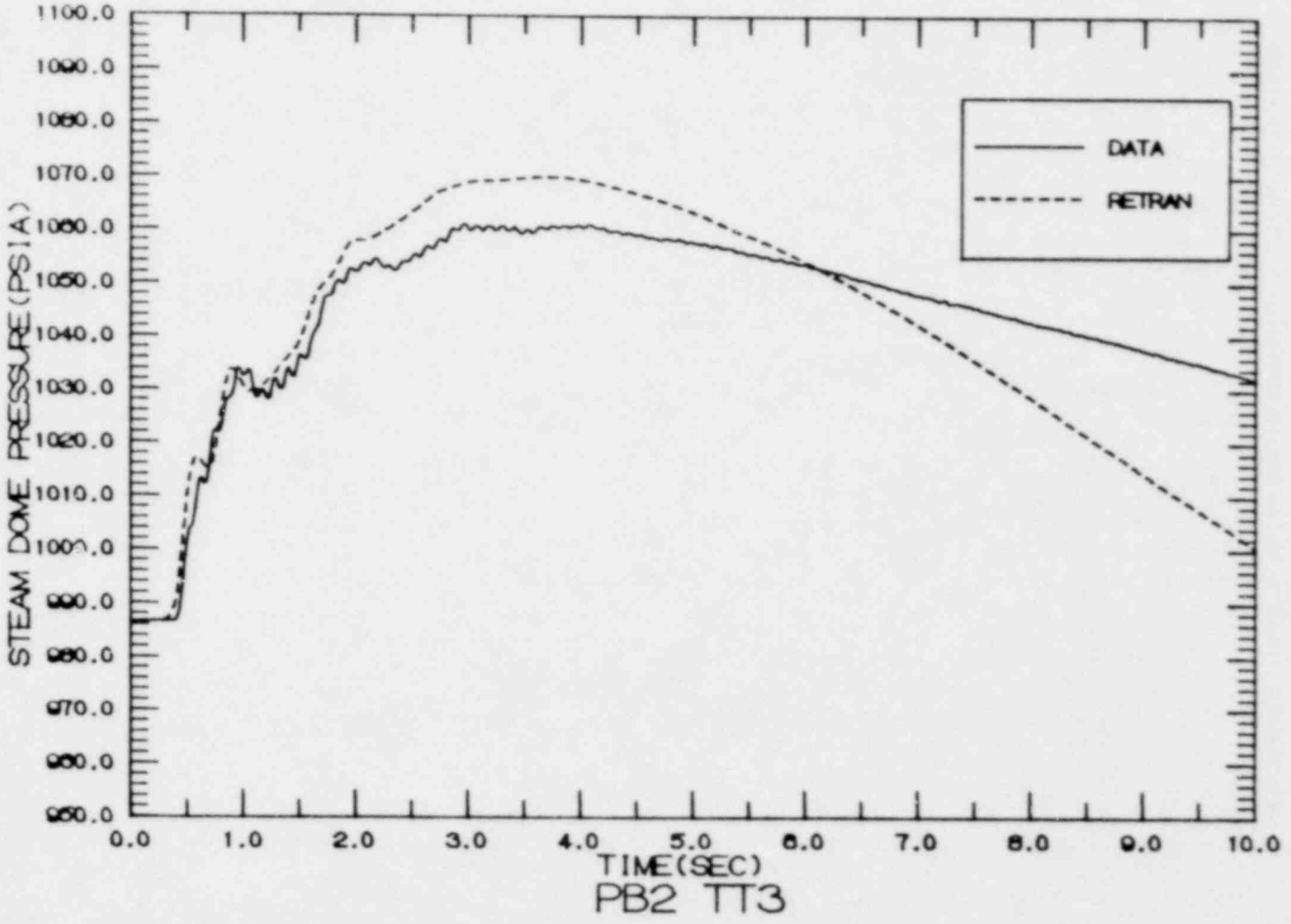

Figure 3.22 Peach Bottom-2 Turbine Trip Test 3
Steam Dome Pressure vs. Time (0.0-10.0 Sec.)

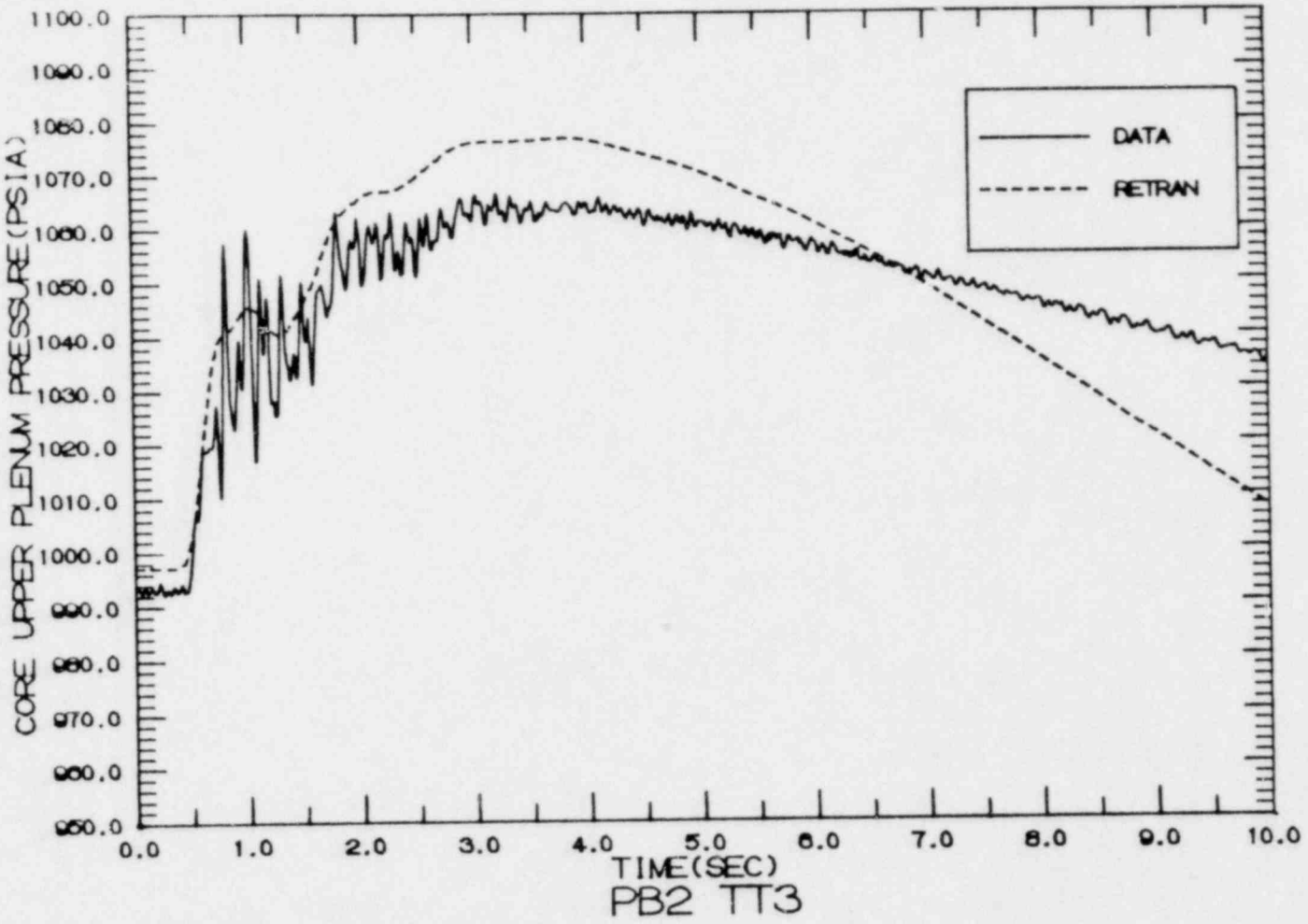

Figure 3.23 Peach Bottom-2 Turbine Trip Test 3
Core Upper Plenum Pressure vs. Time (0.0-10.0 Sec.)

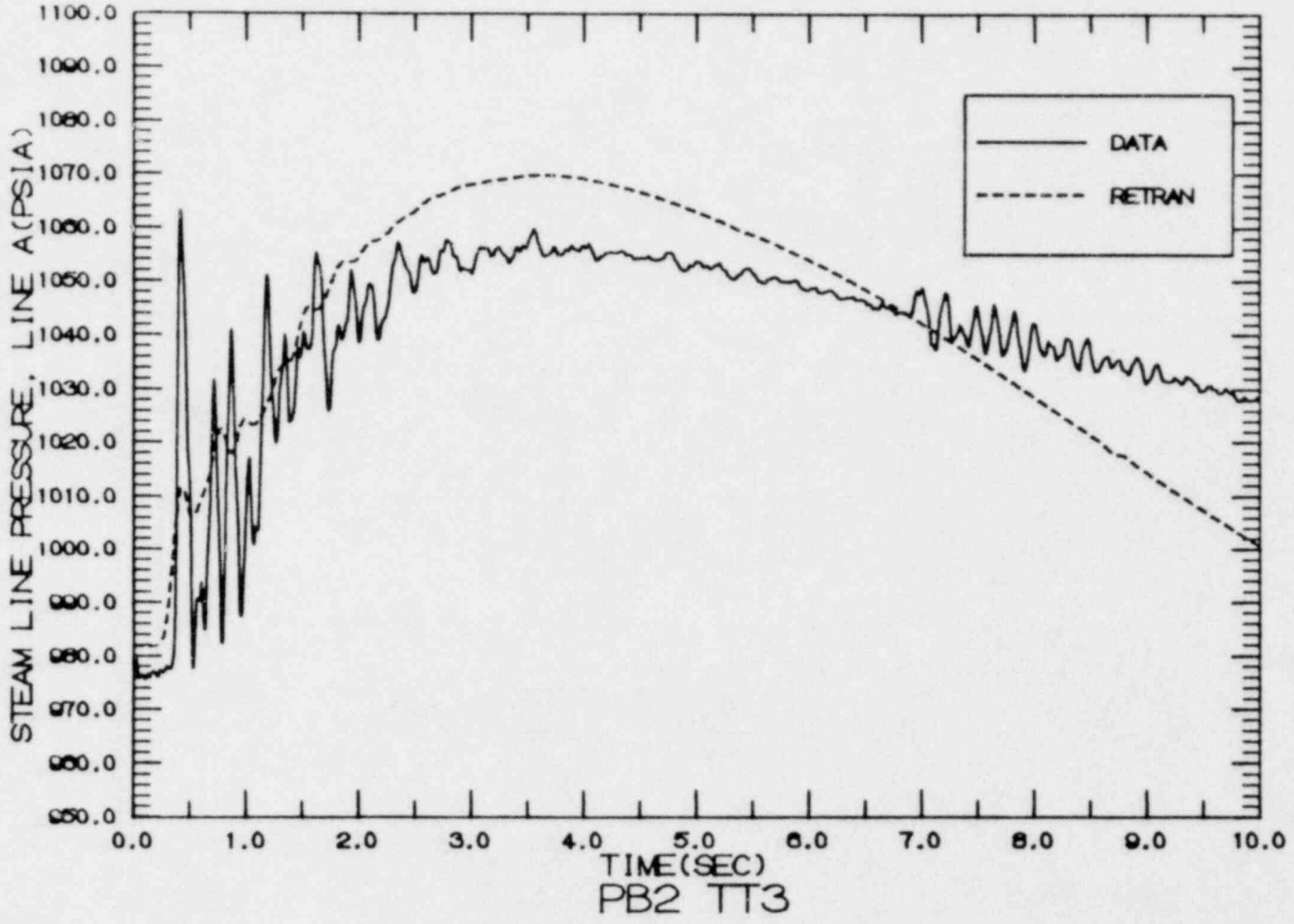

Figure 3.24 Peach Bottom-2 Turbine Trip Test 3
Steam Line A-Pressure at Flow Element vs. Time

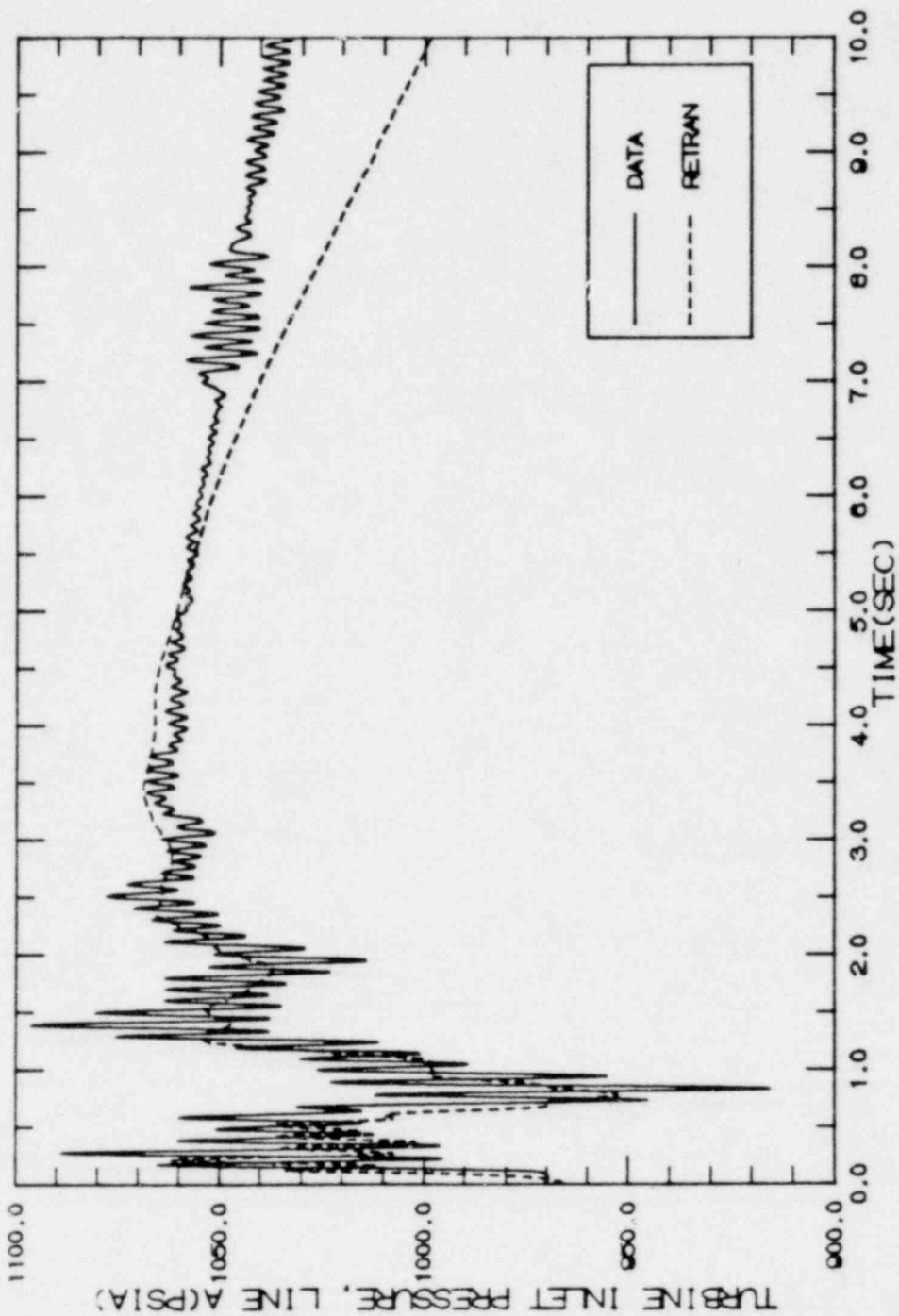

Figure 3.25 Peach Bottom-2 Turbine Trip Test 3
Steam Line A-Turbine Inlet Pressure vs. Time

APPENDIX

APPENDIX A

RETRAN TRANSIENT SIMULATIONS FOR VERMONT YANKEE

A.1.0 INTRODUCTION

The results presented in the following sections are for two specific Vermont Yankee startup test transients (a recirculation pump trip and a generator load rejection) and four operational transients (turbine trip without bypass, loss of feedwater heating, stuck-open relief valve and anticipated transient without scram) that were simulated to demonstrate the ability of the RETRAN model in predicting the course of such transients.

A.2.0 RECIRCULATION PUMP TRIP TEST

The purpose of this section is to document and describe the simulation of a single recirculation pump trip startup test. The test selected to be simulated was performed at Vermont Yankee Nuclear Power Station in February 1974 as part of the 100% power startup test program. The test basically consisted of tripping the Loop A recirculation pump by opening the generator field excitation breaker and taking data on a strip chart recorder until steady-state conditions were reached. Reactor initial conditions were 96% of rated power and 97% of rated core flow. It should be noted that the recirculation flow system was in the manual mode of operation. Hence, the Loop B recirculation pump operated at constant speed during the test. No unusual events occurred during the test.

A pump trip transient for a boiling water reactor results in a decrease in core flow. Due to the thermal inertia of the fuel, heat transfer to reactor coolant decreases at a slower rate than core flow. Core average

void fraction is primarily a function of core flow and energy transfer to the coolant. Since these two parameters decay at different rates, the core average void fraction goes through a maximum during the transient. The neutron flux level is primarily influenced by the void reactivity during this period of the transient. Hence, the neutron flux goes through a minimum during the transient.

The opening of the generator field excitation breaker results in the recirculation pump's motor being isolated from its power supply, a motor-generator set. The coastdown of the pump is governed by the mass moment of inertia of the pump and drive motor, the head-flow-speed and torque-flow-speed characteristics of the pump, and the hydraulic response of the system. As the drive flow of the coasting loop decreases, the total dynamic head developed by its pump decreases and, since the other pump continues to operate, at some point in time flow through the jet pump diffusers of the inactive pump reverses.

A.2.1 Geometric Description

The nodalization used for the simulation is the same as presented in Figure 2.1 with the following exceptions: the steam line and active core region are represented by three volumes as opposed to six and twelve; and a hot channel is explicitly represented.

A.2.2 Modeling Techniques/Option

Brief descriptions of the more important aspects of the model are given below.

A.2.2.1 Core Region

The core region is modeled with seven volumes: three axial volumes for the hot channel; three axial volumes for the average core; and one volume for the core bypass region. The fuel is modeled as a conductor with internal heat generation. Three heat conductors are used to model heat transfer from the average core region to the bypass region through the fuel channels. This energy path is ignored for the hot channel. Junction loss coefficients were developed from plant core pressure drop measurements and known loss coefficients for the inlet orifices. The Baroczy two-phase friction multiplier is used to calculate wall friction losses.

A.2.2.2 Recirculation System

Both loops of the recirculation system are modeled. The ten jet pumps per loop are modeled as a single volume. All loss coefficients associated with a loop with the exception of the jet pump suction and drive nozzles are calculated values. The recirculation pumps are modeled by overlaying available pump vendor data on the built-in curve. Rated values for the mass moment of inertias of the pump and its drive motor are used. The motor generator set has not been modeled.

A.2.2.3 Downcomer Region

The downcomer is split into two volumes. The upper portion is modeled as a non-homogeneous volume (thermodynamic equilibrium between phase is assumed) with a large bubble separation velocity. The bottom portion of the downcomer is a homogeneous volume. Mixing of the subcooled feedwater and saturated liquid from the steam separators occurs in this volume.

A.2.2.4 Steam Separators

The steam separators are modeled as a non-homogeneous volume. A bubble gradient of 0.8 is used. Bubble separation velocity is calculated by the code during the steady-state initialization. Inlet and steam outlet loss coefficients are based on NSSS vendor overall pressure drop data from prototype testing [3]. Junction effective inertias for the inlet and steam outlet are based on physical dimensions. The effective inertia for the liquid outlet is taken from a previous analysis [11].

A.2.2.5 Kinetics

(This modeling is substantially different than that described in Section 2.3.3.)

The point reactor kinetics option of the code is utilized. Void and Doppler reactivity data for this analysis are based on vendor supplied curves [12]. Power squared weighting of the reactivity data is used. In this analysis, all heat is assumed to be transferred through the fuel (i.e., no direct moderator heating).

A.2.2.6 Initialization

The steady-state initialization option is used. The pressure and quality in the core upper plenum (volume 1) is specified. The feedwater junction enthalpy is allowed to be biased to satisfy the heat balance.

A.2.3 Calculations and Results

A.2.3.1 Initial Conditions

Initial conditions for the test were 96% of rated power and 97% of rated core flow. The RETRAN simulation is based on 100% rated conditions. Hence, comparisons to test results are made on a normalized basis.

A.2.3.2 Loop A Drive Flow

A comparison of the Loop A recirculation pump mass flow rate as predicted by RETRAN with the measured test data is presented in Figure A.2.1. The RETRAN prediction is below the data for approximately the first four seconds. This behavior is expected since the field breaker trip is simulated as an instantaneous cutoff of line current to the pump motor while, in actuality, the line current decays over a finite period of time. From the test data, it is seen that the flow does not start to decrease until about one second after the initiation of the trip. At about four seconds into the simultation, RETRAN predicts a stepwise increase in drive flow which is not shown in the data. Just prior to this time, flow reverses through the Loop A jet pump suction nozzle and shortly thereafter flow reverses through the Loop A jet pump diffuser. The magnitude of the rate at which the reverse suction flow increases is very high (Figure A.2.7). It appears that this discontinuity in jet pump suction reverse flow rate is the cause of the drive flow increase. The exact time at which reverse flow occurs in the test is not certain. From the drive flow data, reverse flow appears to occur at five seconds. The earlier prediction of reverse flow by RETRAN is consistent with the assumption of an instantaneous cutoff of line current to the pump motor. Further out in time, the RETRAN prediction is above

the data. The exact reason for this overprediction has not yet been determined. It could well be attributed to inaccuracies in scaling test data from the strip chart.

A.2.3.3 Core Flow and Core Plate Differential Pressure

Figure A.2.2 shows a comparison of core flow as predicted by RETRAN to the test data. Core flow was calculated at the time of the test based on core plate differential pressure measurements. Figure A.2.3 shows the calculated versus measured response for core plate differential pressure. The agreement for both variables is fairly good during the first four seconds. RETRAN underpredicts the data once jet pump reverse flow occurs.

A.2.3.4 Steam Flow and Steam Dome Pressure

Figure A.2.4 is a comparison of the calculated and measured steam flow. The agreement is quite good in light of the fact that the pressure control system is not modeled.

Figure A.2.5 is a plot of measured versus calculated decrease in steam dome pressure. RETRAN predicted less of a decrease in steam dome pressure than was measured from four seconds to twenty-three seconds. Steam dome pressure response is extremely sensitive to the net mass flow rate of steam into the dome region. Hence, it is possible to get good agreement for core flow and steam flow and yet still not get good agreement for the pressure change response.

A.2.3.5 Core Power

Figure A.2.6 is a comparison of core power as predicted by RETRAN and Average Power Range Monitor (APRM) measurements. Unfortunately, the APRM recorder trace went off scale at 2.4 seconds into the test. Agreement looks reasonable during this initial portion of the test. RETRAN also predicted that the core power experienced a minimum during the test as is expected for this transient. The long-term power is below the measured data. This is largely attributed to modeling feedwater flow with a constant flow, constant enthalpy fill junction. In the long-term feedwater flow and enthalpy decrease due to reduced steam flow. If properly modeled, this behavior would tend to increase core power due to the increased core inlet subcooling.

A.2.4 Summary of Results

RETRAN predictions prior to reverse flow through the Loop A jet pumps agree reasonably well with the data. Examination of the predictions shows that a sudden increase in jet pump suction flow at the time of reversal led to a sudden increase in drive flow and an underprediction of core flow and core plate pressure differential from four to ten seconds. This behavior has since been traced to an improper discontinuity in the momentum mixing term associated with the jet pump model. This term has been properly formulated in the current model (Section 2).

A.2.5 Conclusions

The predicted results were in good agreement with measured results until jet pump flow reversal was predicted. It should be noted that this

problem is only of concern during a flow reversal in the jet pumps, which is not encountered in any of the following analyses. Until this problem is corrected, RETRAN will not be applied to problems in which significant recirculation flow asymmetries occur.

A.3.0 GENERATOR LOAD REJECTION TEST

This section documents and describes the simulation of a generator load rejection startup test. The test selected to be simulated was performed at Vermont Yankee Nuclear Power Station on March 29, 1974 as part of the 100% power startup test program. The plant conditions prior to the start of the test were as follows:

Reactor Power	93.7% (Rated = 1593 MWt)
Reactor Core Flow	98.5% (Rated = 48 x 10^6 lb/hr)

The recirculation pump speed control system was in the master manual mode. The sequence of events upon initiation of the test is given in Table A.3.1. A brief description of the test and the turbine control system response is given below. The reader is cautioned that the current plant protective response to a generator load rejection is different than the one described below which was in effect at the time of the test.

The test was initiated by tripping the generator output breakers, isolating the generator from the grid. The resultant loss of load caused the turbine generator system to overspeed with a rapid rate of acceleration. This acceleration was sensed by the acceleration relay in the turbine control system causing the following functions to occur:

1. Fast closure of the turbine control valves and opening of the bypass

valves (105% steam flow capacity).

2. The select rod insert feature is actuated, scramming a pre-selected group of control rods which provide sufficient negative reactivity to compensate for the positive reactivity added by the cold water which enters the vessel due to loss of feedwater heating.

3. A signal is generated which, after a thirty second delay, triggers the establishment of a new high flux scram point of 90% of full power.

The turbine control system functioned as expected during the test. A turbine trip occurred 38.5 seconds into the transient necessitating a manual reactor scram. The turbine trip was believed to be caused by a high reactor water level. It should be noted that the simulation is performed only for the first 27 seconds of the test. Hence, the turbine trip is not modeled.

Test data were taken on a slow speed strip chart recorder. Normal plant instrument sensors were used for measurements. The accuracy of this instrumentation is provided in Section 7 of the plant FSAR [1]. Test data used for comparisons in this report were obtained by manual scaling of the strip chart traces.

A.3.1 Geometric Description

The nodalization scheme used in this analysis was the same as shown in Figure 2.1 except that a two volume jet pump model was used instead of a one volume model, and the active core region and steam line each comprised three volumes instead of twelve and six.

A.3.2 Calculations and Results

Two analyses were performed. One in which the point kinetics option of the code was used to predict core power and the other in which the transient core power was input. The former analysis is referred to as the "base case" in this report. The simulation was run out to 27 seconds by which time the actual test measurements had reached steady-state.

A.3.2.1 Initial Conditions

Initial conditions for the test were 94% of rated power and 99% of rated flow. Since the RETRAN simulation is based on 100% rated conditions, most of the comparisons are made on a normalized basis. In cases where absolute results are compared, no biases have been applied. It is expected that the transient response of these variables would not be significantly affected by the slightly different initial conditions.

The steady-state initialization feature of the code was used to initialize the problem. The convergence criteria were relaxed to a maximum enthalpy error of .05 Btu/lb and a maximum junction acceleration pressure drop error of .0005 psi. The problem converged in 17 iterations with the largest enthalpy error being .0002 Btu/lb and the largest acceleration pressure drop error being 2×10^{-6} psi.

A.3.2.2 M-G Set Generator Speed

During a generator load rejection, the motor of a M-G set, which is part of the station auxiliary load, speeds up due to the increased speed and frequency of the main turbine-generator. The M-G set generator, which is coupled to the motor by a hydraulic drive, also initially speeds up.

However, the M-G set speed controller reacts to maintain the generator at the constant setpoint speed. As a result of these two competing effects, the generator speed goes through a maximum during the early portion of the transient.

A comparison of the M-G set generator speed as predicted by the model with the test data is presented in Figure A.3.1. The model slightly overpredicts the peak speed. However, the general agreement is quite good. It should be noted that the test data does not show a change in the M-G set generator speed for the first second, although the main turbine-generator is speeding up during this time. In order to model this phenomena, a one second delay block was placed between the function generator representing the transient main turbine generator frequency and the M-G set electrical motor torque logic.

A.3.2.3 Core Inlet Flow

Figure A.3.2 presents a comparison of the model prediction of core inlet flow to the test data. The initial rise and drop in the model prediction is due to the rise and drop in steam dome pressure predicted at this time. The abrupt change in slope at about one second is where the pump begins to speed up, following the M-G set generator. The model slightly underpredicts the peak core flow. The overall agreement is quite good. The anomalies in the core flow prediction occurring at approximately 13 seconds and 26 seconds are due to a numerical problem associated with the small volumes representing the throat section of the jet pumps. (This problem has been eliminated in the current version of the Vermont Yankee model.)

A.3.3.4 Core Power

Figure A.3.3 presents the core neutron power prediction to the test APRM measurement. The model initially predicts a slight rise in power due to an initial increase in steam dome pressure. The start of the select rod insert at 0.4 seconds caused the rapid decrease in neutron population. The rise in core power at 1.0 seconds is due to the increasing core flow. The local maximum at about 3.3 seconds corresponds to the peak core flow prediction. The model overpredicts the neutron power from this point on with agreement improving as the transient steadies out. There are too many unknowns associated with the input reactor kinetics data to really make a conclusive explanation about the discrepancies between the test data and the model prediction. (The Void and Doppler reactivity data used for this analysis was taken from the reactor vendor core design report.) In order to get a feeling for the validity of the input data, the RETRAN calculation of net reactivity was compared to the reactivity necessary to calculate the measured APRM trace. The latter was determined by solving the point kinetics equation for reactivity with the RHOINV computer code [10]. The comparison is shown in Figure A.3.4. The overall shape of the RHOINV curve is pretty well matched. It is seen that RETRAN overpredicts the initial reactivity decrease and subsequent rise. This is indicative of too much worth associated with the select rod insert reactivity and perhaps too negative a void coefficient.

A.3.3.5 Steam Dome Pressure

A comparison of the model prediction for steam dome pressure decrease with the test data is presented in Figure A.3.5. The model initially

predicts a slight rise in steam dome pressure and then slightly overpredicts the pressure decrease for the first 7 seconds. After this time, the model predicts a rise in steam dome pressure which is not reflected in the data. The overprediction in steam dome pressure is primarily due to the overprediction of core power during this portion of the simulation. (See Section A.3.3.9 for confirmation of this statement.)

A.3.3.6 Vessel Steam Flow

Figure A.3.6 presents the comparison of vessel steam flow as predicted by the model to the test data. Unfortunately, the strip chart trace is unintelligible after 11 seconds. During the first 2 seconds, the data shows two distinct local maximums and two distinct local minimums. The model predicts these, although the magnitudes are slightly off. Agreement during the first 8 seconds is reasonably good. At about 10 seconds into the simulation, the predicted steam flow has reached a minimum and begins to rise. The data at this point shows that steam flow is still decreasing. The reason for the discrepancy is the overprediction of core power during this time. (See Section A.3.3.9 for confirmation of this statement.)

A.3.3.7 Feedwater Flow

A comparison of the model prediction of feedwater flow to the test data is presented in Figure A.3.7. The feedwater flow initially rises due to the rapidly dropping sensed level response. The flat portion of the prediction is due to the modeling of a maximum feedwater flow of 115% rated flow. Although the test data shows normalized feedwater flow above 115%, the actual values were below 115% of rated flow. The overall agreement

is reasonable. The model slightly underpredicts the flow after approximately 10 seconds. This is probably, in part, due to the fact that the feedwater flow model does not take into account reactor pressure. (This phenomena has been accounted for in the current Vermont Yankee feedwater flow control system model). The decreasing vessel pressure would tend to make the feedwater pumps run out.

A.3.3.8 Sensed Water Level

The sensed water level prediction of the model is compared with the test data in Figure A.3.8. The fluctuations in sensed water level predicted initially correspond to the initial fluctuations in steam flow. The level drops rapidly during the first 5 seconds due to the collapsing of voids in the core region and the decreasing of vessel steam flow. The model does not predict the rapid rise in level occurring at approximately 4.5 seconds. This rise in the data may be indicative of some inertial effects in the water level measuring instrument or perhaps some wave phenomena inside the vessel. The prediction shows better agreement with the data as the transient tends to steady out.

A.3.3.9 Results Obtained With Core Power Input

In order to better evaluate the thermal-hydraulics and control system modeling, a run was made in which core power versus time was specified based on the measured APRM test trace. Comparisons of the model predictions to the base case and measured test data are presented in Figures A.3.9 through A.3.14.

The M-G set generator speed and core inlet flow results are shown

in Figures A.3.9 and A.3.10, respectively. The generator speed response in essentially identical to base case prediction. The core flow prediction is in better agreement with the data than the base case. This is primarily due to the reduced quality in the core associated with the lower power transient. The same anomalies associated with the small jet pump throat volume occurred.

The vessel steam flow and steam dome pressure predictions are shown in Figures A.3.11 and A.3.12, respectively. The steam flow prediction is considerably below the base case prediction from 10 seconds until the end of the simulation. The slope of steam flow prediction agrees fairly well with the data from 8 to 11 seconds. The steam dome pressure predicted by the model is in better agreement with the data than the base case. This is because steam dome pressure tends to follow core power in a BWR.

Figures A.3.13 and A.3.14 present the feedwater flow and sensed water level comparisons, respectively. The feedwater flow prediction stays at the maximum flow condition longer than the base case and drops off at a more rapid rate. This behavior is due to the sensed water level and vessel steam flow predictions of the model. As seen from Figure A.3.14, the sensed water level prediction shows a decreasing water level from 5 to 11 seconds, while the base case shows a rising level. The level error is dominant during this period, hence, a higher feedwater flow is predicted. The more rapid decrease is due to the lower steam flow prediction, which produces a higher steam-feedwater flow mismatch error signal. The lower water level prediction is due to the greater void collapse in the core associated with the lower transient behavior of core power. The slope of the water level rise near the end of the transient is in better agreement with the data than the base

case.

A.3.4 Conclusions

Based on the analysis performed, the following conclusions are made.

With respect to the adequacy of the RETRAN computer code:

(1) The code is flexible enough to model all major components of the reactor system which are of importance in this type of transient.

(2) No major shotcomings which would prevent the code from analyzing events of the generator load rejection type were discovered.

With respect to the adequacy of the Vermont Yankee RETRAN model:

(1) Good overall agreement with most of the measured test parameters was obtained using the point kinetics feature of the code. In the case of the steam dome pressure prediction, the lack of agreement with the data during the late portion of the transient was attributed to the overprediction of core power during this period.

(2) When the measured core power was input to the code, core flow and steam dome pressure predictions improved indicating that a better core power prediction would yield better thermal-hydraulic results.

(3) The very good results obtained for M-G set generator speed and core flow indicate that the assumptions made concerning the electrical torque calculation are reasonable approximations to reality.

A.4.0 TURBINE TRIP WITHOUT BYPASS TRANSIENT

This section presents the results of an analysis of the Turbine Trip Without Bypass (TTWOB) transient for Vermont Yankee Nuclear Power Station. Results of sensitivity studies performed on steam line nodalization, time step sizes, and fuel rod thermal models are also included. The transient was initiated from rated power and rated flow conditions.

A.4.1 Description of the Turbine Trip Without Bypass Transient

The TTWOB transient is one of the pressure increase category transients. In this transient, the turbine is tripped and it is assumed that the steam bypass valves which will normally open to relieve pressure fail to operate. The scram signal is received from a position switch on the turbine stop valve. The scram signal is generated when the stop valves are 10% closed.

The transient is initiated by closure of the turbine stop valves. Once these valves are closed, the steam flow leaving the vessel decreases. Since the core is continuing to generate power with a reduced steam flow, the reactor vessel pressure increases. The pressure continues to increase until the safety relief valves open. This rise in pressure causes a reduction in the core voids which result in a core power increase. The power continues to rise until the new voids generated by higher power, the Doppler reactivity feedback, and the scram reactivity feedback override this positive effect and begin to reduce the power. The rise in core power is followed by a rise in fuel centerline temperature and fuel rod surface heat flux. This results in a decrease in critical power ratio (CPR).

The basic sequence of events as modeled in RETRAN for the TTWOB transient are shown below for end of cycle operating conditions (all control rods withdrawn). The control rod insertion times assumed for this analysis exceed those required by the current plant technical specifications:

Time (sec)	Events
0.0	Steady-state initialization of the model.
10E-10	Arbitrary input time to begin closing turbine stop valves.
0.01	Scram is initiated by position switch when the turbine stop valves are 10% closed.
0.1	Turbine stop valves are fully closed.
0.278	Control rods begin to move.
6.0	Control rods are fully inserted.

All events important to the reactor system's response to the TTWOB are essentially over by about 8.0 seconds, therefore, the transient simulation was ended at 8.0 seconds.

A.4.2 Model Description

The nodalization scheme used for the TTWOB transient was the same as shown on Figure 2.1, with the exception of the steam separator (volume 3), steam line, and active core region nodalization. The model used for TTWOB simulation assumed thermodynamic equilibrium between the separated phases in volume 22. In the current version of the model, thermal non-

equilibrium effects are accounted for. Three fluid volumes were used to represent the steam line, i.e., volumes 52, 53, 54, and 55 (see Figure 2.1) were represented by one volume.

The key feature, the closure of the turbine stop valve, was modeled assuming a linear closure rate. The stroke time for the valve is 0.1 seconds (full open to full shut). The scram was initiated at the 10% closed position of the turbine stop valve.

The reactor kinetics data were taken from the Cycle 2 reload licensing submittal. The initial conditions of RETRAN model were based on 100% power (1593 Mwt) and 100% flow (48 x 10^6 lb/hr). The model was initialized using the self initialization feature of RETRAN. The built-in convergence criteria were relaxed (enthalpy error being = .05 Btu/lb and error in acceleration pressure drop being = .0005 psi) and the problem converged in 17 iterations. The reactor dome pressure (volume 22) was initialized to 1020 psia which is approximately the observed value at rated conditions.

A.4.3 Results

Various modeling options and techniques were tried in simulating the TTWOB transient in order to arrive at an optimum converged solution. The results of these sensitivity studies are presented in the following sections. First, a time step sensitivity study was performed.

A.4.3.1 Time Step Sensitivity Study

There were three cases evaluated. The differences between the three cases are summarized on Table A.4.1, which also shows the differences in computer processing time between the cases. Base case and case #1 were executed using the automatic time step control feature available in RETRAN with minimum and maximum time step sizes shown in Table A.4.1. In case #2, a fixed time step size of 0.005 seconds was used throughout the transient.

Figure A.4.1 shows the comparison of normalized core power between the three cases. As soon as the turbine stop valves start to close, the pressure in the vessel starts rising due to reduced steam flow. This rise in pressure causes a reduction in core voids which results in a core power increase. The scram was initiated when the turbine stop valves were 10% closed. The power continues to rise until the new voids generated by the higher power, the Doppler reactivity feedback, and the scram reactivity feedback override the positive void reactivity effect and begin to reduce the power. The power reached a maximum of 206% of the initial and the power peak occurred at 0.8 seconds in the transient.

Figures A.4.2 and A.4.3 show the comparisons of the steam dome and steam line pressure response. The steam line pressure reaches the lowest relief valve setpoint at approximately 1.11 seconds. The peak pressure in the steam line at the safety and relief valves reaches a maximum of 1162.15 psia at 3.69 seconds. The steam dome peak pressure is approximately 1161.98 psia at 3.92 seconds.

Figure A.4.4 shows the RETRAN calculation of the core inlet flows.

The core inlet flow increases are primarily due to the changes in steam dome pressure, which causes the core voids to decrease, resulting in a net decrease in two-phase pressure drop. A total increase of about 5.5% in core inlet flow is predicted by RETRAN.

Figure A.4.5 shows the comparison of RETRAN calculations of the core average surface heat flux. Core average surface heat flux decreases initially due to the pressurization effect on saturation temperature and the heat transfer coefficient. Subsequently, the core average surface heat flux reaches a maximum of 109 percent at about 1.06 seconds.

A.4.3.2 Steam Line Nodalization Sensitivity

The base case nodalization of the steam line included three volumes plus a bypass piping volume. The first two volumes were selected to model the pressure at the relief valves and to allow modeling of the main steam line isolation valves. The remainder of the steam line piping was treated as one volume except for the bypass piping. This approach resulted in a relatively large volume for the third steam line volume. A nodalization study was performed with this relatively large volume broken up into four equal volumes resulting in a total steam line nodalization of six approximately equal volumes.

The first test case was run with this six volume steam line model and is referred to in the remainder of this discussion as the six volume case. A second case was set up in which the relatively large volume was broken up into eight equal volumes resulting in a total steam line nodalization of ten volumes. This case is referred to in the remainder of this discussion as the ten volume case.

Figures A.4.6 through A.4.10 show the comparison of results based on this steam line nodalization scheme discussed above. Figure A.4.6 shows the power response for the three cases. The six volume case predicted 2.9% higher power than the base case, and the ten volume case predicted 3.6% higher power than the base case. Figure A.4.7 shows the steam dome pressure response for these cases. The six volume case pressure in the steam dome was 3.25 psi higher than the base case, and the ten volume pressure in the steam dome was 3.35 psi higher than the base case. Figure A.4.8 shows the steam line pressure response for the three cases. The six and ten volume cases show oscillations in pressure in the early part of the transient and later tend to damp out. Figure A.4.9 shows the core inlet flow response for these cases. High core flow predictions are seen for the six and ten volume cases at approximately the same time the steam line goes through a pressure oscillation. Figure A.4.10 shows the core average surface heat flux response for the three cases. Average surface heat flux predicted by the six and ten volume cases is slightly less than the base case prediction.

Figure A.4.20 shows the response of average surface heat flux, cases that used volume average weighting for the density show a higher peak than the base case.

A.4.3.3 Fuel Rod Thermal Models Sensitivity

The following sections present the results of the sensitivity studies performed on fuel-to-clad gap conductance and radial nodalization of the fuel and clad regions.

Sensitivity studies on gap conductance were performed assuming a constant gap conductance across the gap. A value of 1000 Btu/hr-ft^{2o}F for the gap conductance was used in the base case. Two more cases were executed with gap conductance values of 500 and 2000 Btu/hr-ft^{2o}F. Figures A.4.11 through A.4.15 show the results of the sensitivity study performed on the gap conductance. Figure A.4.14 shows that the average surface heat flux reached a maximum of 110.5% with a gap conductance of 2000.0 Btu/hr-ft^{2o}F. The average surface heat flux reached a maximum of 109% in the base case. The surface heat flux reached a maximum of 107.5% when the gap conductance of 500 Btu/hr-ft^{2o}F was used. Figure A.4.11 shows that the case with gap conductance of 500 Btu/hr-ft^{2o}F predicted the highest neutron power. During the transient, higher gap conductance will lead to faster heat transfer from the fuel to the moderator/coolant, which generates more steam voids. This fast conversion of fuel energy into steam voids in the core helps to mitigate the transient due to the negative reactivity feedback effect. Therefore, the neutron power response of the system with higher values of gap conductance will be less severe. Figures A.4.12 and A.4.13 show that the pressure response of TTWOB transient is insensitive to the value of gap conductance.

A sensitivity study was performed to measure the effects of radial nodalization of the fuel and clad regions on the system response and computer running time. The base case utilized six nodes in the fuel pin and eight nodes in the cladding region. The gap in all cases was represented by one node. Figures A.4.16 through A.4.20 show the transient response to the radial nodalization schemes used in fuel and clad regions. Results indicate that the lesser the number of nodes in the fuel and clad, the higher the

surface heat flux and lower the peak power. The pressure response of the system was found to be insensitive to the number of radial nodes used to represent the fuel and clad.

In an effort to examine the effect of clad nodalization on the transient response, another case (see Figure A.4.16) was executed with two radial nodes in the clad region. The fuel was represented by six radial nodes as in the base case. The results indicated that there was essentially no change in the average surface heat flux prediction between the base case and the case with reduced clad radial nodes.

A.4.4 Conclusions

The overall purpose for performing the present study was to evaluate the predictive capabilities of RETRAN and identify sensitive parameters and models in RETRAN that influence the operational transient response of the reactor system.

The conclusions reached on the basis of this study are summarized below:

- RETRAN predicts the expected behavior of the reactor to a Turbine Trip Without Bypass transient.
- The results are sensitive to steam line nodalization up to six approximately equal volume nodes. Any increases in the number of nodes beyond six did not significantly change the predicted results.
- Sensitivity studies on gap conductance indicate that the average surface heat flux response is sensitive to the values used. Pre-transient

gap conductance and characteristics input for the Vermont Yankee RETRAN model for application will be derived from a detailed thermal effects calculation for steady-state fuel rod, FROSSTEY [17].

- The radial nodalization schemes used to represent the fuel and clad indicate that the TTWOB transient response is relatively sensitive to the number of radial nodes used to represent the fuel. It appears that about 6 fuel nodes are sufficient.

- Time step sensitivity study indicated that a maximum time step size of .001 seconds up to 0.5 seconds in the transient and a maximum time step size of .01 later on can be a good "first cut" value to be used in TTWOB transient (with relief valves modeled as negative fills).

A.5.0 LOSS OF FEEDWATER HEATER TRANSIENT

This section presents the results of an evaluation of the sudden loss of feedwater heating capability. This results in a relatively slow power increase due to the increase in moderator density in the core region which occurs with colder feedwater injection. This evaluation is of particular interest because of the use of the enthalpy transport delay option in RETRAN, which allows the user to more accurately track the temperature changes in various regions of the reactor.

A.5.1 Description of the LOFWH Transient

A loss of steam flow to a feedwater heater, or bypass of flow around the feedwater heater, can result in the introduction of colder feedwater into the reactor. This will result in an increase in core inlet subcooling, and subsequently, a reduction in the core average void fraction. This

increase in moderator density will cause an increase in core power until a new steady-state value is reached.

A.5.2 Model Description

As mentioned before, the enthalpy transport delay option of RETRAN was exercised in this transient in order to track the enthalpy "front" associated with the decrease in feedwater temperature. Temperature changes move through some regions (such as piping) essentially as a front. That is, the incoming fluid does not completely mix with the fluid within the particular region, but only displaces it. The standard RETRAN method for determining the junction enthalpy is to homogeneously mix incoming fluid with the contents of the particular region; thus, the outlet enthalpy begins to respond immediately to changes at the inlet. The transport delay model considers the movement of fluid through a region as a slug. In other words, the fluid coming into a region at time (t) leaves the region at time ($t+\tau$) where τ represents the time required to transport that fluid through the volume. For further details see Reference 2. A brief description of some aspects of the models relevant to the LOFWH transient and sensitivity studies are given below.

In order to account for the movement of colder feedwater as a slug, the lower part of the downcomer region was divided into four volumes. The top volume (volume 4, see Figure A.5.1) of the lower downcomer represents a mixing region where feedwater mixes with the fluid in that region. The middle downcomer volume (volume 41) is situated between the bottom of volume 4 and the jet pump suction. Volume 42 represents the volume in the lower downcomer region existing between volume 41 and the outlet to the

recirculation line. Volume 43 represents a stagnant volume sitting below the recirculation line outlet. Due to the inactivity of this volume, it was modeled as a homogeneous volume. The upper portion of the downcomer region (volume 23) is modeled as a non-homogeneous volume with a high bubble separation velocity. Liquid level in volume 23 represents the reactor water level.

Initial conditions were 100% power (1593 Mwt) and 100% flow (48 x 10^6 lb/hr). The model was initialized using the self initialization feature of RETRAN. It was assumed that the feedwater temperature dropped $100^{o}F$ instantaneously at the reactor inlet. In other words, mixing in the piping between the feedwater heater and the reactor inlet nozzle was ignored.

A.5.3 Results

Two cases were evaluated: one with and one without the enthalpy transport delay option. Figure A.5.2 shows the comparison of core power for the two cases. As expected, both cases ultimately reach the same higher power level, which is about 118% of rated power. There are some variations between the two cases earlier in the transient which can be associated with the changes in core flow as discussed later.

Figure A.5.3 shows the jet pump exit enthalpy. The effect of the transport delay model is quite evident in this figure. Without transport delay, the enthalpy change is a gradual change. In the transport delay case, the enthalpy remains essentially constant until the colder fluid reaching the induced nozzle passes through the jet pump exit, then a sharp decrease in jet pump enthalpy is seen. The enthalpy then remains approximately constant until the colder fluid has passed through the

recirculation loop and out the jet pump. At that time, there is another sharp decrease in the jet pump exit enthalpy. These sudden changes in jet pump exit enthalpy results in sudden changes in the density of the coolant exiting the jet pumps, which result in small, but noticeable, drops in jet pump flow (Figure A.5.4). This momentary change in jet pump flow is reflected in total core flow (Figure A.5.7) and core power (Figure A.5.2).

Figure A.5.5 shows the steam flow, feedwater flow and reactor water level behavior during the transient for the two cases. Feedwater flow is responding as expected to the change in reactor water level and the steam flow - feedwater flow mismatch.

Figure A.5.6 is a comparison of the steam dome pressure predicted by the two cases. Both the cases predict an overall increase of approximately 7.3 psi in steam dome pressure, which is a result of the increase in steam flow noted above.

Time step sensitivity studies were performed on both cases. Cases were run with a maximum time step size ranging between 0.001 seconds and 0.01 seconds for the first 0.5 seconds of transient time. For the remainder of the transient a maximum time step size ranging between 0.01 seconds and 0.1 seconds was used. It was found that the transient solution was relatively insensitive to the range of time step sizes tested. However, with a maximum time step size of 0.01 seconds in first 0.5 seconds of the transient and a maximum time step size of 0.1 seconds in the remainder of the transient resulted in substantial savings in the computer processing time.

A sensitivity study on the mesh interval size used in the enthalpy

transport delay model was also performed. The RETRAN model used for this study contained only two volumes in the downcomer region, that is, volume 23 and volume 4 (see Figure A.5.1). In other words, volume 4 was a lumped representation of volumes 4, 41, 42 and 43 (see Figure A.5.1) which were used to model the downcomer region in the previous cases. As a "first cut" value, a mesh interval size of approximately 1 foot was selected. Later, cases were run with mesh interval size of approximately 2 feet, 1/2 foot, and 1/10 of a foot. It was quite evident from the results that mesh interval size had essentially no effect on the time-dependent behavior of parameters of interest. The agreement among the results predicted by different mesh intervals was quite good.

A.5.4 Conclusions

RETRAN predicts the expected behavior of the loss of feedwater heater transients. From a core reload licensing analysis viewpoint, the maximum power level reached is of utmost interest because of the potential effect of exceeding fuel cladding integrity safety limits; therefore, the use of the enthalpy transport delay option is of little interest. However, from a transient simulation viewpoint, the enthalpy transport delay option probably provides a somewhat more realistic prediction of the course of the transient, and thus should be used for operator training or simulator input purposes.

A.6.0 STUCK-OPEN RELIEF VALVE TRANSIENTS

A stuck-open relief valve can lead to steam condensation instability at high suppression pool temperatures. RETRAN has been used to predict the reactor pressure decay and the amount of steam released to the

suppression pool for a variety of postulated incidents. These results have been used to develop a set of acceptable operating procedures and pool temperature limits for the Vermont Yankee Nuclear Power Station [13].

A.6.1 Description of a SORV Event

The events that were analyzed using RETRAN which would result in relatively high suppression pool temperatures due to a stuck-open relief valve included a stuck-open S/RV during power operation, and a stuck-open S/RV during hot standby conditions.

A stuck-open S/RV during power operation could be initiated by a downward drift in the S/RV actuation setpoint or a failure in the electrical circuits causing a false "open" signal to be sent to the valve actuator. During a stuck-open S/RV event, the suppression pool will be heated by the condensation of the steam generated in the reactor vessel and released to the suppression pool through the S/RV(s). The sources of energy available to generate steam include:

a) nuclear fission (prior to scram),

b) fission product decay (following scram),

c) sensible heat of the fuel,

d) sensible heat of structures (reactor vessel, piping, internals),

e) internal energy of the reactor coolant.

A.6.2 Model Description

In order to accurately evaluate the reactor's response to stuck-

open relief valve events, given the multiplicity of energy sources, RETRAN was used to simulate the course of these transients. A schematic of the nodalization scheme used in RETRAN is shown in Figure A.6.1. This model was collapsed from a more detailed reactor model (see Figure 2.1) in order to better suit the model to the long transients under consideration. The control system shown in Figure A.6.2 represents the feedwater system under manual control following reactor scram. This control model incorporates models for trip monitoring, a flow integrator to keep track of the amount of feedwater added to the reactor and a linearization function generator. This scheme was used to account for enthalpy changes as the hot feedwater was flushed from the feedwater system following a reactor scram.

A.6.3 Results

The collapsed model, along with the feedwater control system described above, was used to evaluate both the stuck-open S/RV during power operation and during hot standby transients. Figures A.6.3 and A.6.4 show a reactor pressure and steam flow through the stuck-open relief valve for the stuck-open relief valve from 100% power case.

Sensitivity studies were performed to evaluate the adequacy of the collapsed version of the detailed reactor model in predicting the course of the transients. It was found that the course of these transients was relatively insensitive to the reduction of details in going from the detailed reactor model (Figure 2.1) to its collapsed version (Figure A.6.1). This reduction in detail resulted in substantial savings in computer processing time.

Time step sensitivity studies were performed to assure that a

converged solution to the transient calculation was obtained. However, it was found that an increase in the maximum time step size from 0.01 seconds to 0.1 seconds resulted in approximately a factor of 8 reduction in computer processing time with little loss in computational accuracy.

A.6.4 Conclusions

RETRAN predicts the expected behavior of the reactor to a stuck-open relief valve transient.

A.7.0 SIMULTANEOUS CLOSURE OF ALL MAIN STEAM ISOLATION VALVES WITHOUT SCRAM

A.7.1 Event Description

This analysis presents the plant response to a simultaneous closure of all main steam isolation valves (MSIV's) with failure of the reactor protection scram function. This particular transient has typically been presented as the most severe anticipated transient without scram (ATWS) event for BWR's.

A.7.2 Model Description

No credit was taken for a recirculation pump trip actuated by a high reactor pressure signal, which would mitigate the pressurization transient. Reactivity data for the analysis was generated by SIMULATE [9], a 3-D core simulator, and reflects actual core conditions at the time the analysis was performed. Important aspects of the model relative to this type of transient are listed below:

- The capacities of the four safety/relief valves and two safety valves were assumed to be 10% greater than the nameplate rated capacities. The basis for this assumption is that the ASME code

uses a conservatism factor of 0.9 in determining nameplate capacity.

- Technical Specification values were used for the pressure setpoints of the above valves.
- A linear valve flow area versus time characteristic was assumed for the MSIV's, with a 3 second closing time. This corresponds to the Technical Specification minimum value for valve closure time.
- The modeling of the upper portion of the downcomer (above the feedwater sparger and below the steam dryers) assumes thermodynamic equilibrium between the vapor and liquid phases.
- In order to take into account the effect of reactor vessel pressure on feedwater flow, a linear correction is made such that at 700 psi above initial steam dome pressure, feedwater flow is zero (pumps are at their shutoff head).
- Point kinetics is used for the core power calculation. Reactivity changes due to moderator density and fuel temperature changes are based on core average values.

A.7.3 Results

The transient results for the case of 85% power/100% core flow are presented. The changes in slope of the lower plenum pressure trace (Figure A.7.1) at approximately 4.3 seconds and 7.5 seconds are due to openings of the safety/relief valves and safety valves, respectively. The effects of these valve openings are clearly seen in the vessel steam flow trace of Figure A.7.2. Careful examination of the core inlet flow trace shows drops in core inlet flow occurring just after the two increases in vessel steam flow. The neutron power and average surface heat flux traces are provided in Figure A.7.3. The first spike in the neutron power trace is due to the rise in power associated with the initial void collapse and the counteracting effect of the subsequent heatup of the fuel which turns over the power response. The underdamped behavior of neutron power is caused primarily by the oscillatory core flow. The average surface heat flux tends

to follow the neutron power trace but is much more damped due to the heat capacitance of the fuel. Figure A.7.4 presents the total reactivity and its components for the transient. From examination of this figure, it is clear that the oscillatory nature of the neutron power is due to the void component of reactivity. The oscillation in moderator density (voids) is due to the oscillatory nature of the core flow.

Although the analysis was performed at 100% core flow, it was recognized that if reduced power operation was required, it may be preferrable to accomplish this by reducing core flow. In order to investigate the sensitivity of the results to the 100% core flow assumption, a run was made with 80% power/70% core flow initial conditions. These initial conditions reflect the 100% power rod line condition for the plant. It was found that the 100% core flow case predicted a slighter higher pressure and earlier pressure peak than the rod line case. The lower pressure outcome of the rod line case is somewhat biased by the fact that its initial lower plenum pressure is less than the 100% core flow case. This is because of the reduced core pressure drop associated with lower core flow case.

A number of sensitivity runs were made to identify important input parameters and modeling techniques. The goal of this sensitivity study was to evaluate the effect of the parameter variation on peak lower plenum pressure for each case. The base case for the sensitivity runs was the 80% power/100% flow case. It was found that the steamline inertial effects, MSIV valve closure rate, and the direct moderator heating fraction have a negligible effect on the peak pressure calculation. The gap conductance value has a significant effect on peak pressure. A lower gap conductance

corresponds to a higher transient "delta fuel temperature" and hence a higher Doppler contribution to the transient reactivity function. This same effect is observed in the case where 1.2 times the base case Doppler reactivity was used as input. The sensitivity to void reactivity was investigated by running a case where .9 times the base case moderator reactivity was used as input. The sensitivity of the peak pressure to variations in either void or Doppler reactivity is slight.

Increasing the size of the upper downcomer volume reduced the peak pressure significantly. This effect is due to the increase in liquid mass inventory of this control volume combined with the modeling assumption that both phases are in thermodynamic equilibrium. All other things being equal, the absolute value of the time rate of change of pressure for a saturated control volume decreases as the liquid inventory increases. The motivation for lowering the volume elevation was to analyze higher power and reduced valve area cases for which more significant drops in water level were expected. If mixture level drops below the elevation of the upper downcomer volume, the code will calculate erroneous results. The failure of the sensitivity run to reproduce the base case results eliminates this modeling technique as a legitimate approach to coping with pressurization transients where large changes in water level are expected.

A.7.4 Conclusions

RETRAN predicts the expected plant response to a simultaneous closing of all the main steam isolation valves followed by a failure of the reactor protection system scram function. The results of the analyses show that peak vessel pressure can be kept below 1500 psig for initial steady-state

power levels of $\leq$85% of rated.

It was found that the equilibrium assumption for the upper downcomer region for pressurization transients is not entirely realistic. Since the performance of the above analysis, non-equilibrium effects in the steam dome and downcomer have been investigated (Section 3.1), found to be important, and incorporated into the model (Section 2.1.1).

TABLE A.3.1

Sequence of Events for GLR Startup Test

Time (Seconds)	Event
0.00	Generator output breakers open.
0.25	Load rejection sensed.
0.27	Control valves start to close and bypass valves start to open.
1.50	Bypass valves cam opened to 95%. Reactor power decreased from 94% to 51%.
1.5-2.0	Main turbine generator reaches maximum speed.
27.00	Reactor power has reached 75%.
38.50	Turbine trip occurs. Reactor scrammed.

TABLE A.4.1

Time Step Sensitivity Study

Case	Time (sec)	Maximum Time Step Size (sec)	Minimum Time Step Size (sec)	Actual Number of Time Steps	Standard No. of Time Steps	CPU* Time (sec)
Base Case	0.0 - 0.5	0.001	0.0001	511	500	80.035
	0.5 - 2.0	0.01	0.0005	665	650	26.97
Case #1	0.0 - 0.8	0.01	0.005	82	80	22.243
	0.8 - 2.0	0.1	0.01	114	92	5.252
Case #2	0.0 - 2.0	Fixed = 0.005, No automatic time step control		401	400	67.595

*Note: CP time is based on CDC 6600 Computer.

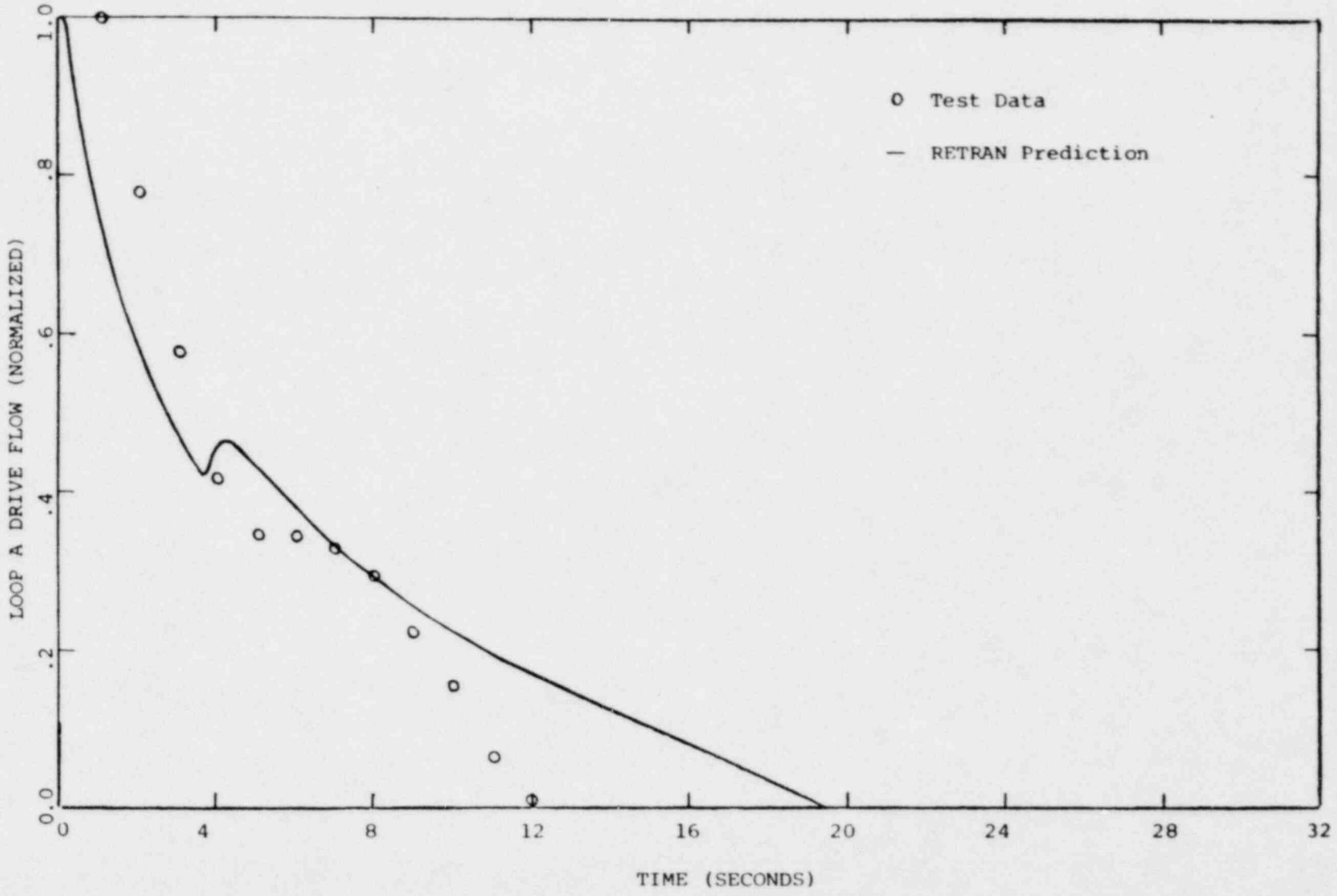

Figure A.2.1
RPT Test, Loop A Drive Flow
Vs. Time

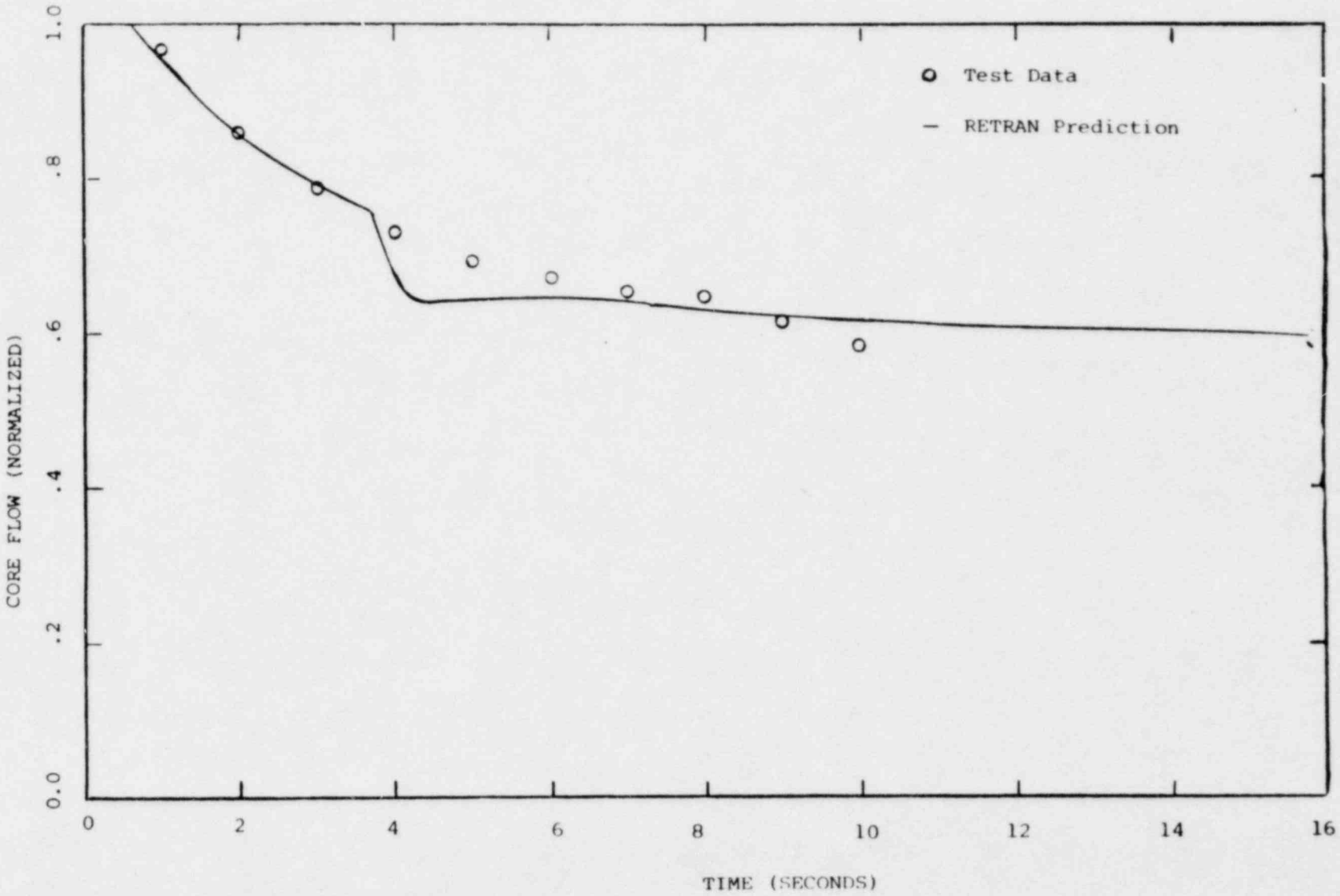

Figure A.2.2
RPT Test, Core Flow
Vs. Time

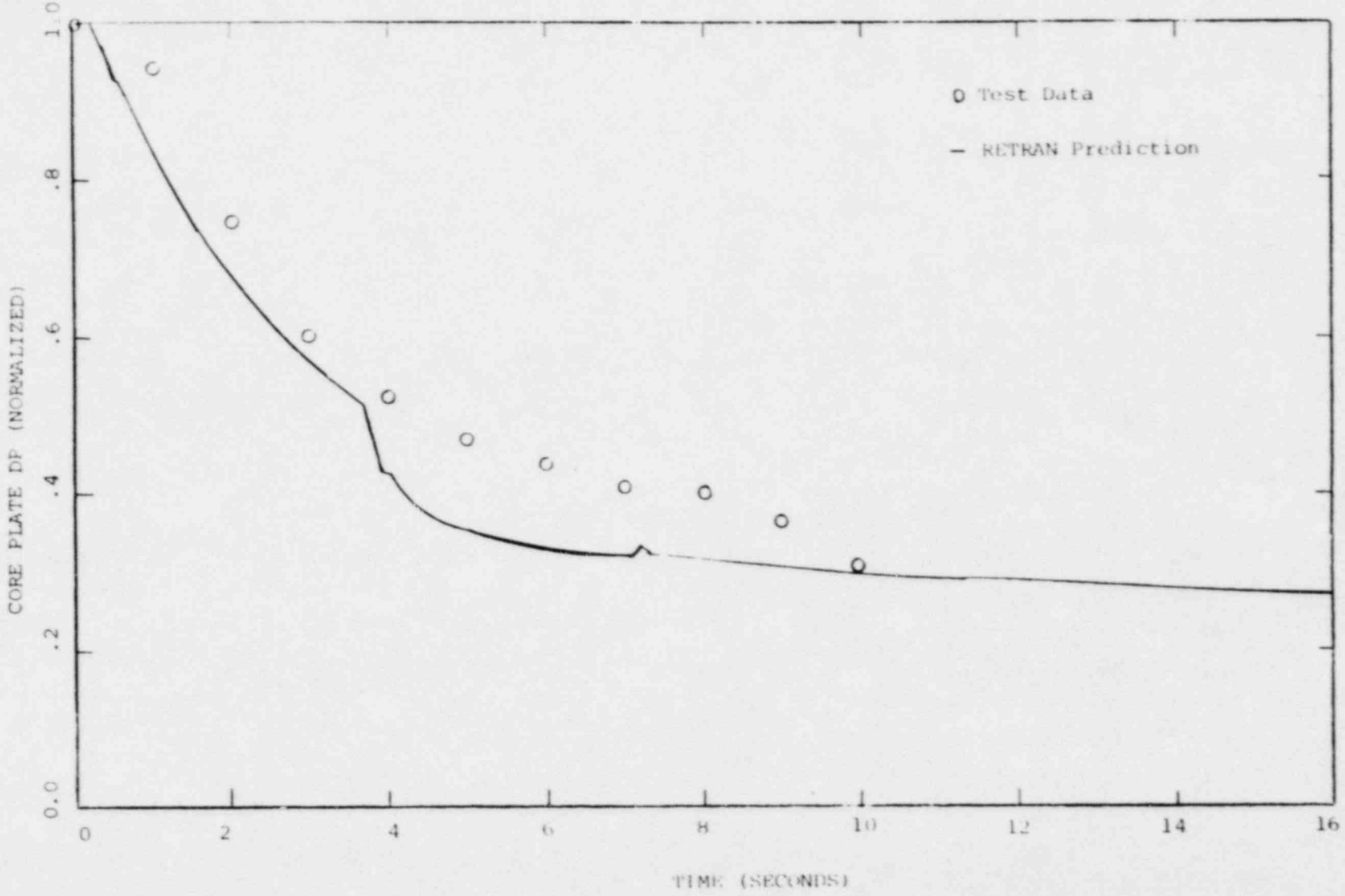

Figure A.2.3
RPT Test, Core Plate Delta P
Vs. Time

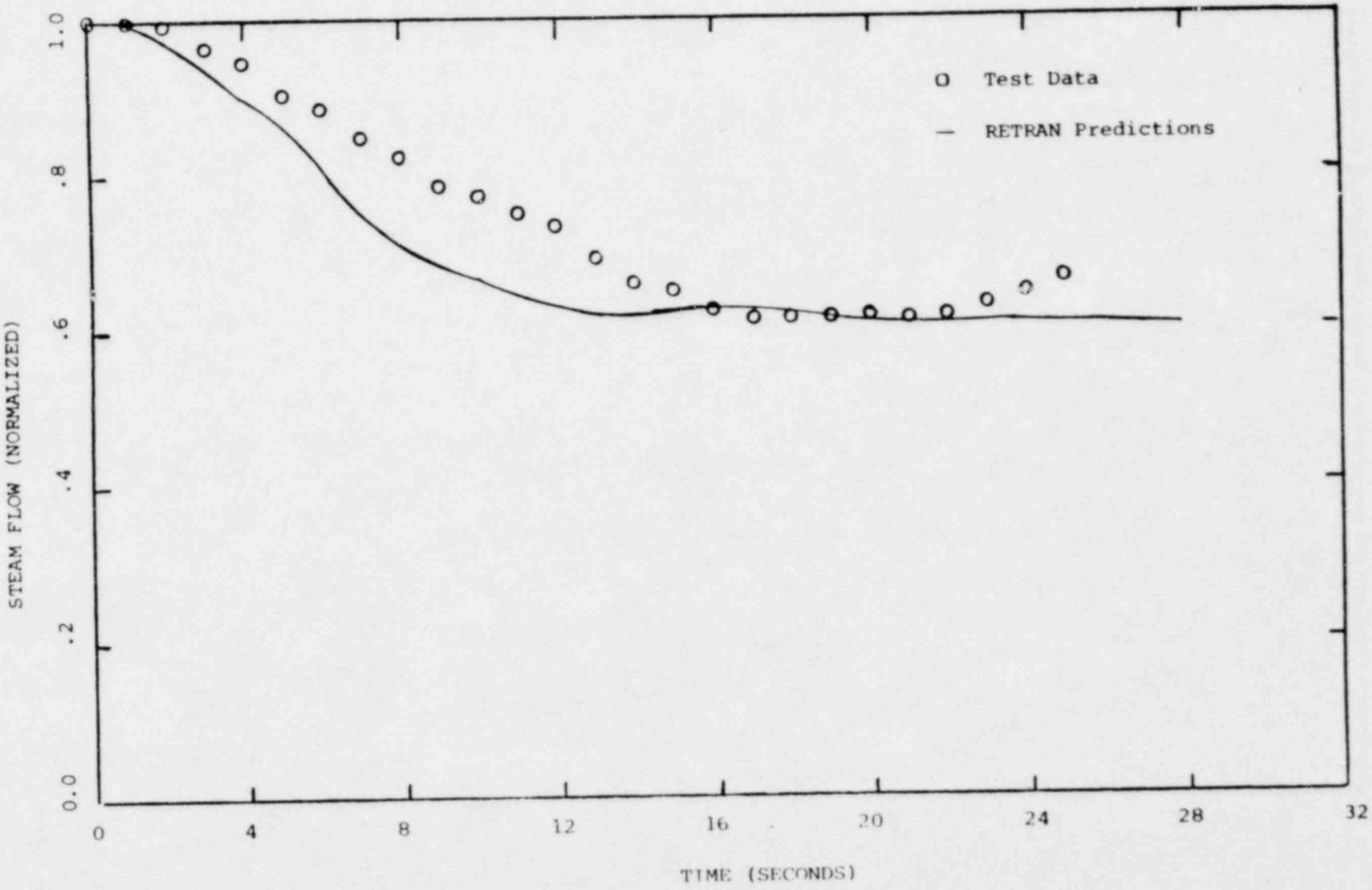

Figure A.2.4
RPT Test, Steam Flow
Vs. Time

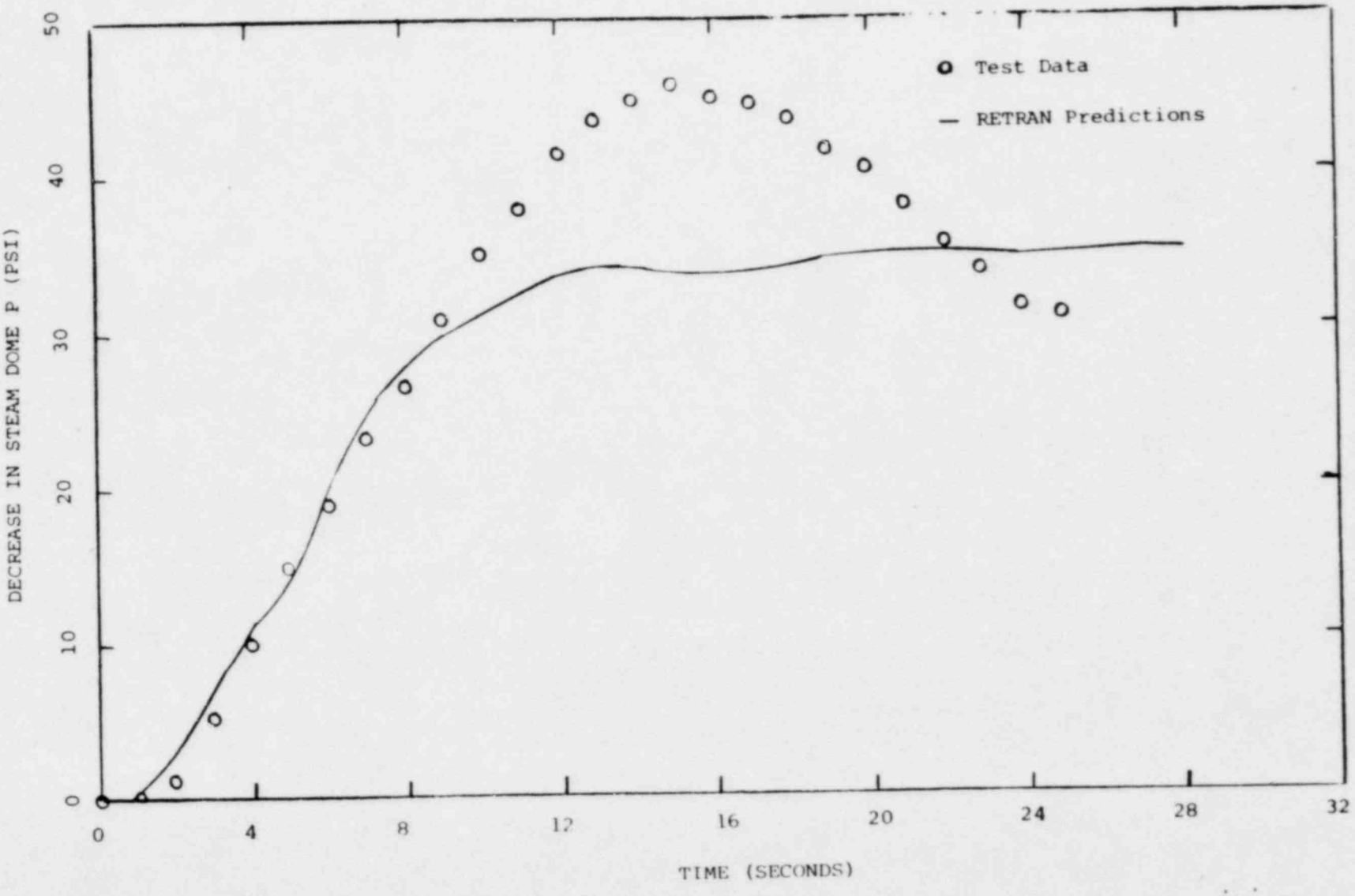

Figure A.2.5
RPT Test, Steam Dome Pressure
Vs. Time

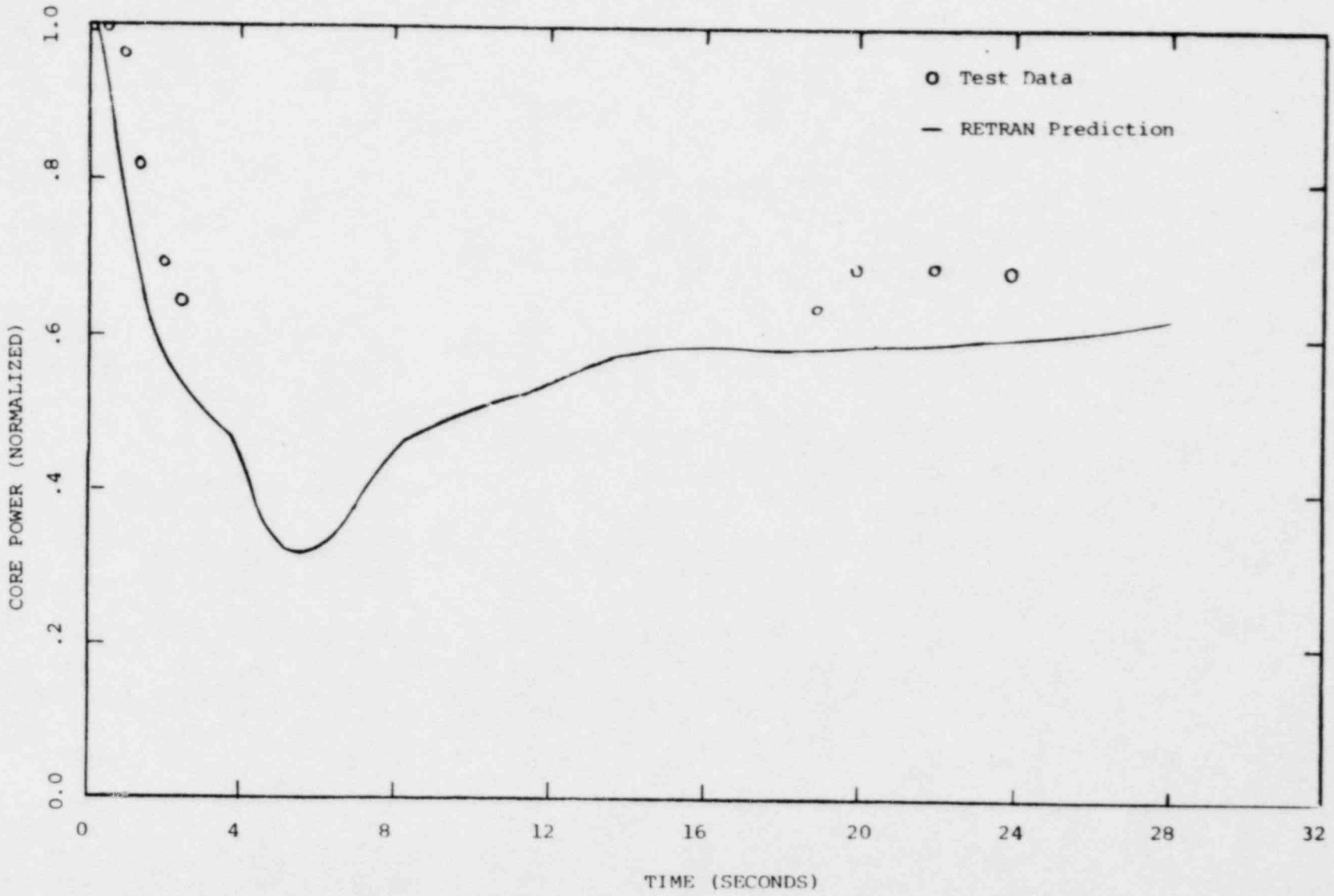

Figure A.2.6
RPT Test, Core Power
Vs. Time

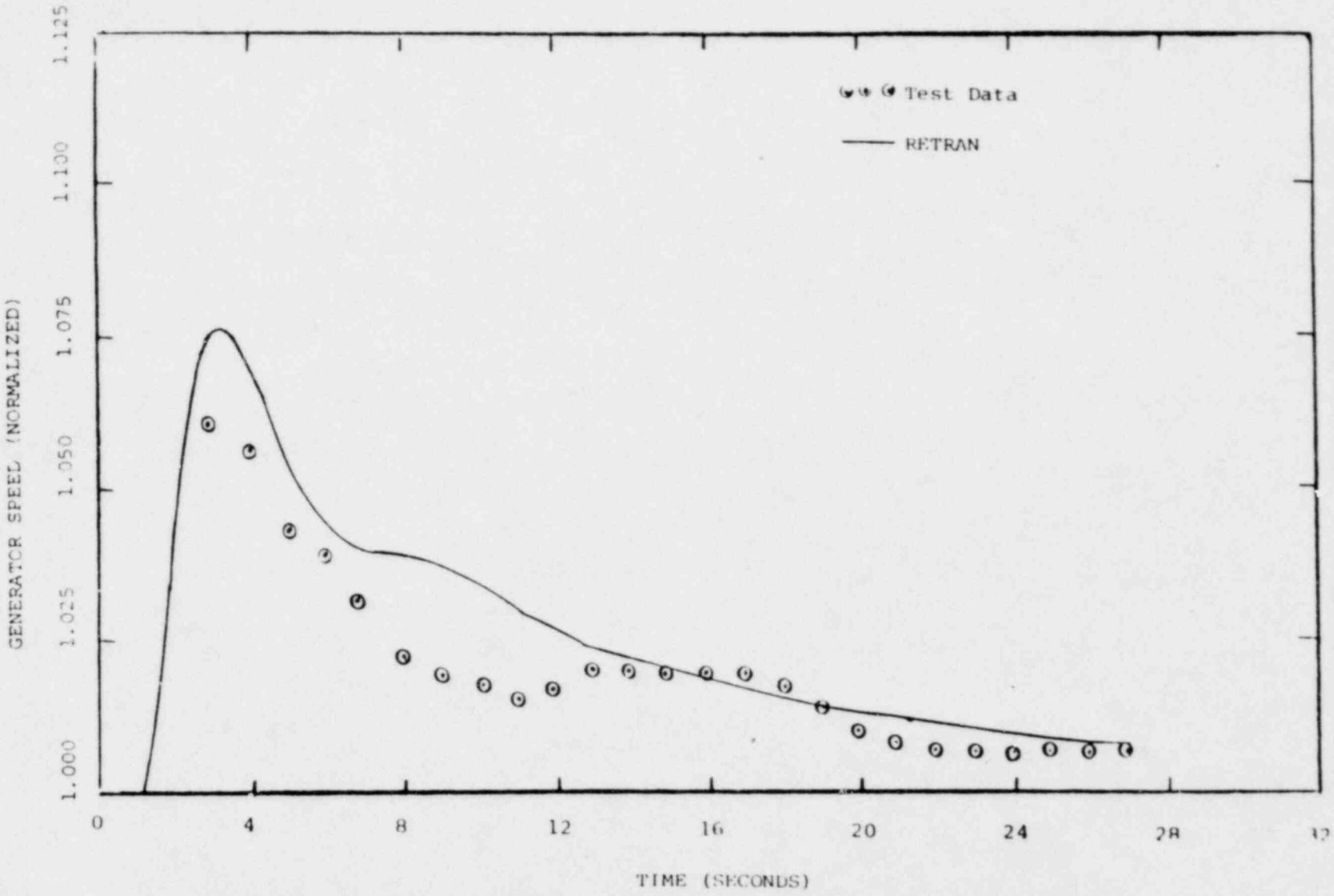

Figure A.3.1
GLR Test, Generator Speed
Vs. Time

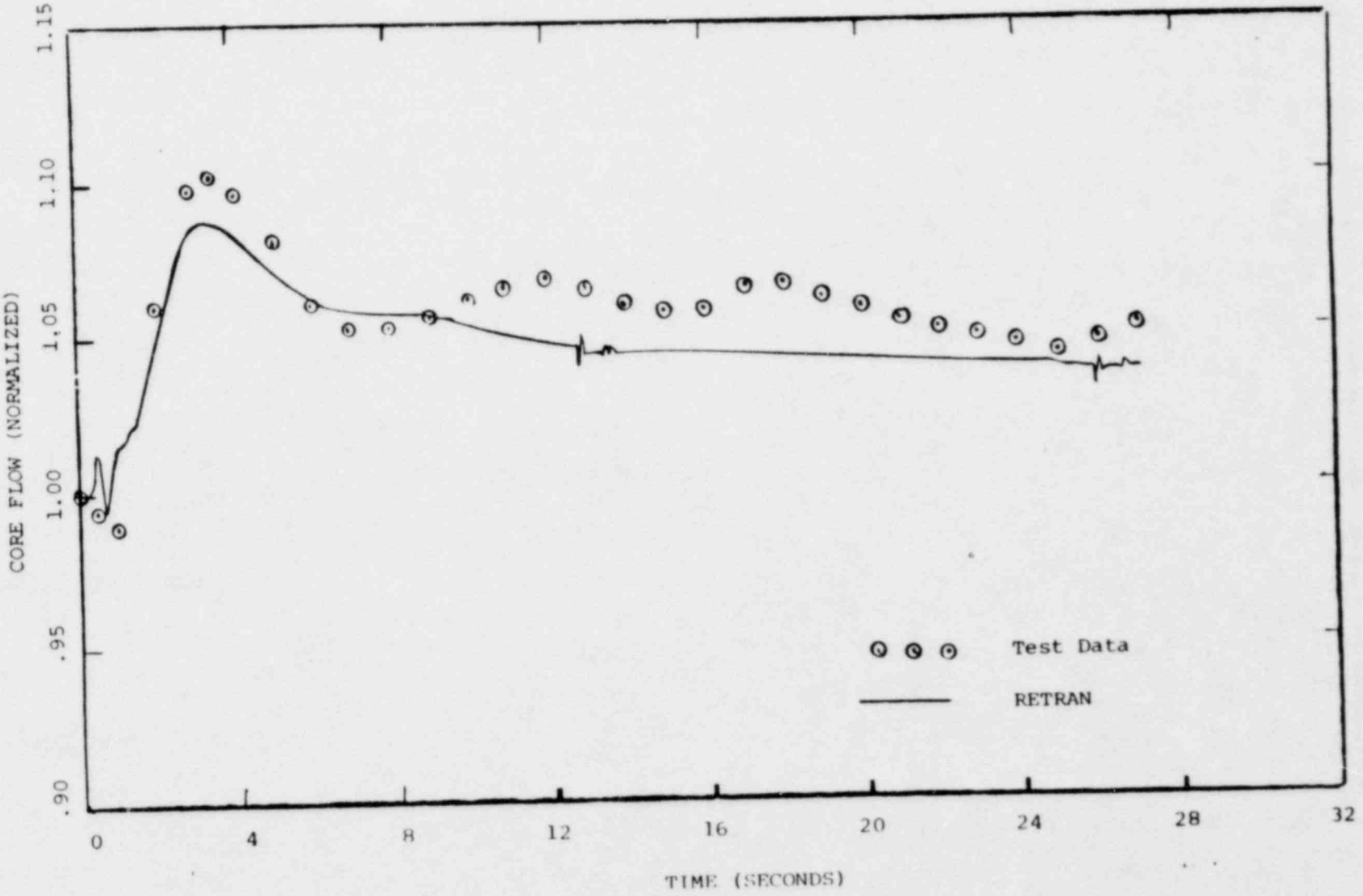

Figure A.3.2
GLR Test, Core Flow
Vs. Time

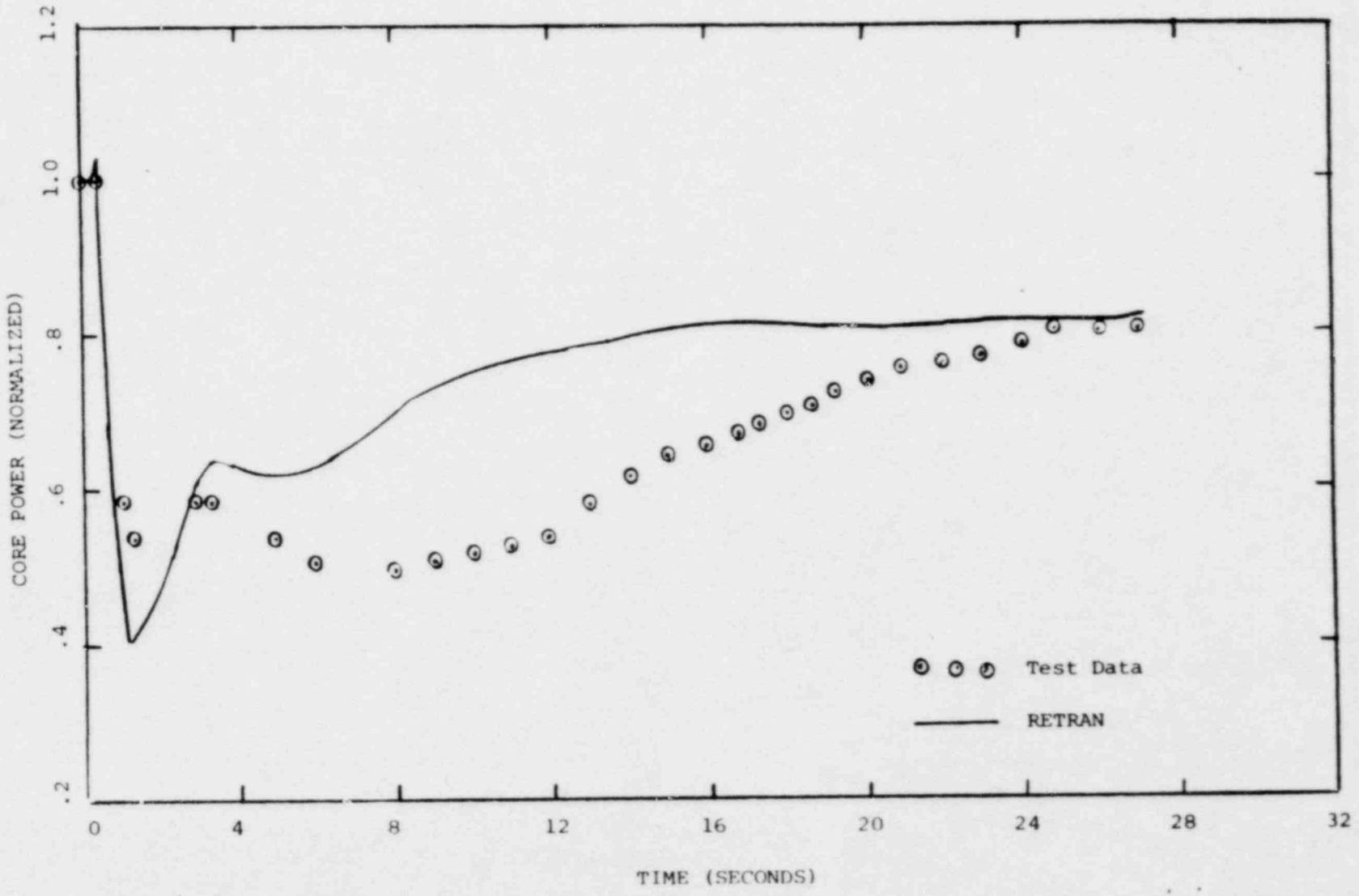

Figure A.3.3
GLR Test, Core Power
Vs. Time

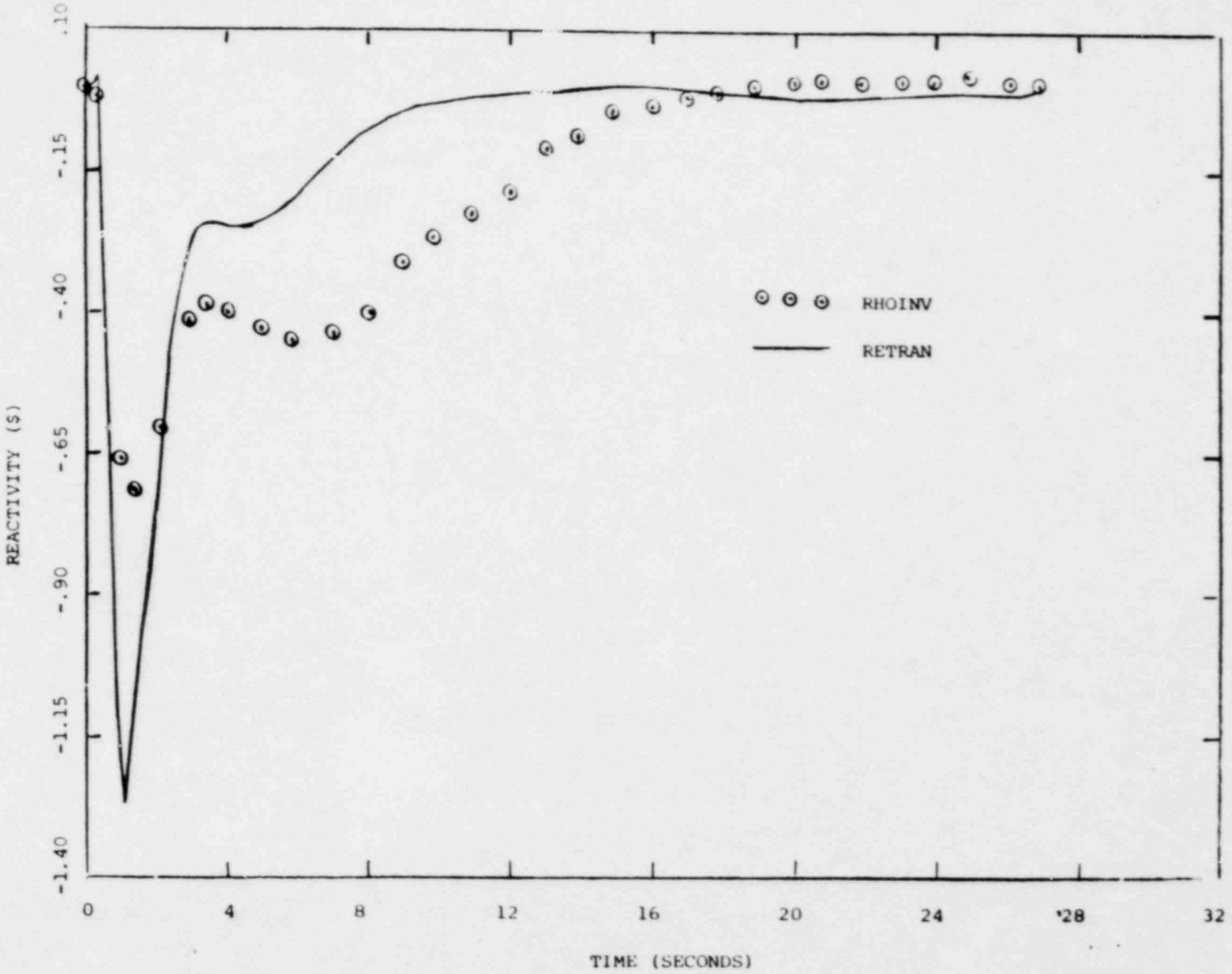

Figure A.3.4
GLR Test, Reactivity
Vs. Time

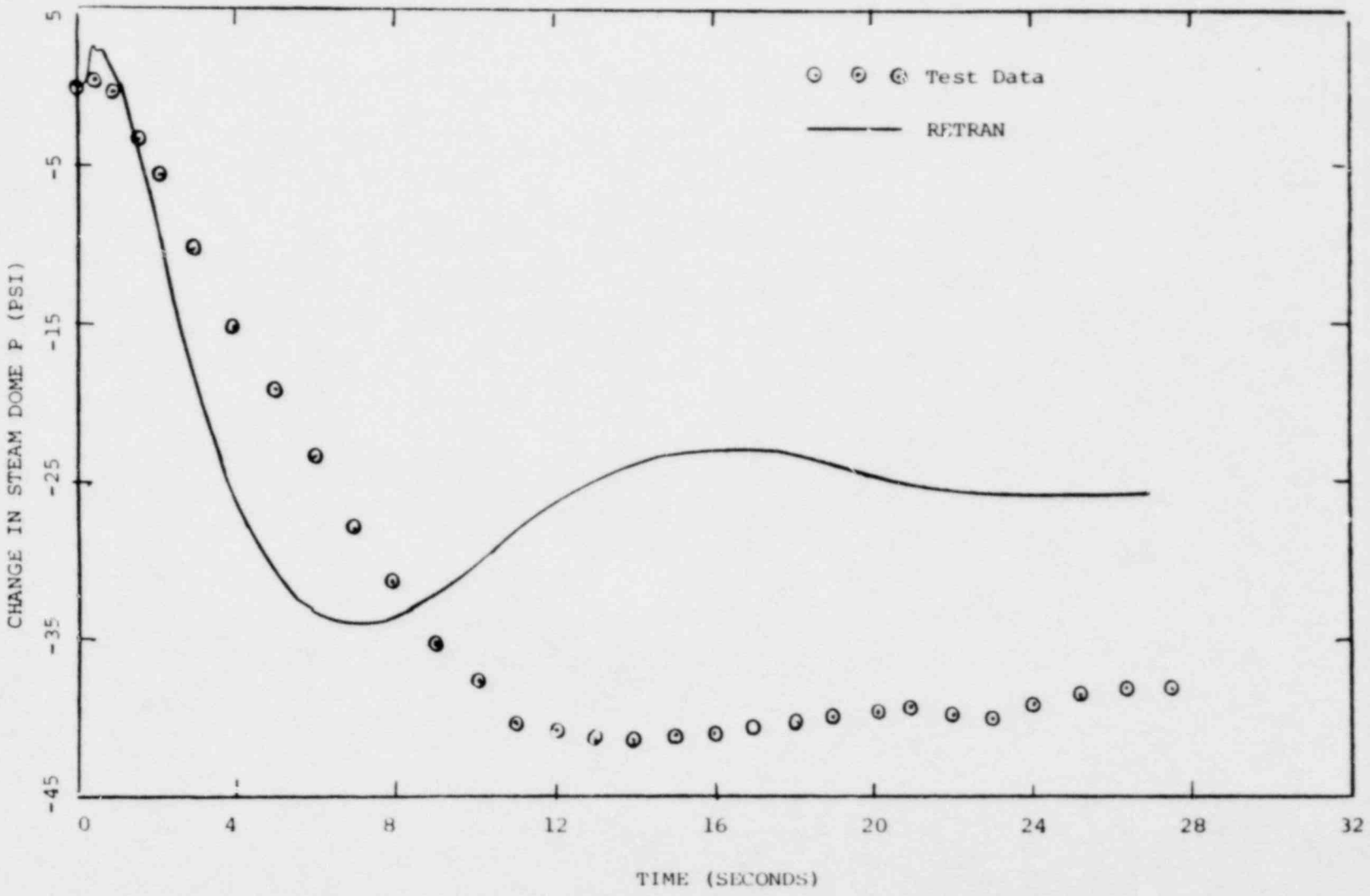

Figure A.3.5
GLR Test, Steam Dome Pressure
Vs. Time

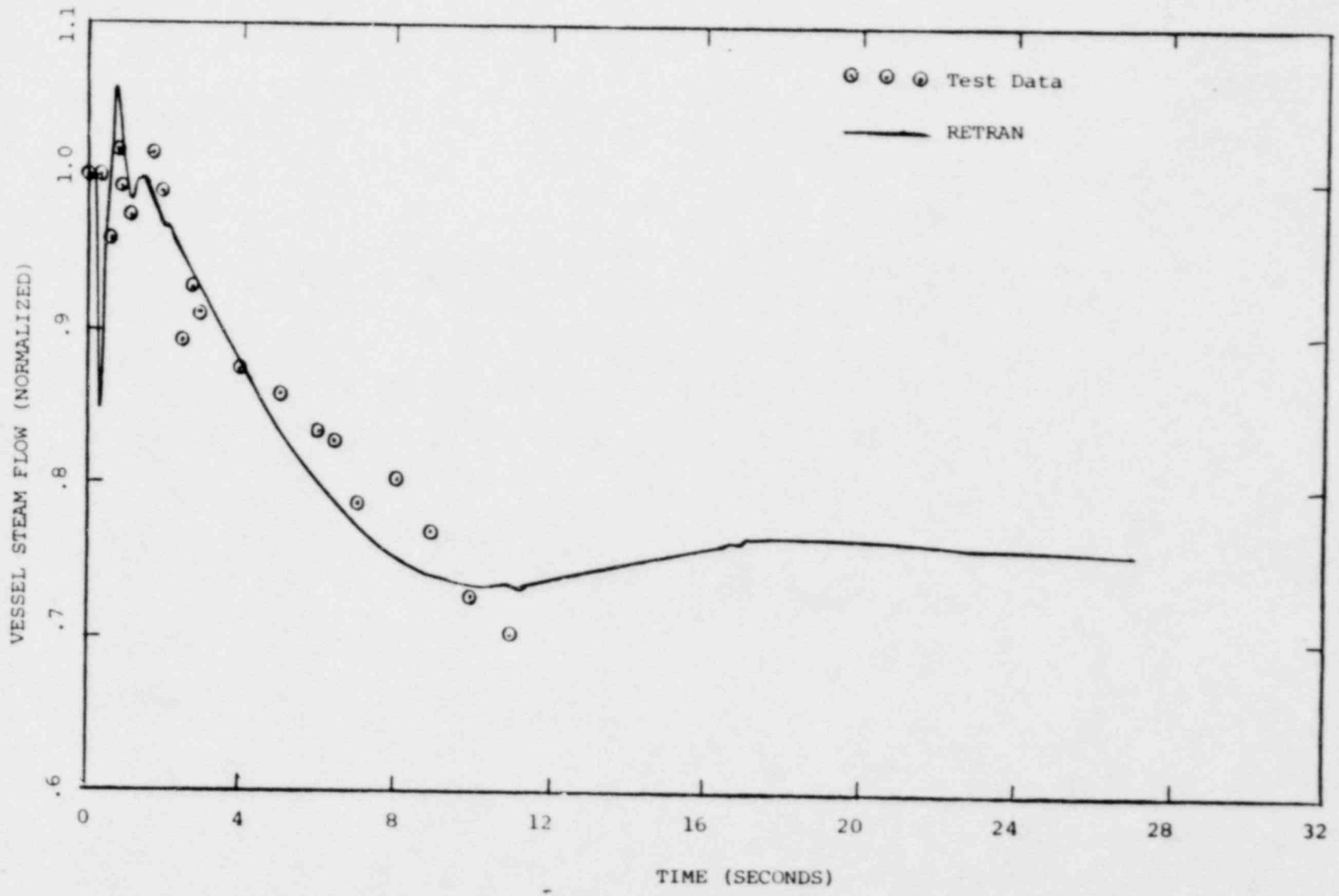

Figure A.3.6
GLR Test, Vessel Steam Flow
Vs. Time

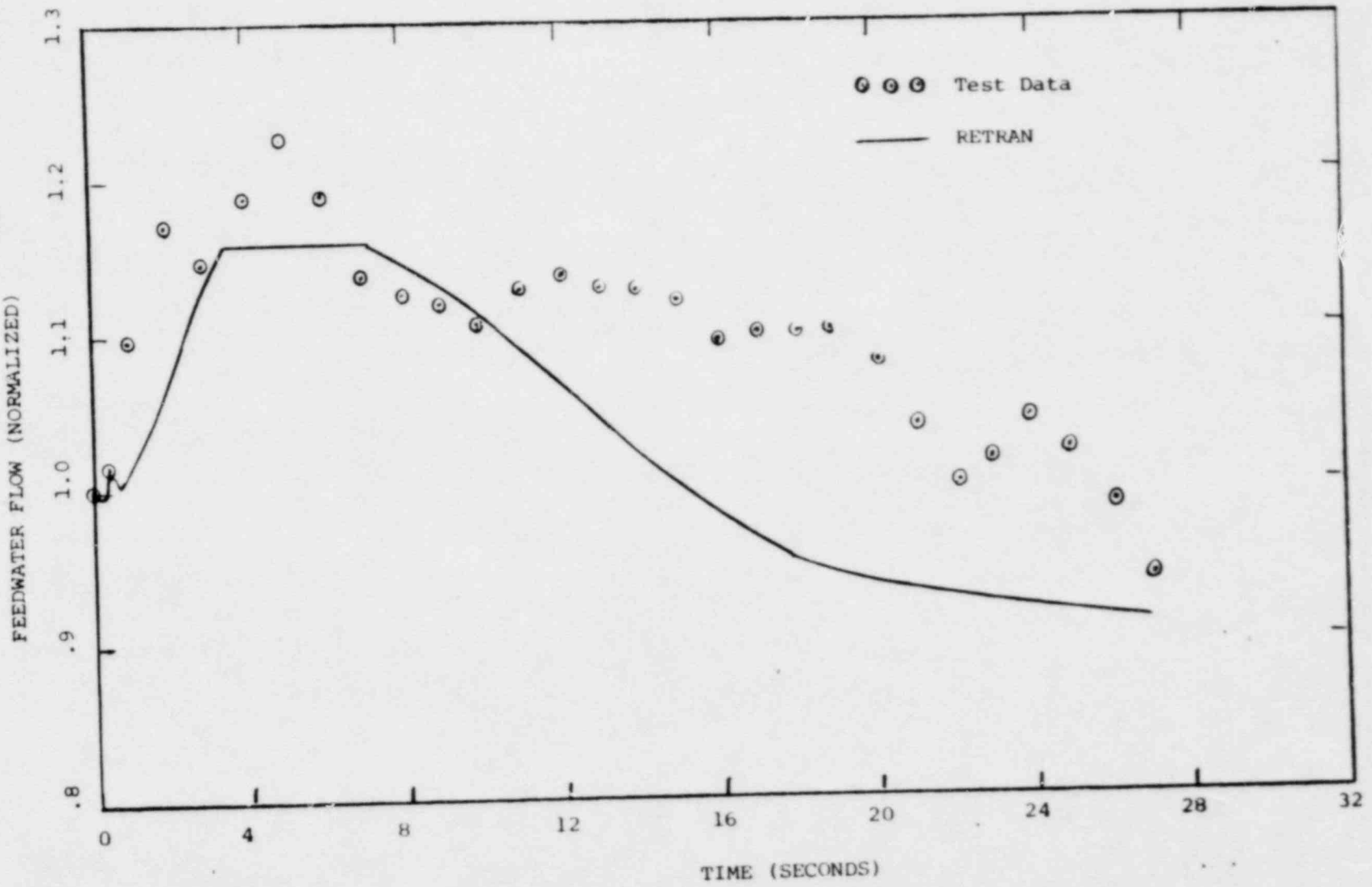

Figure A.3.7
GLR Test, Feedwater Flow
Vs. Time

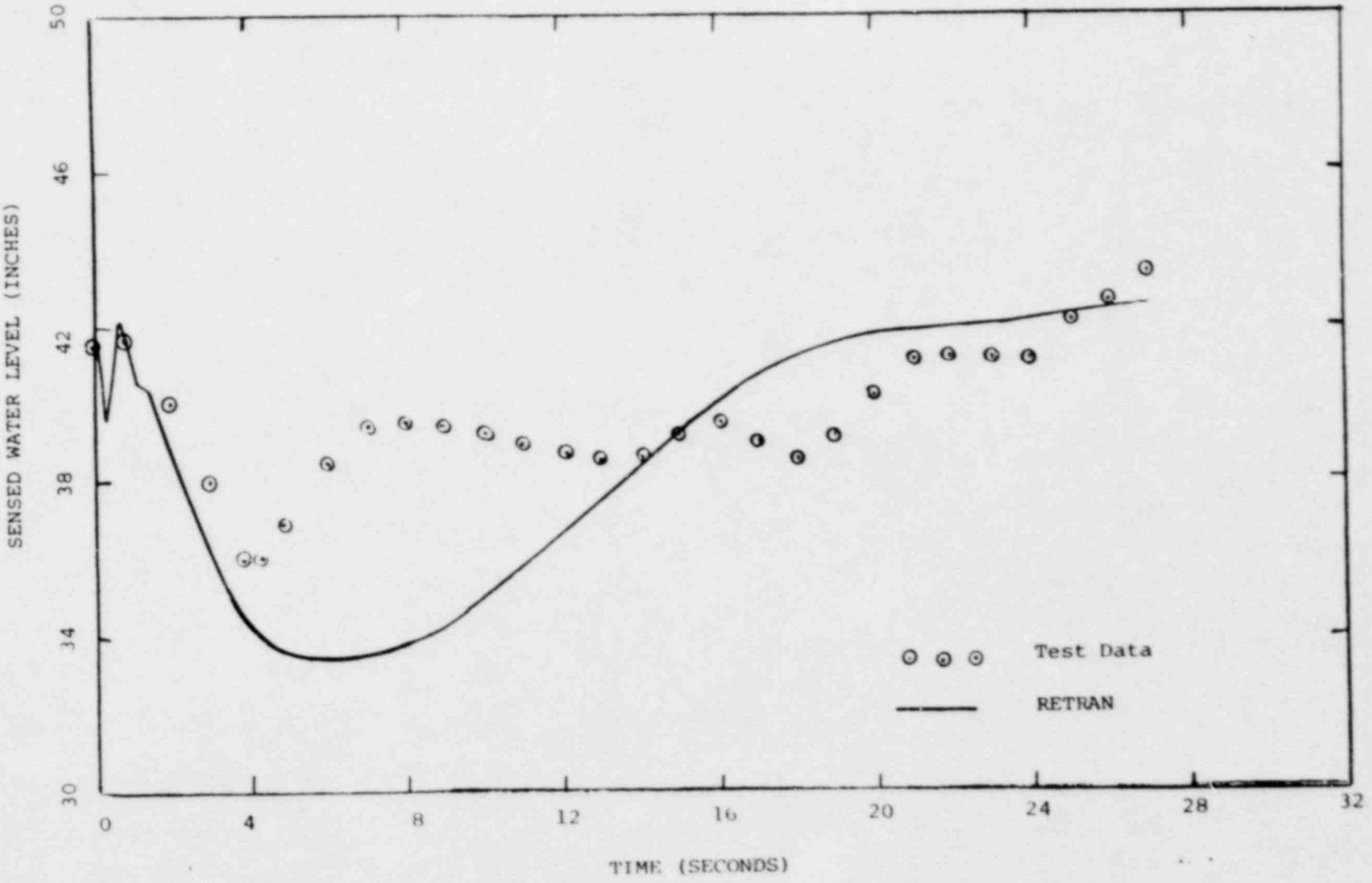

Figure A.3.8
GLR Test, Sensed Water Level
Vs. Time

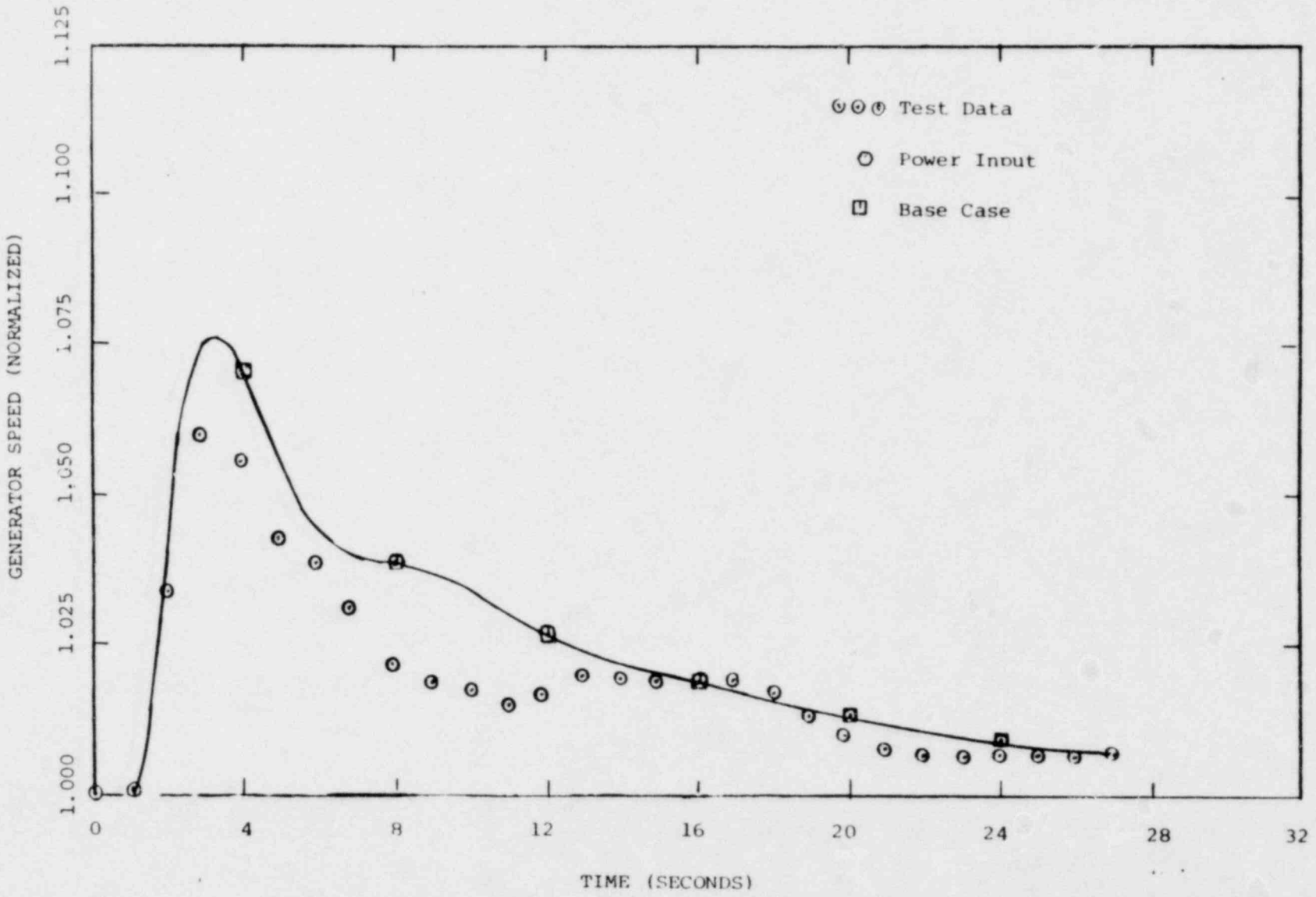

Figure A.3.9
GLR Test, Generator Speed
Vs. Time (Power Input Case)

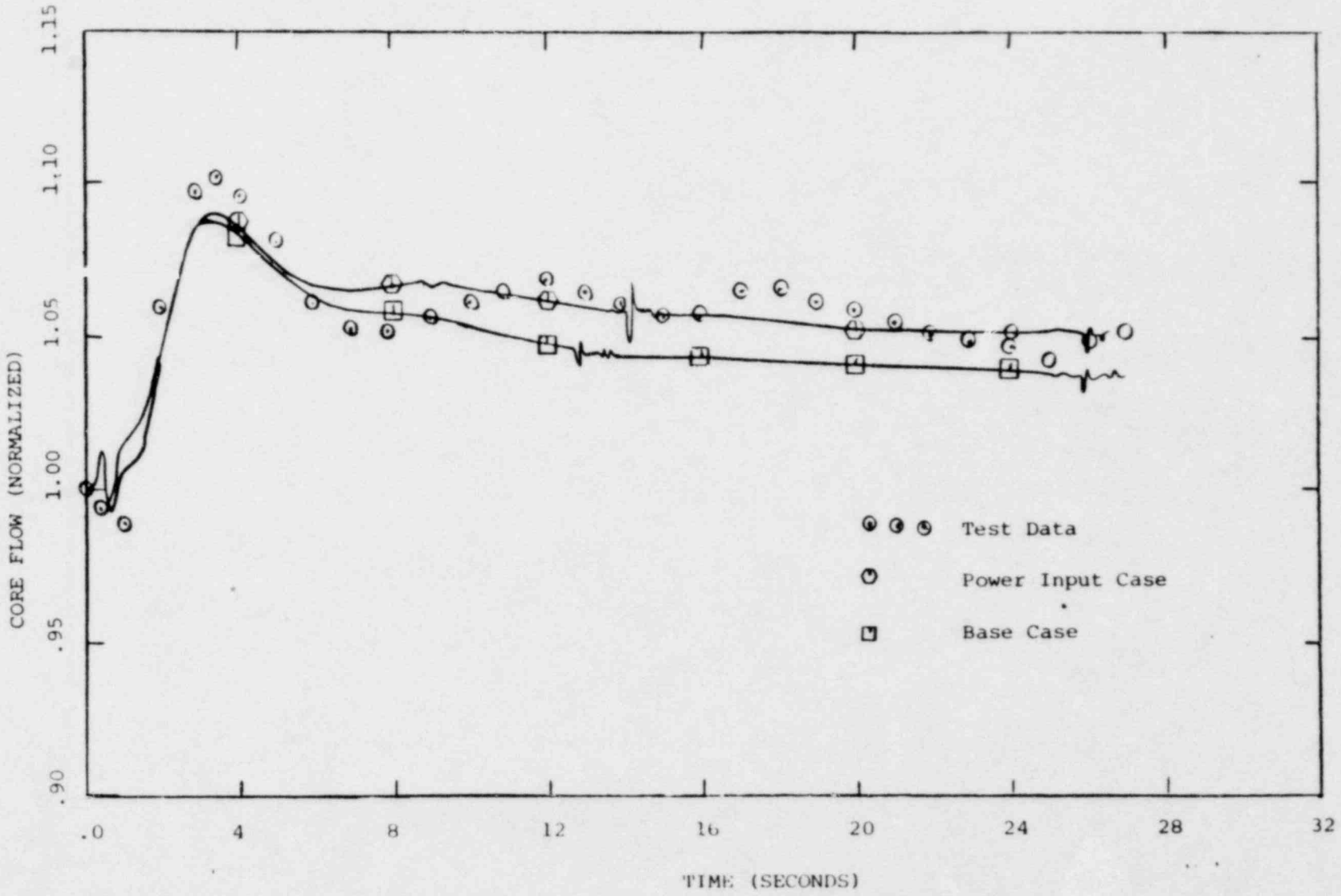

Figure A.3.10
GLR Test, Core Flow
Vs. Time (Power Input Case)

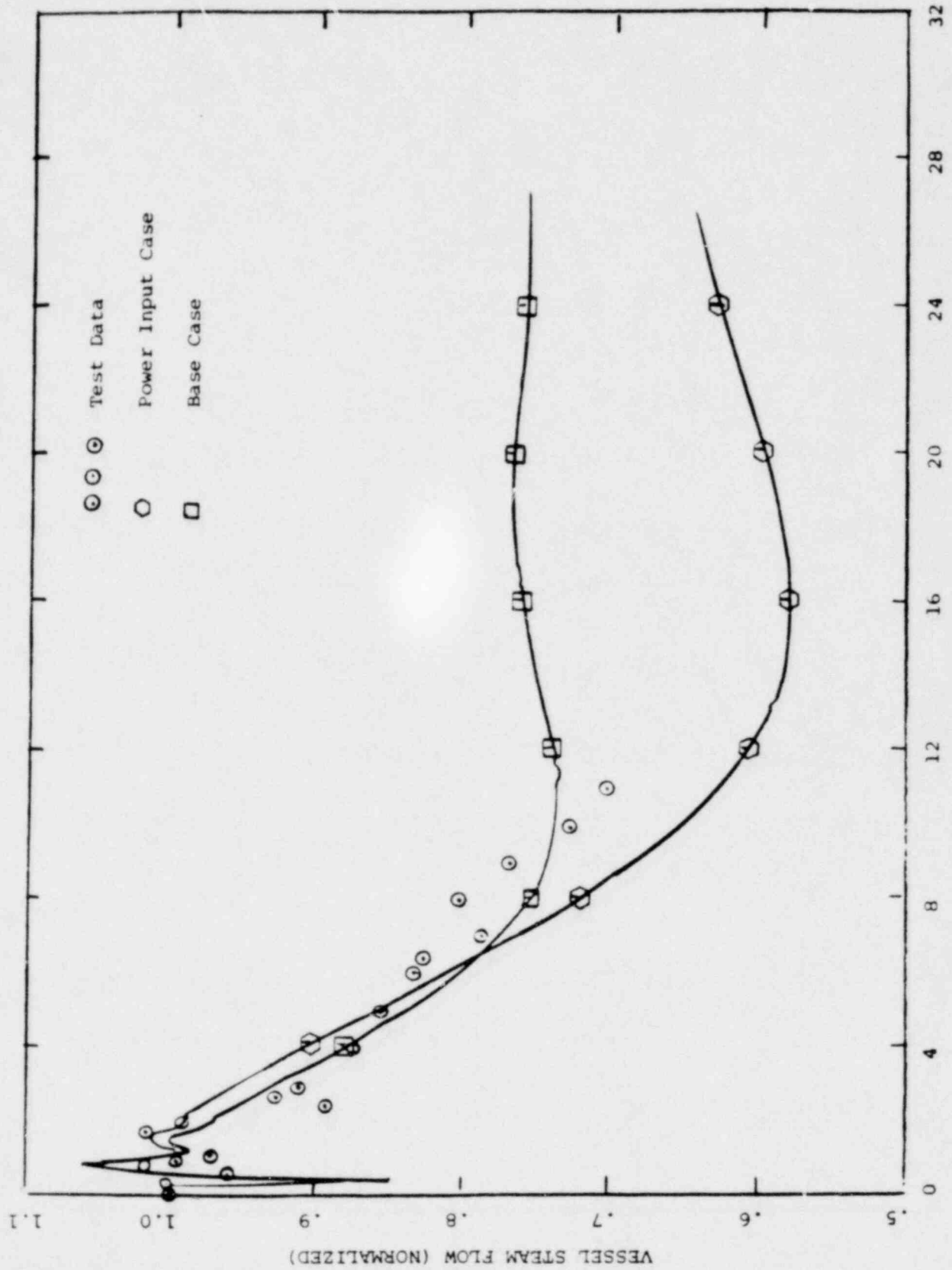

Figure A.3.11
GLR Test, Vessel Steam Flow
Vs. Time (Power Input Case)

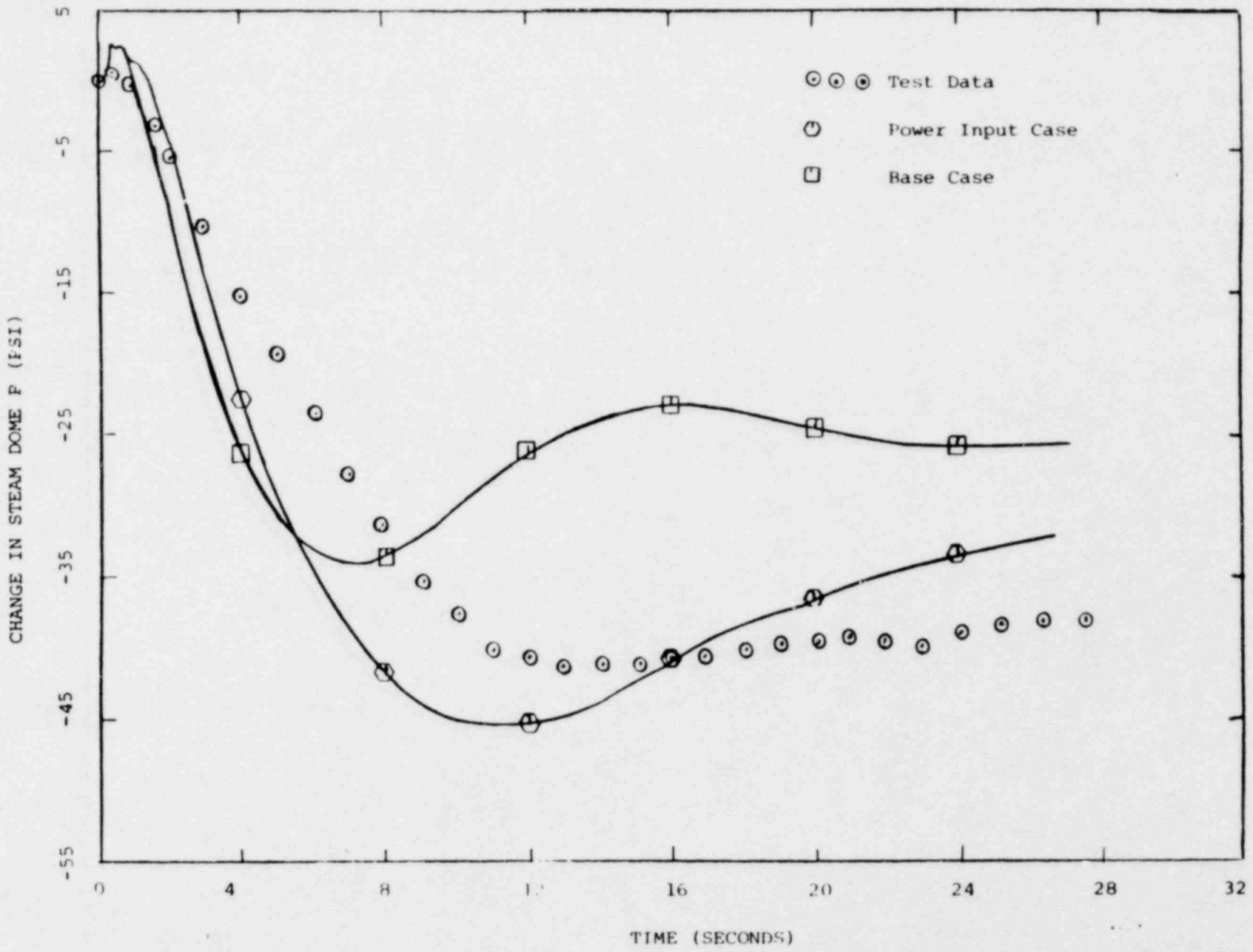

Figure A.3.12
GLR Test, Steam Dome Pressure
Vs. Time (Power Input Case)

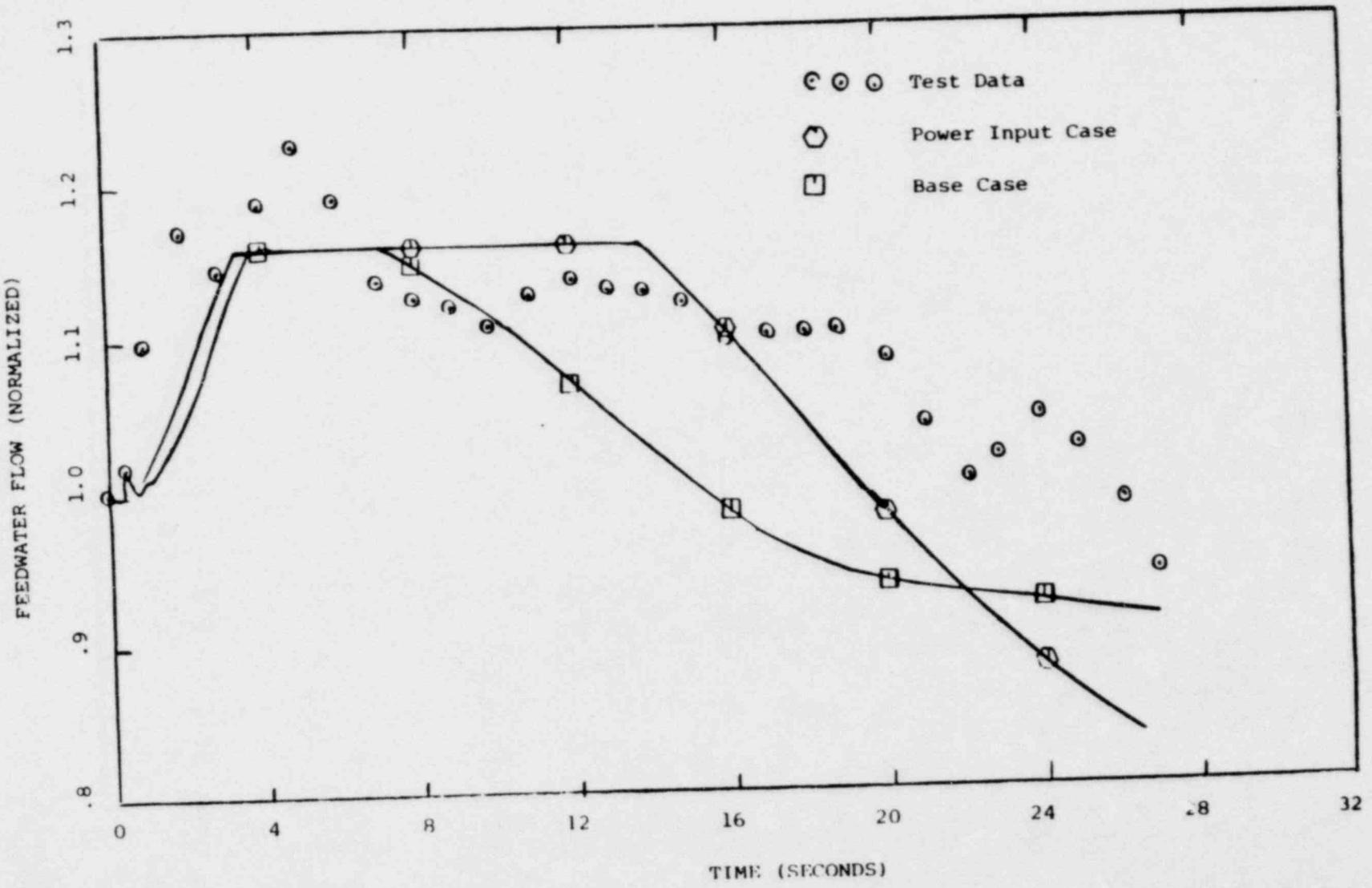

Figure A.3.13
CLR Test, Feedwater Flow
Vs. Time (Power Input Case)

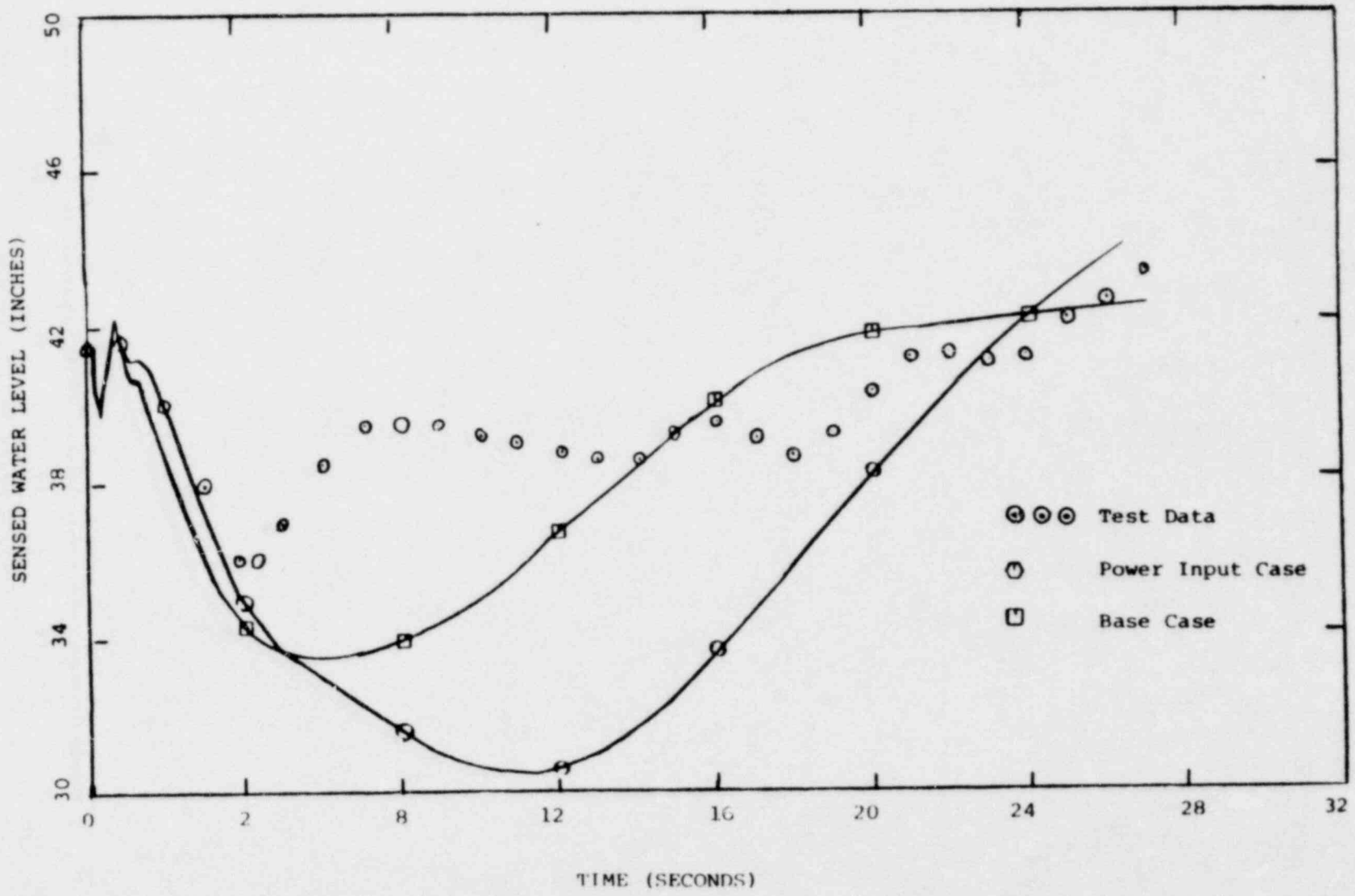

Figure A.3.14
GLR Test, Sensed Water Level
Vs. Time (Power Input Case)

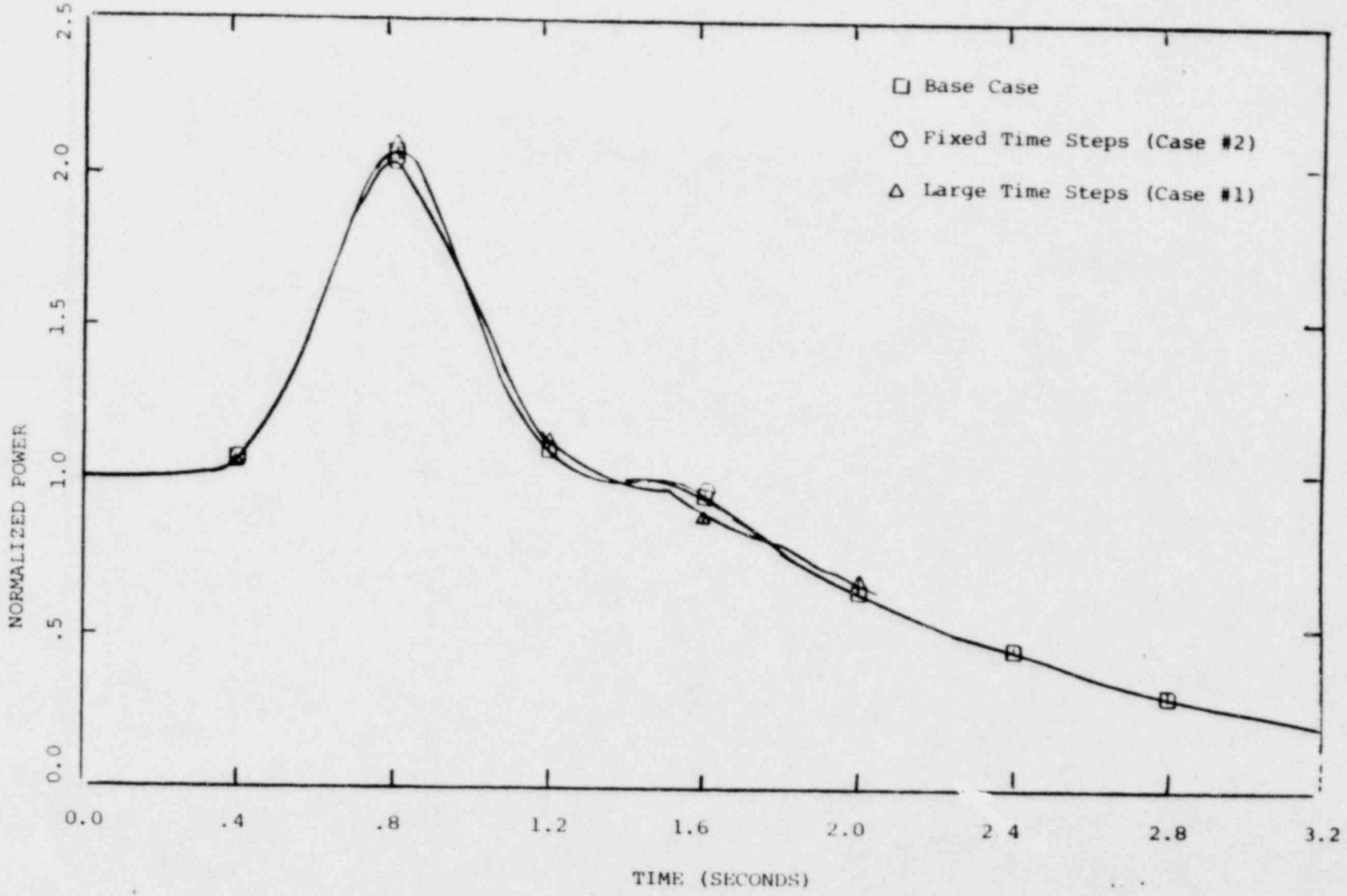

Figure A.4.1
TTWOB, Time Step Sensitivity,
Power Vs. Time

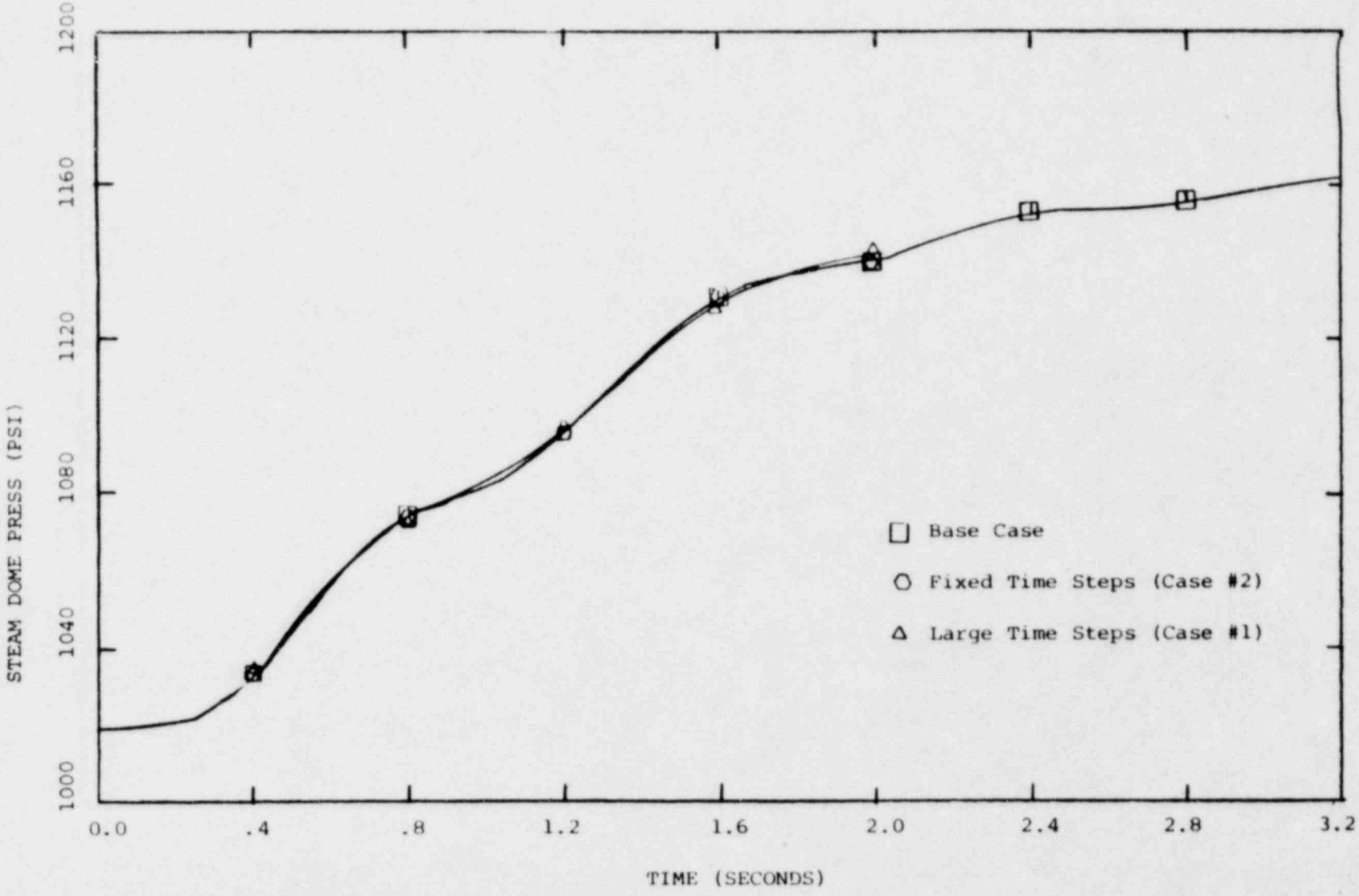

Figure A.4.2
TTWOB, Time Step Sensitivity,
Steam Dome Pressure
Vs. Time

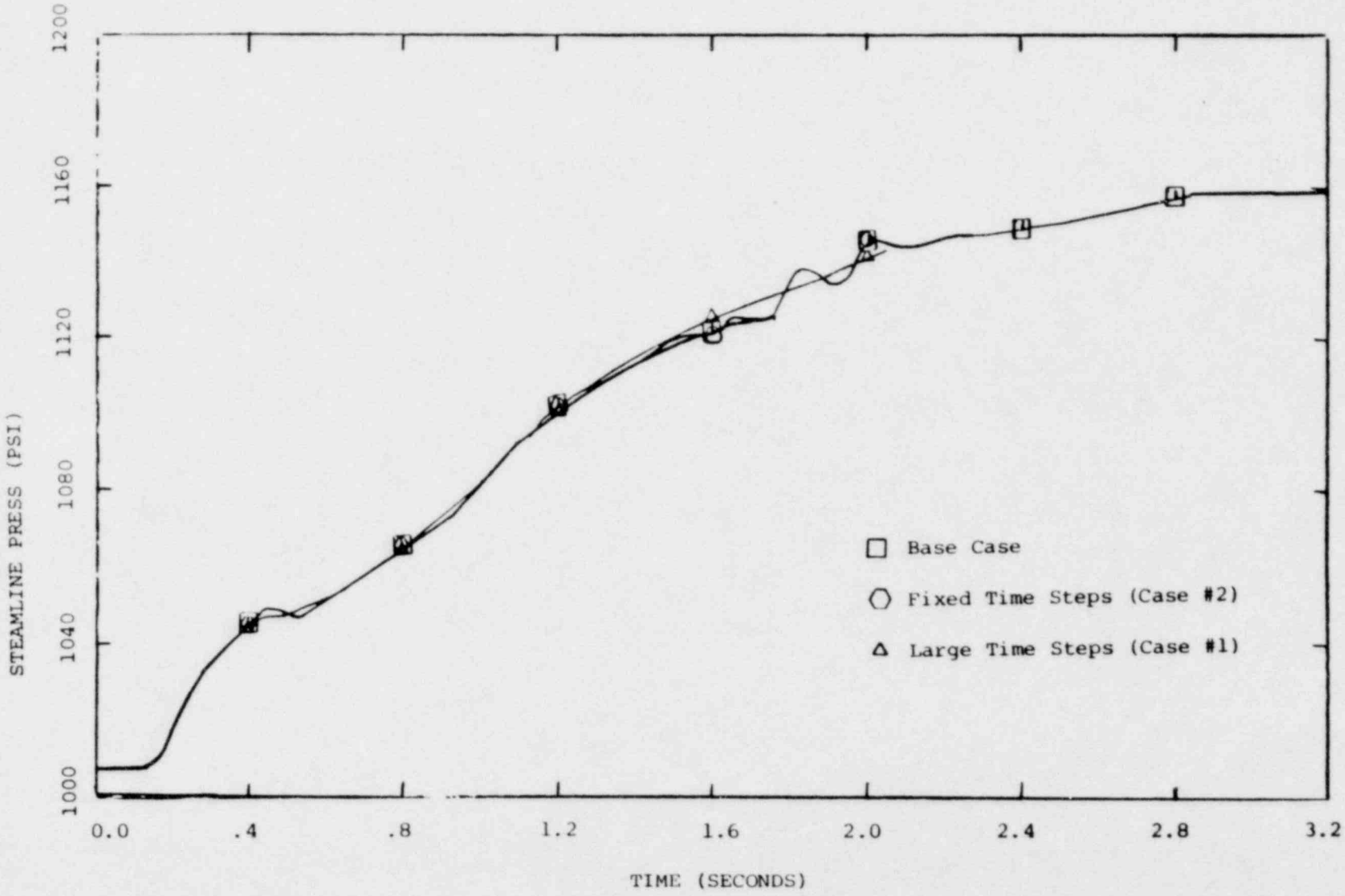

Figure A.4.3
TTWOB, Time Step Sensitivity,
Steam Line Pressure
Vs. Time

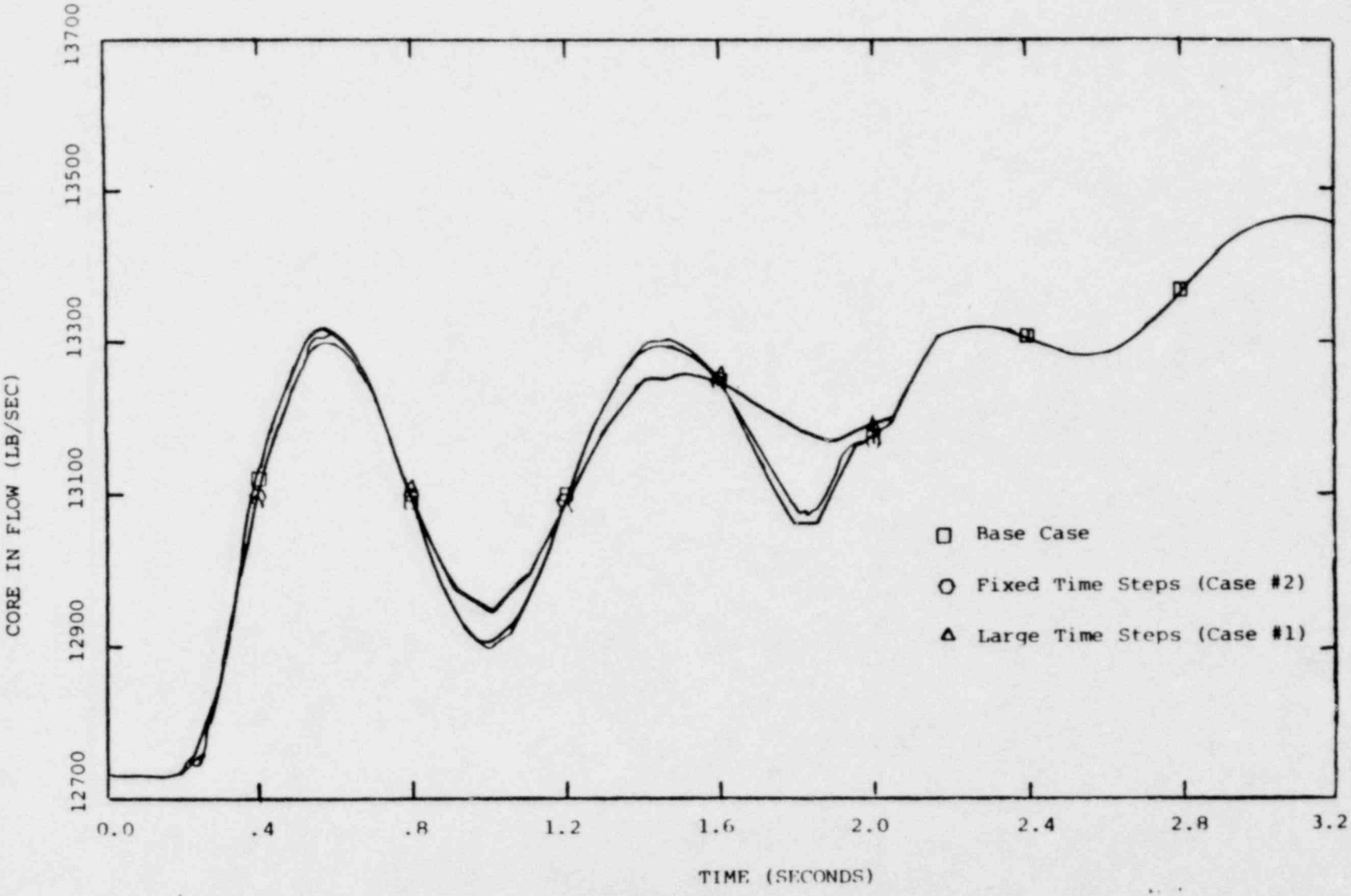

Figure A.4.4
TTWOB, Time Step Sensitivity,
Core Flow Vs. Time

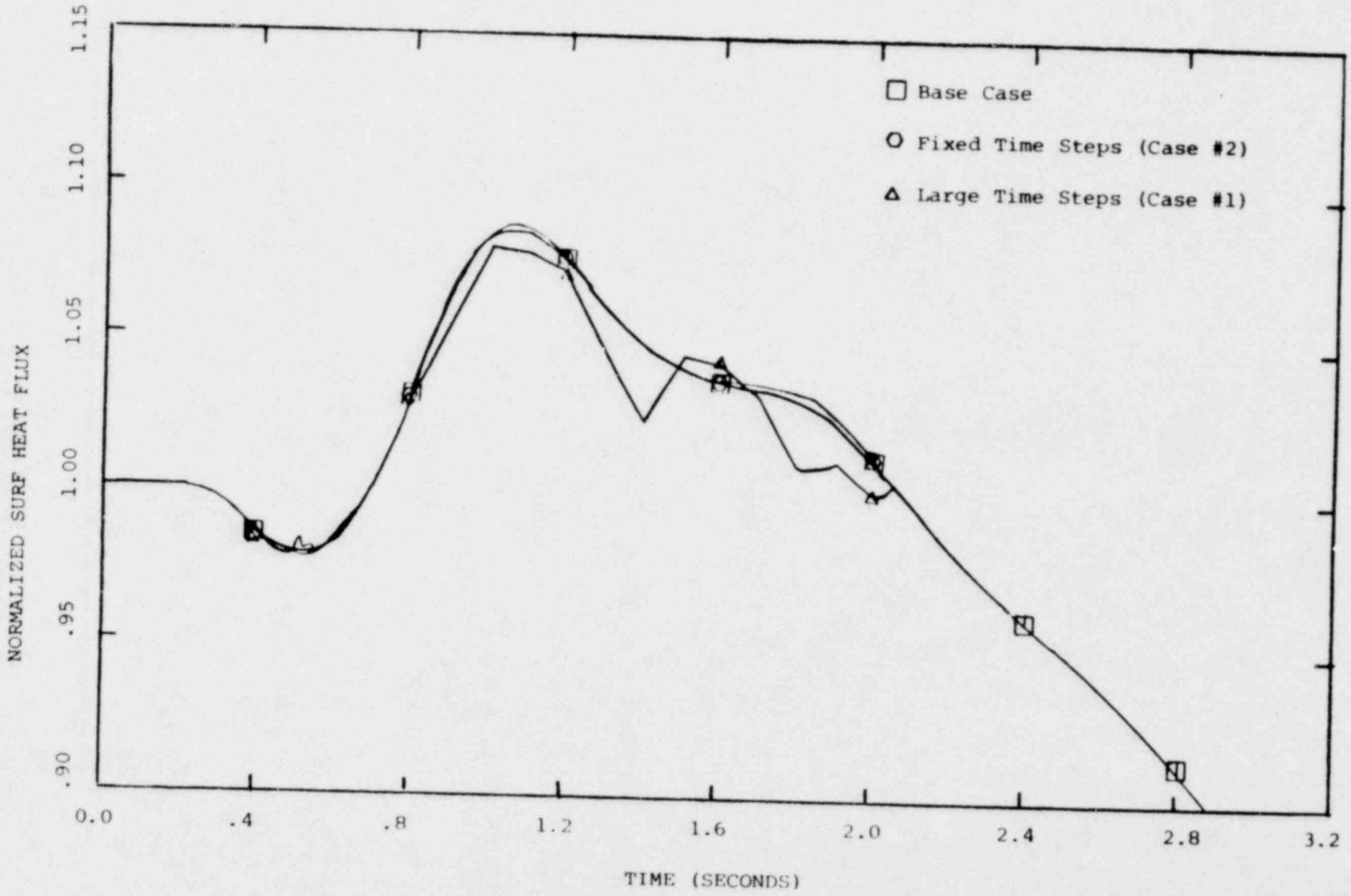

Figure A.4.5
TTWOB, Time Step Sensitivity,
Core Heat Flux Vs. Time

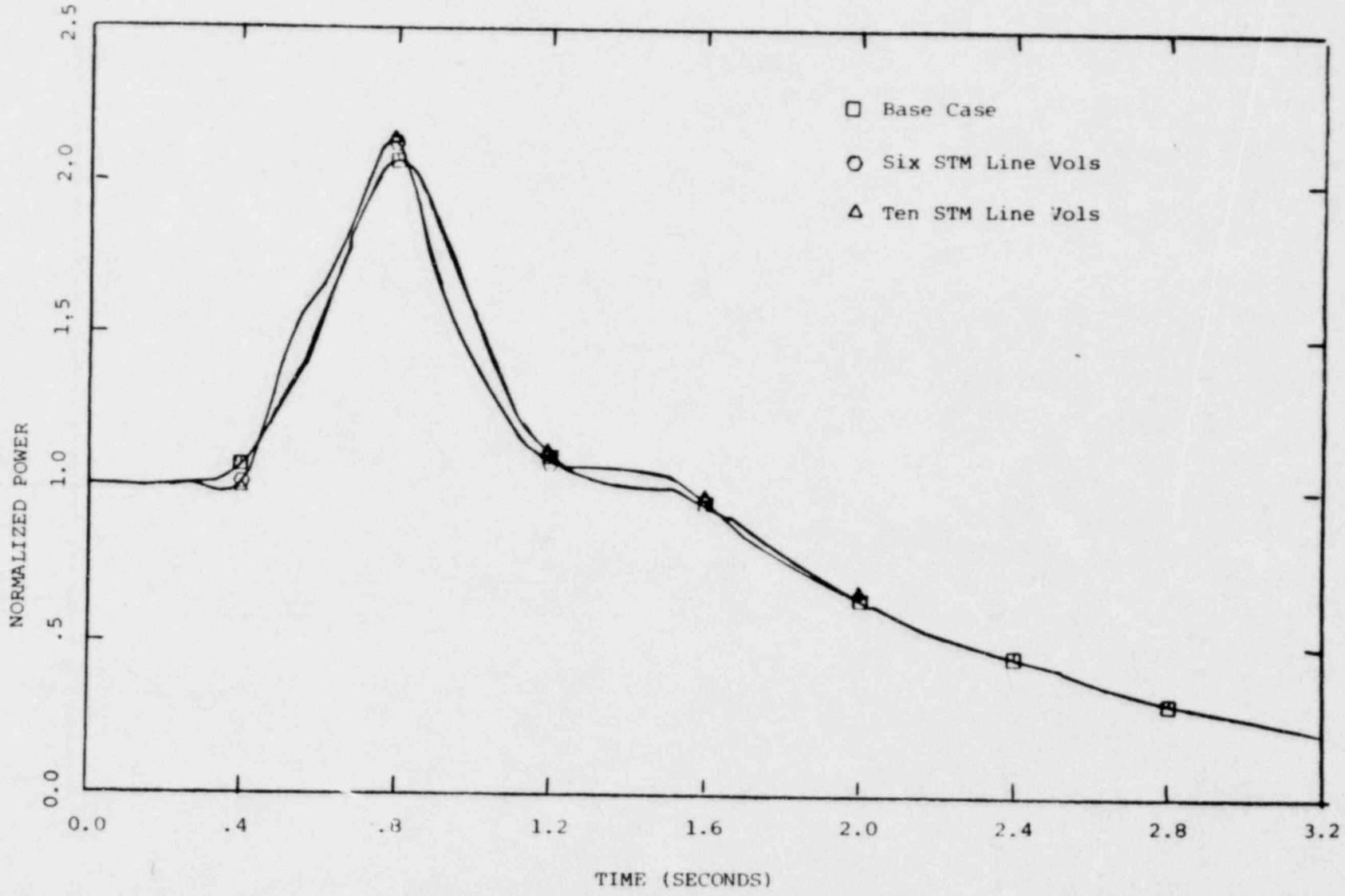

Figure A.4.6
TTWOB, Steam Line Nodalization
Study, Power Vs. Time

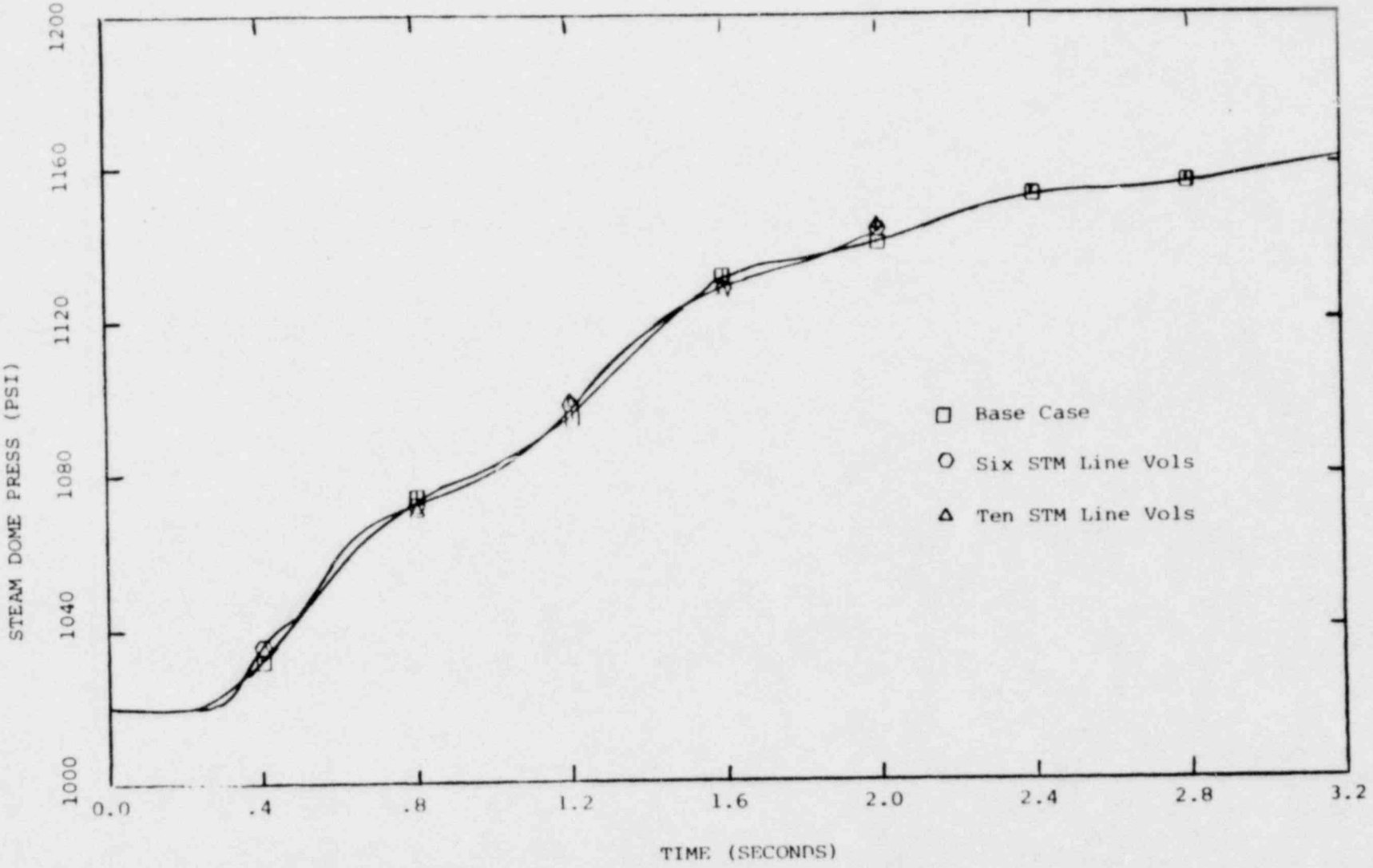

Figure A.4.7
TTWOB, Steam Line Nodalization
Study, Steam Dome Pressure
Vs. Time

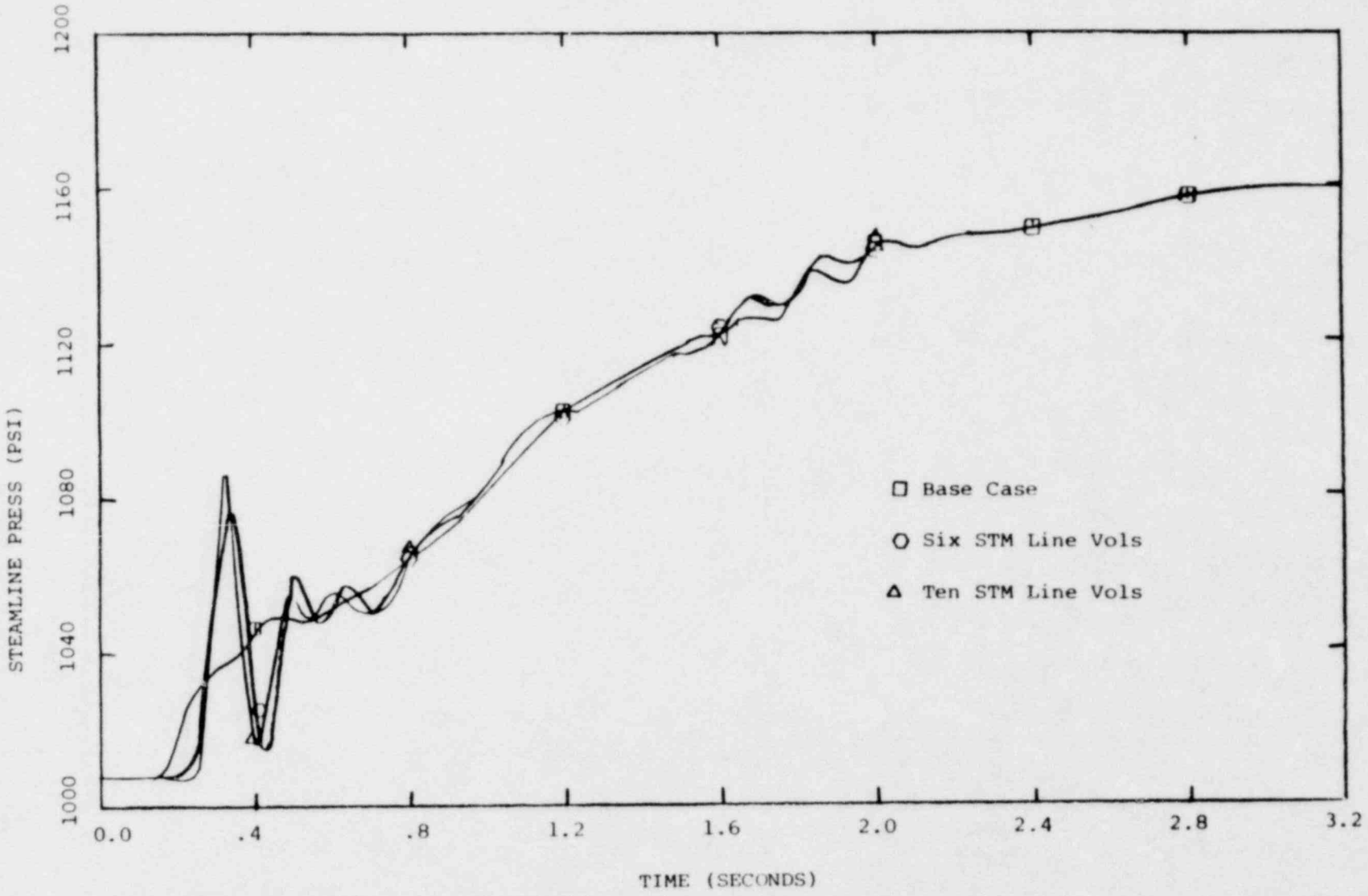

Figure A.4.8
TTWOB, Steam Line Nodalization
Study, Steam Line Pressure
Vs. Time

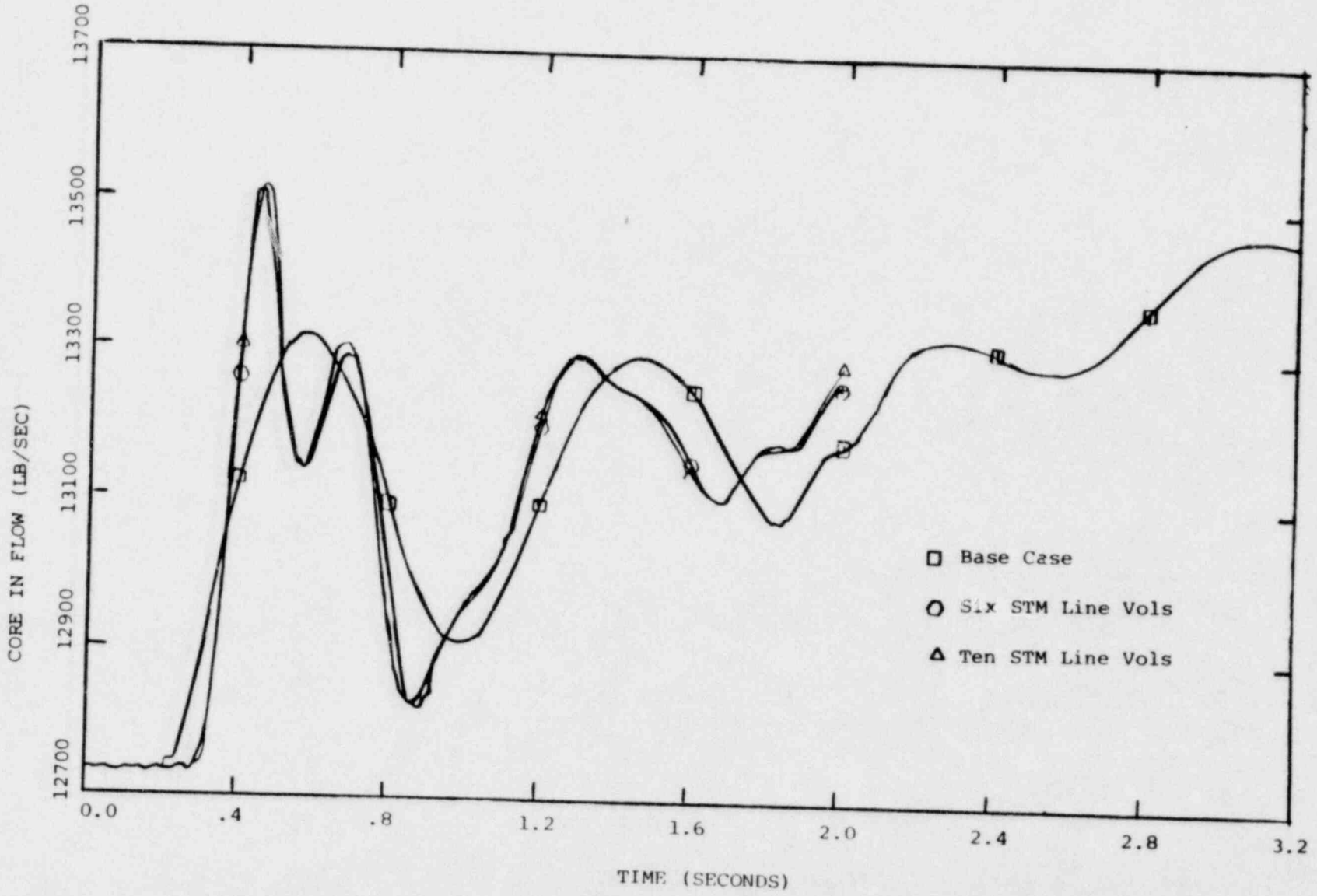

Figure A.4.9
TTWOB, Steam Line Nodalization
Study, Core Flow Vs. Time

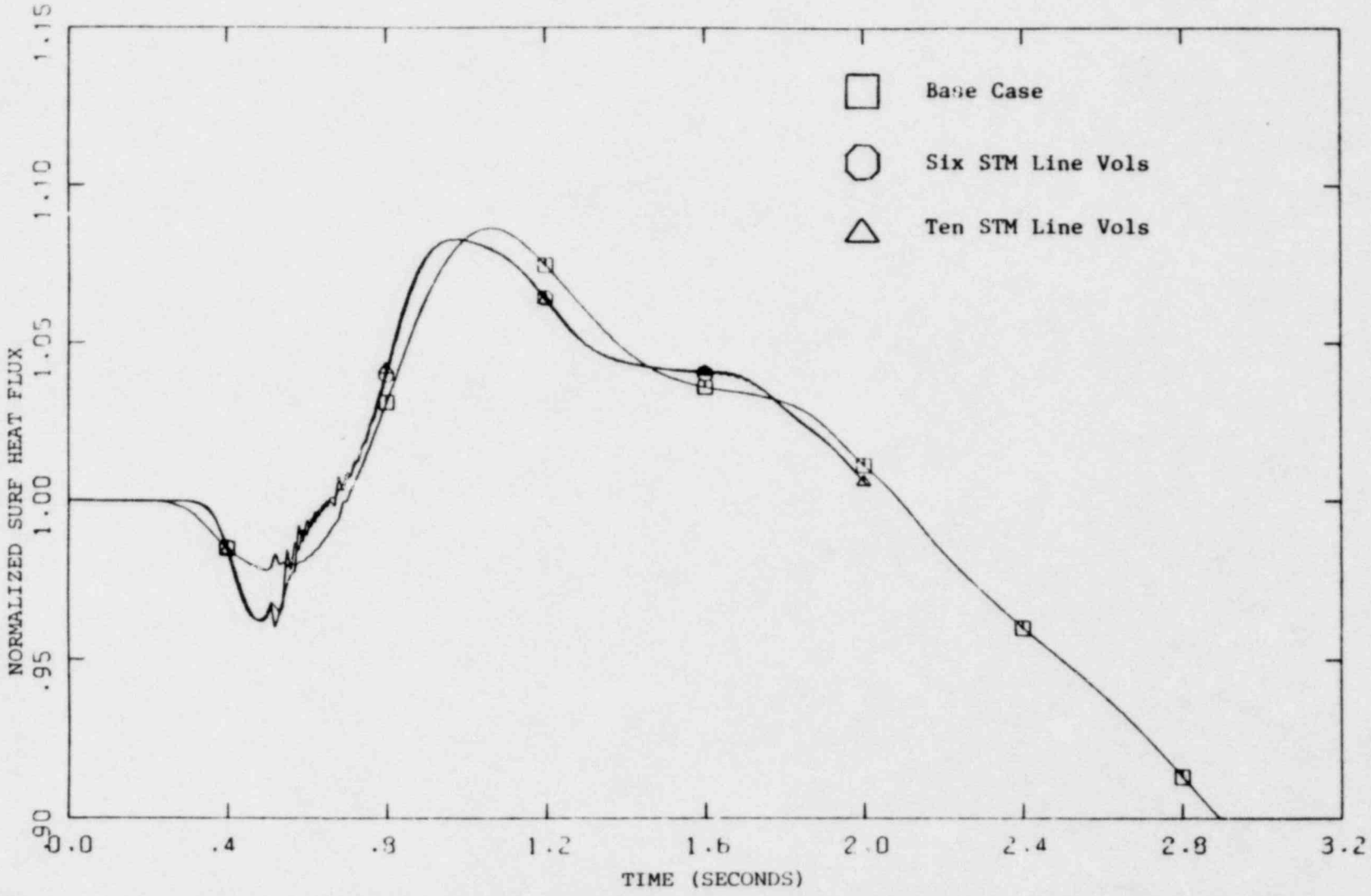

Figure A.4.10
TTWOB, Steam Line Nodalization
Study, Core Heat Flux
Vs. Time

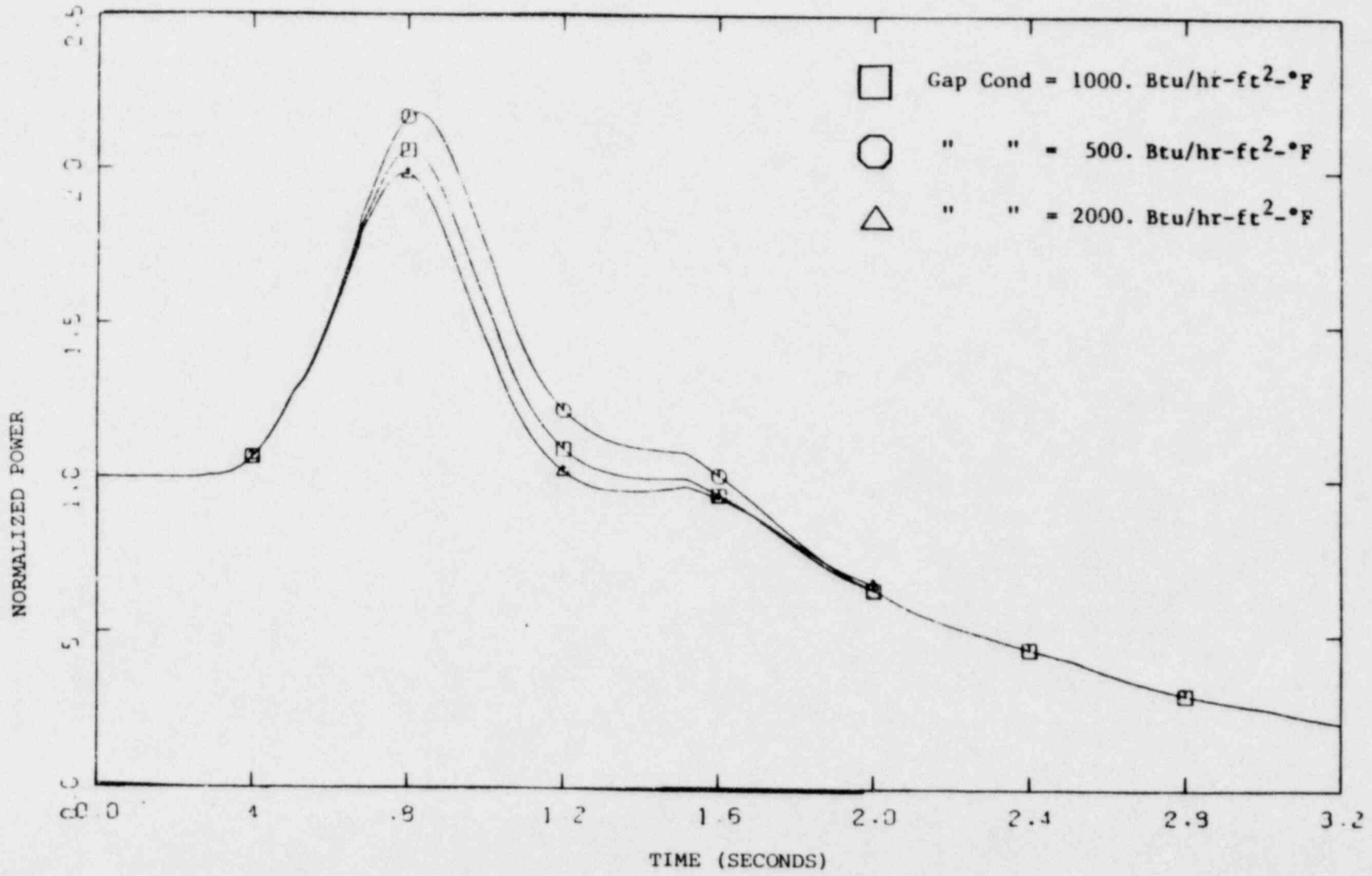

Figure A.4.11
TTWOB, Gap Conductivity Study,
Power Vs. Time

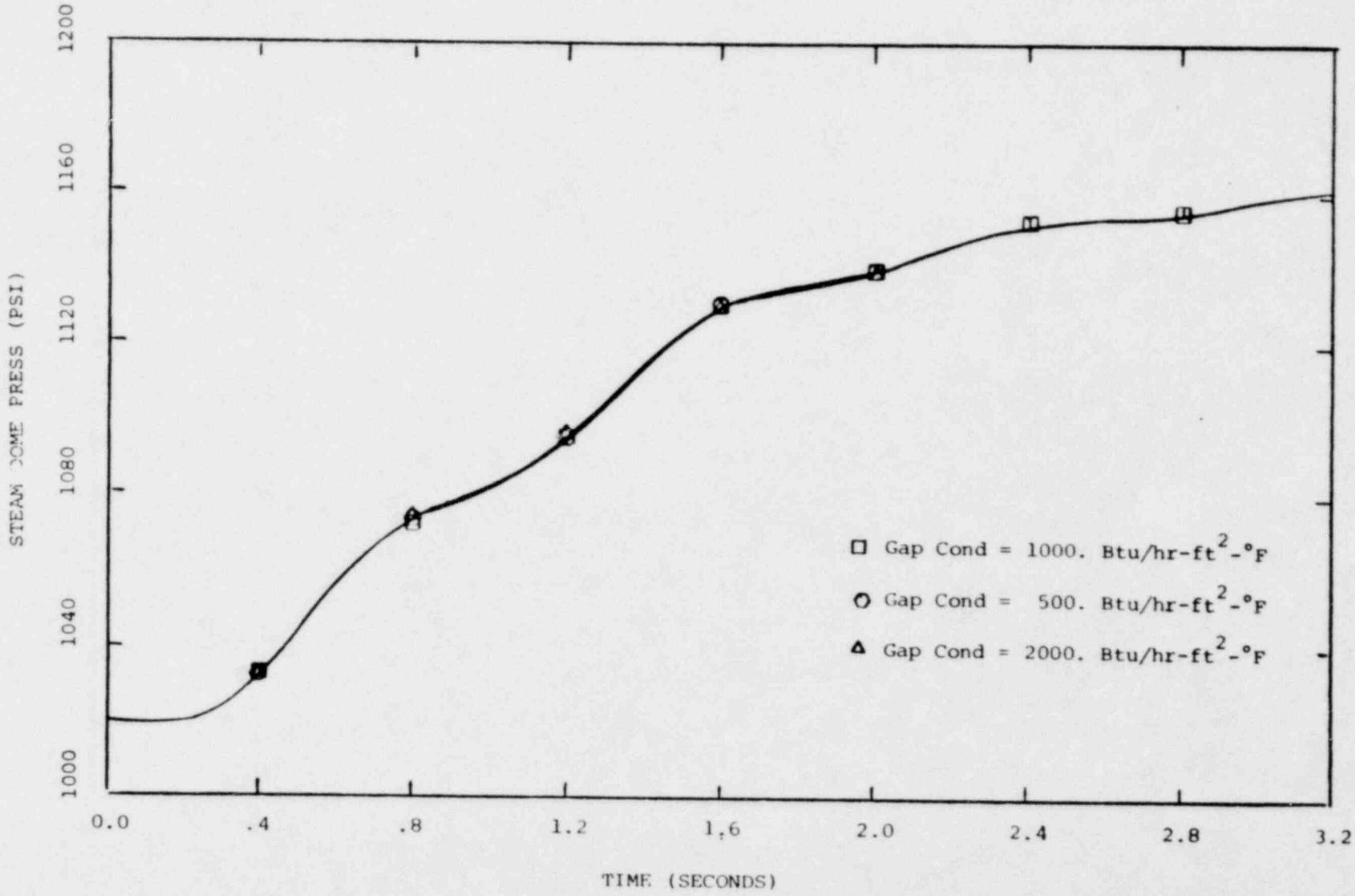

Figure A.4.12
TTWOB, Gap Conductivity Study,
Steam Dome Pressure
Vs. Time

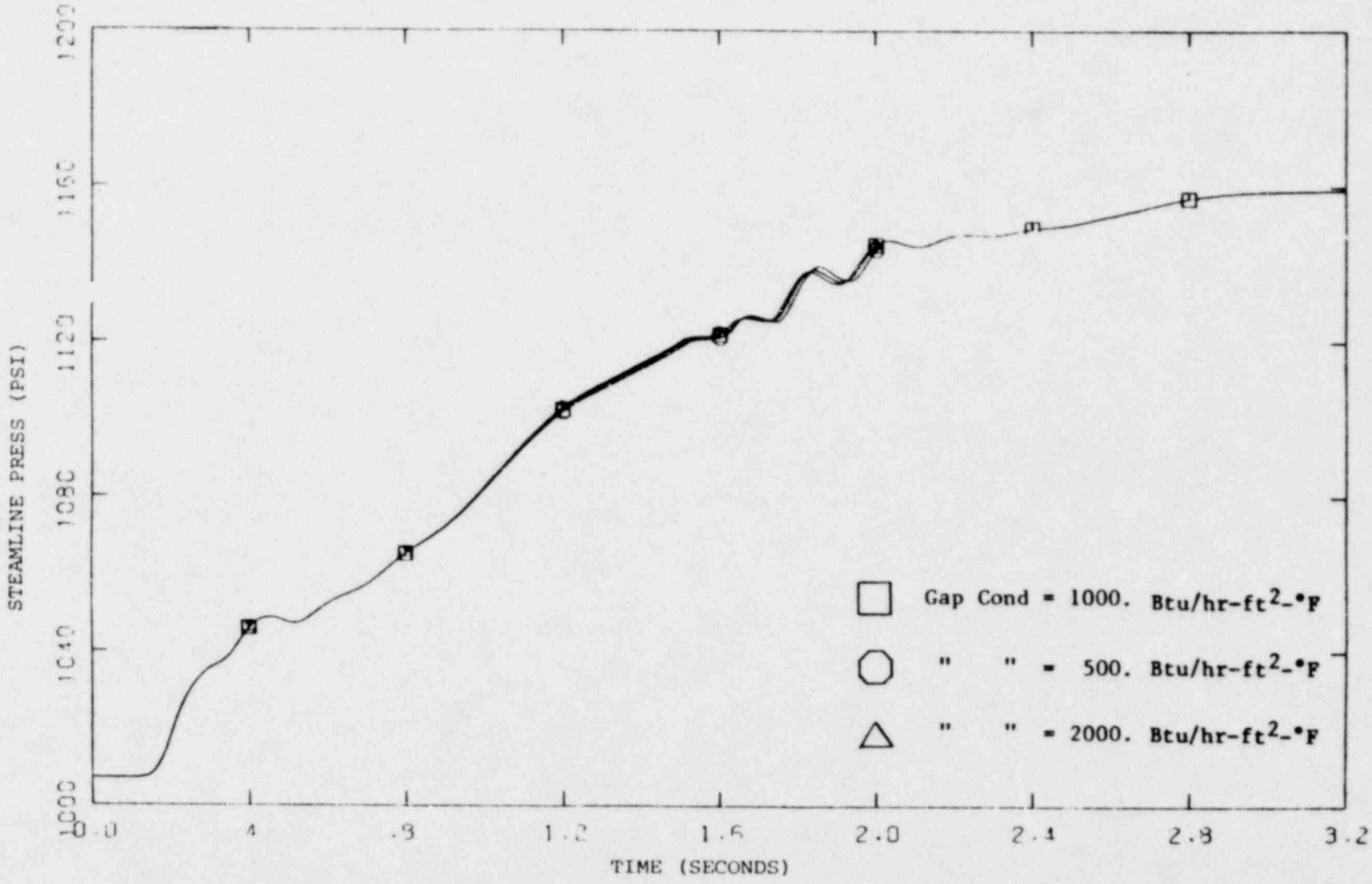

Figure A.4.13
TTWOB, Gap Conductivity Study,
Steam Line Pressure
Vs. Time

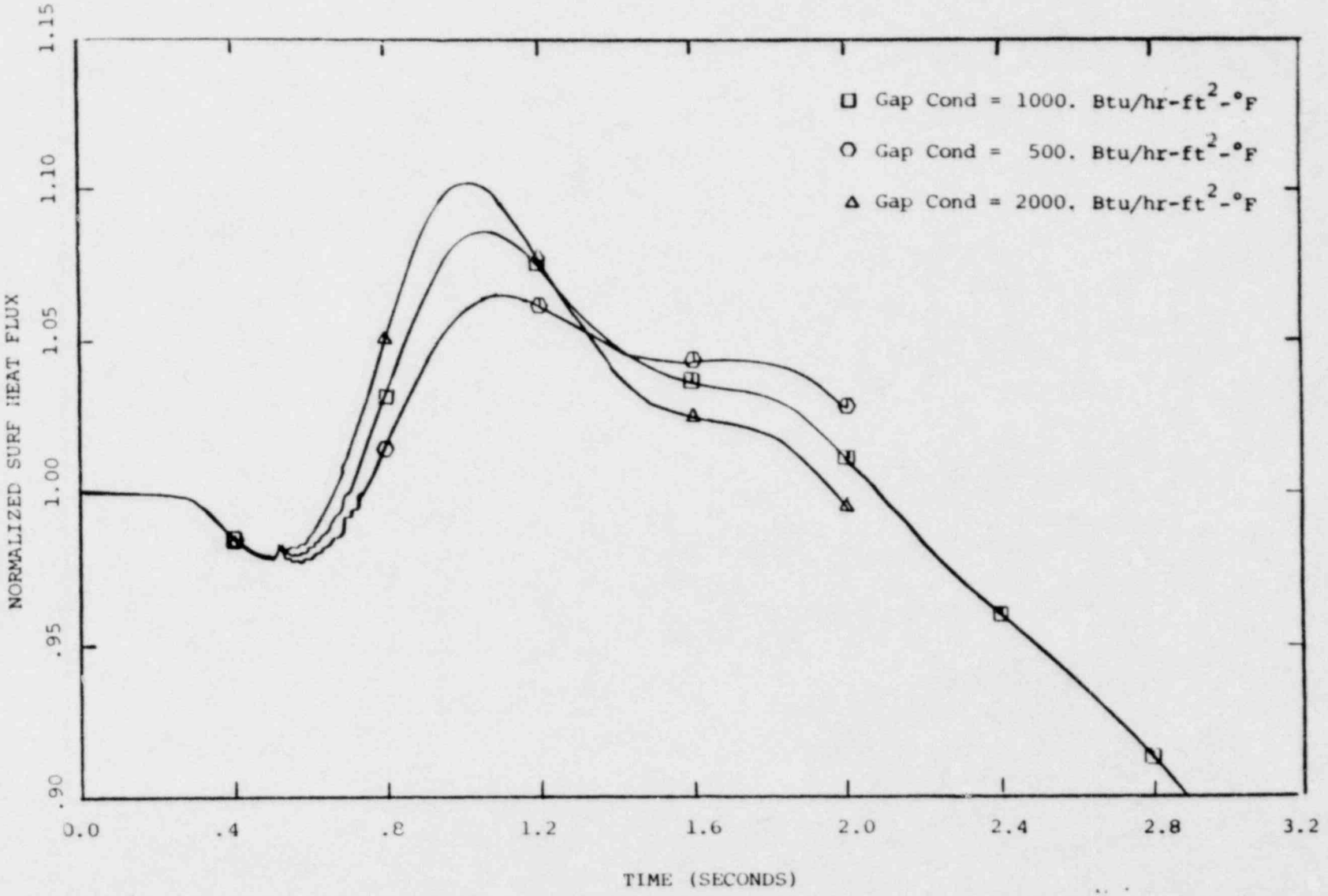

Figure A.4.14
TTWOB, Gap Conductivity Study,
Core Heat Flux
Vs. Time

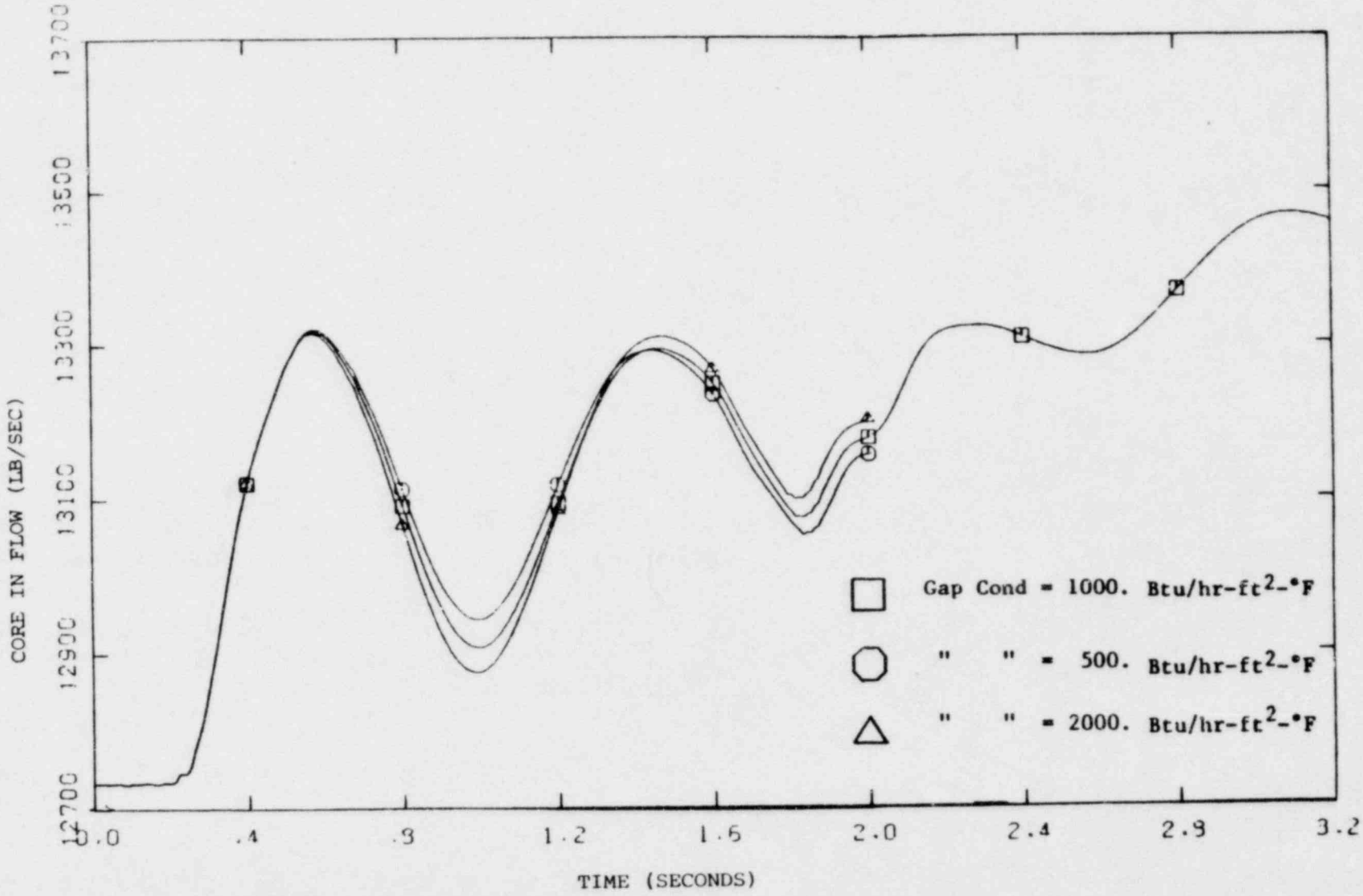

Figure A.4.15
TTWOB, Gap Conductivity Study,
Core Flow
Vs, Time

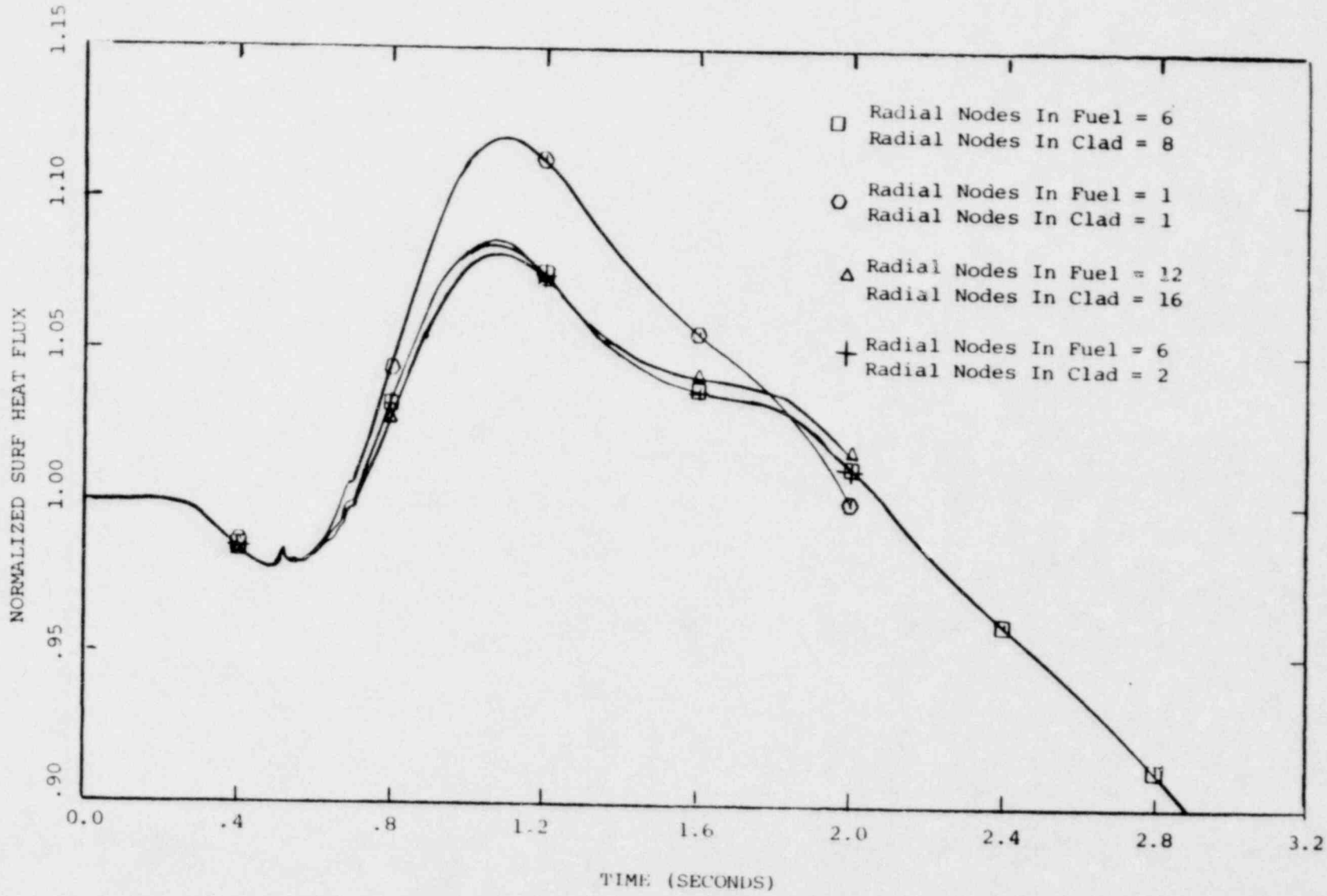

Figure A.4.16
TTWOB, Core Radial Nodalization
Study, Core Heat Flux
Vs. Time

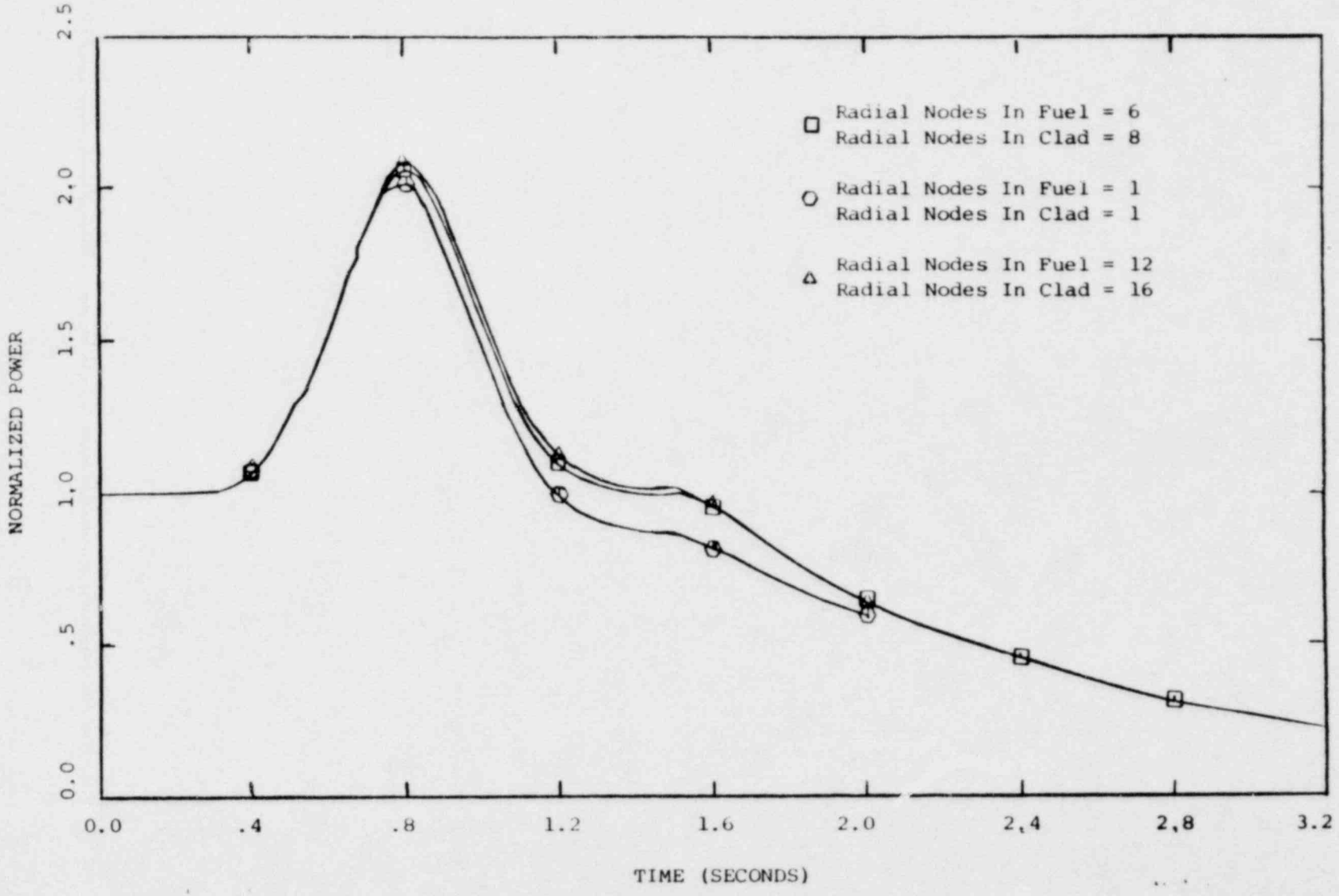

Figure A.4.17
TTWOB, Core Radial Nodalization
Study, Power Vs. Time

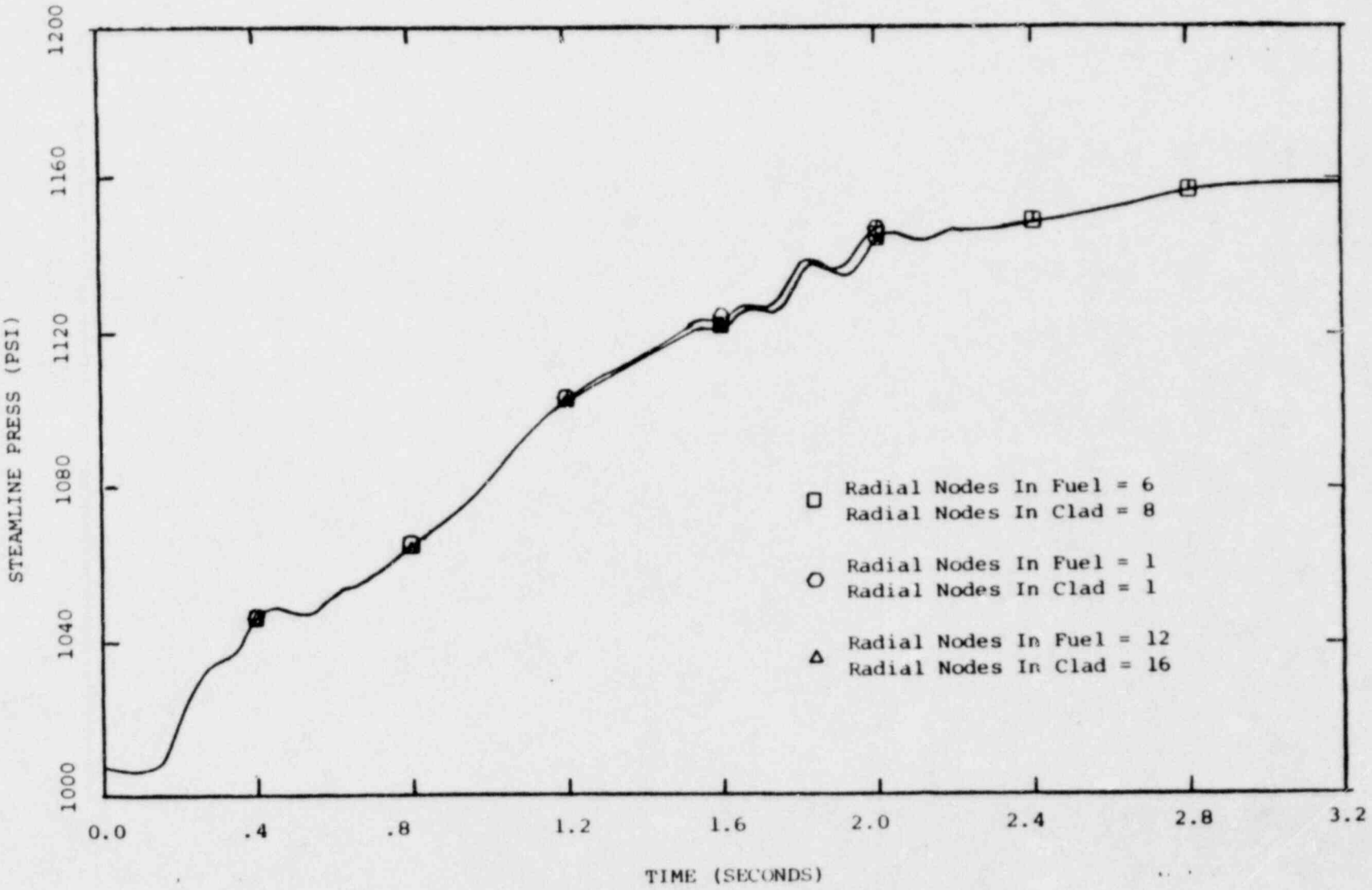

Figure A.4.18
TTWOB, Core Radial Nodalization
Study, Steam Line Pressure
Vs. Time

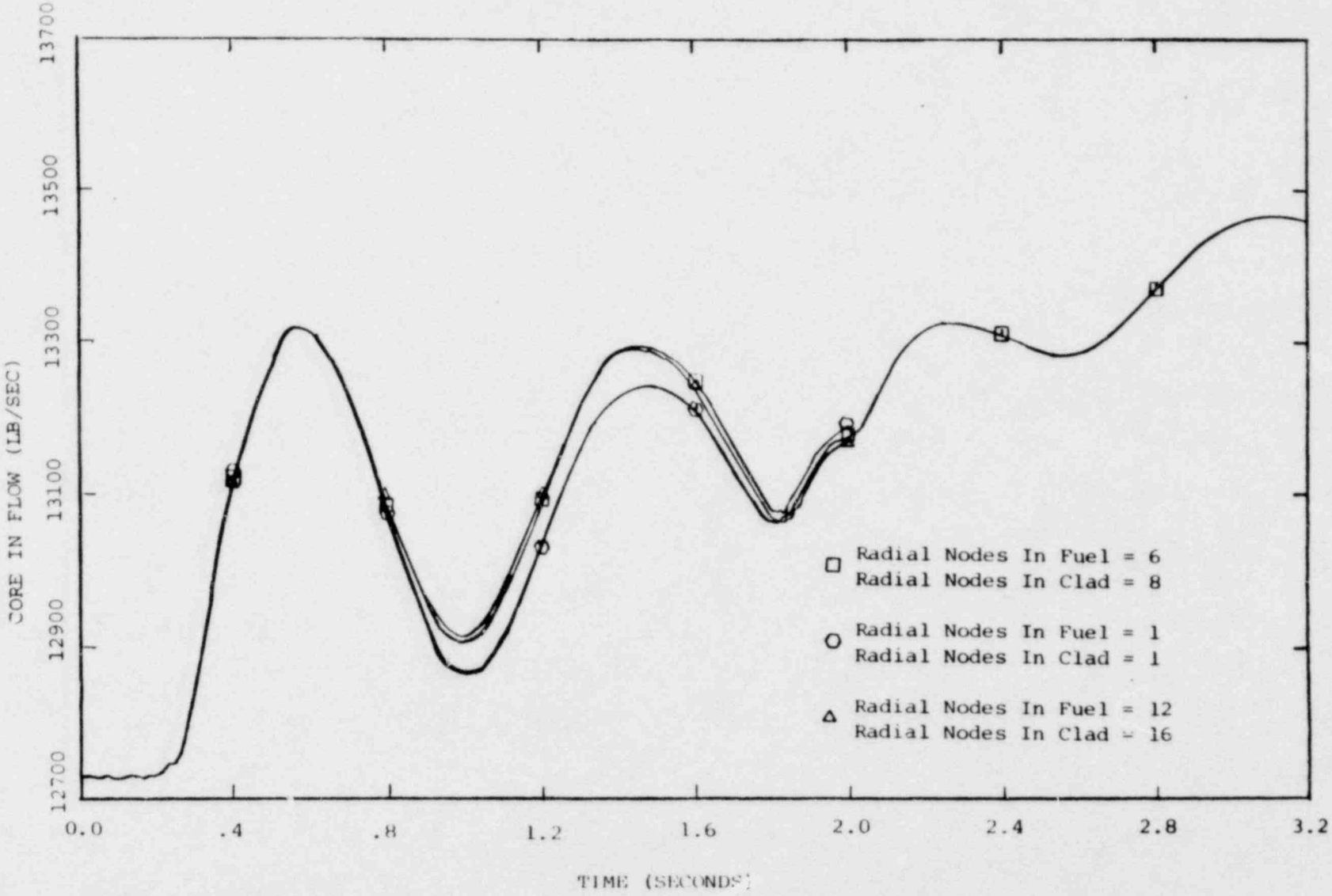

Figure A.4.19
TTWOB, Core Radial Nodalization
Study, Core Flow Vs. Time

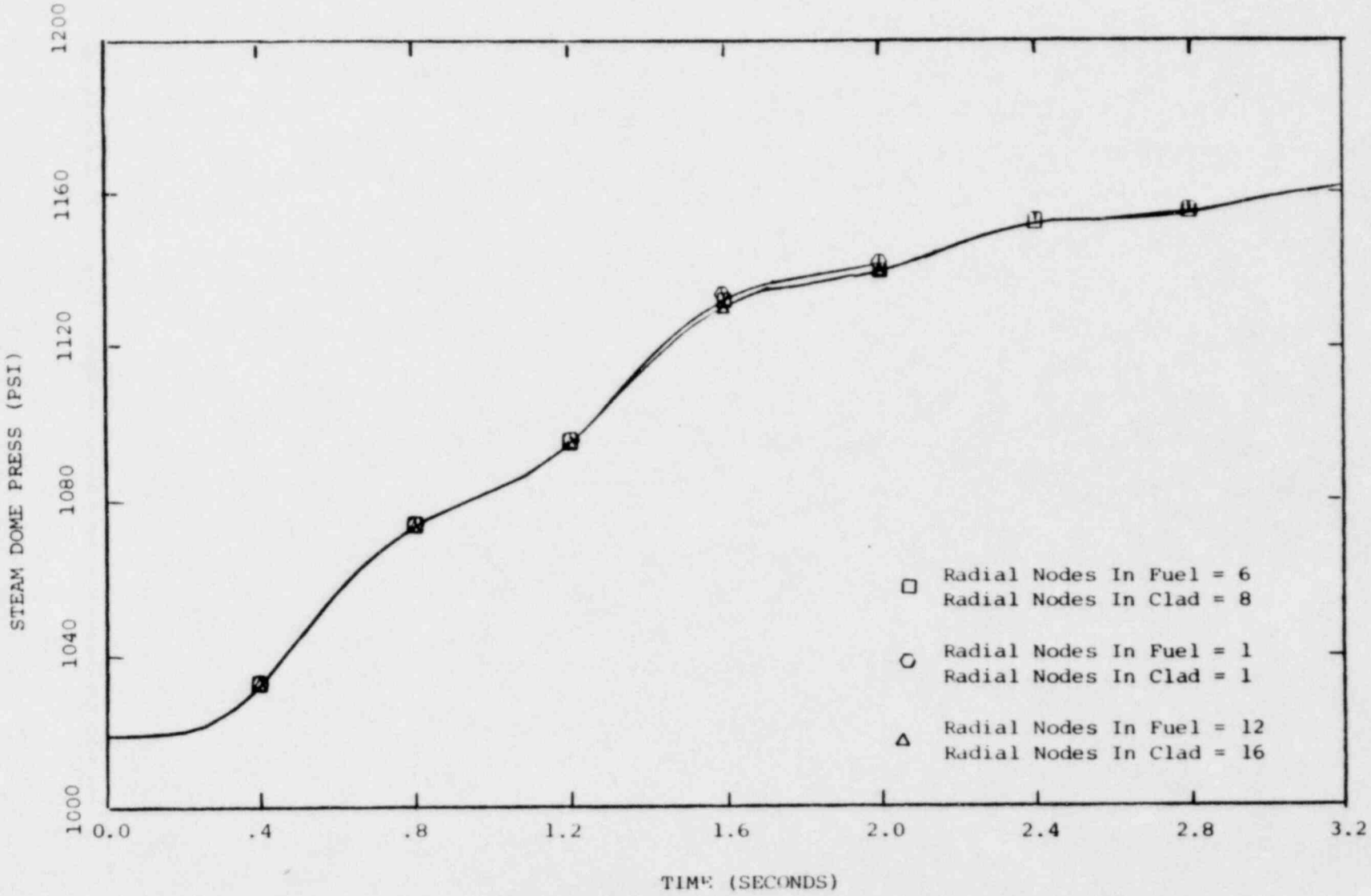

Figure A.4.20
TTWOB, Core Radial Nodalization
Study, Steam Dome Pressure
Vs. Time

VERMONT YANKEE RETRAN MODEL

FOR

LOSS OF FEEDWATER HEATER TRANSIENT

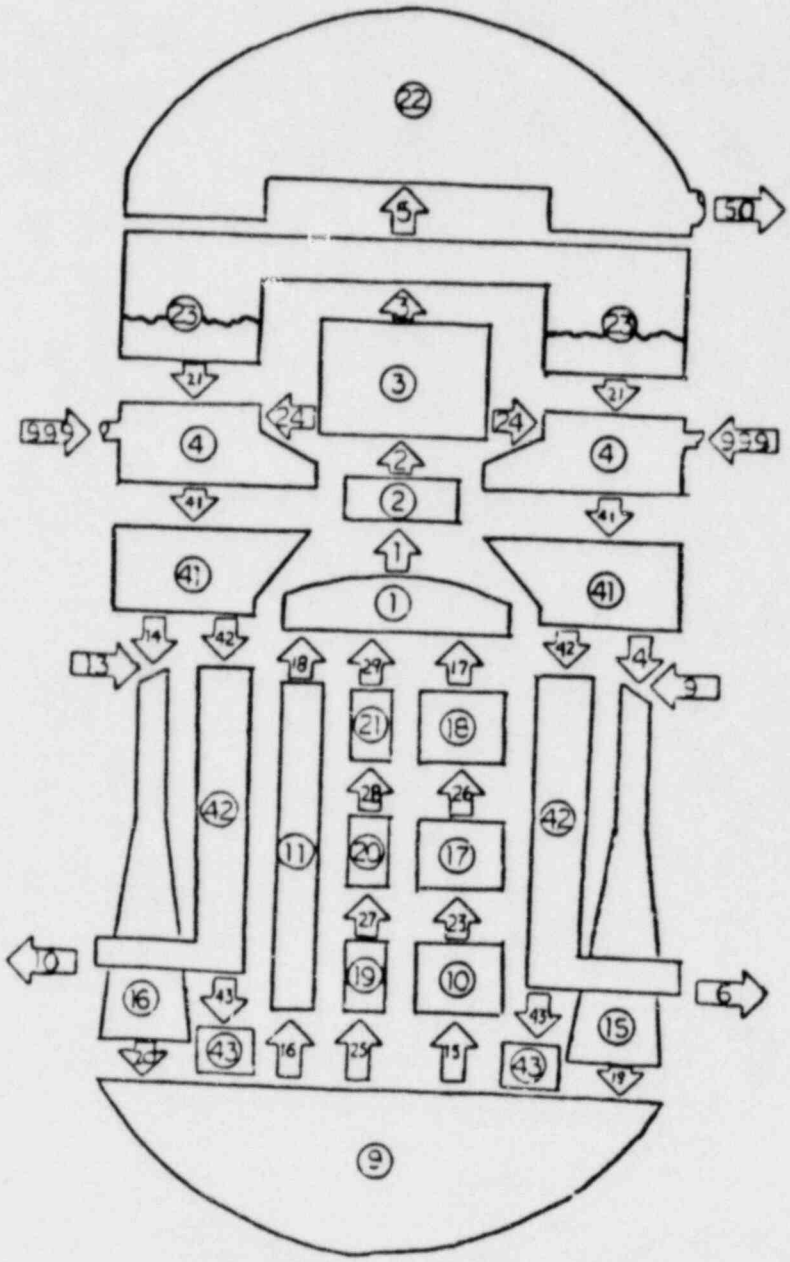

Figure A.5.1
LOFWH, Nodalization Scheme

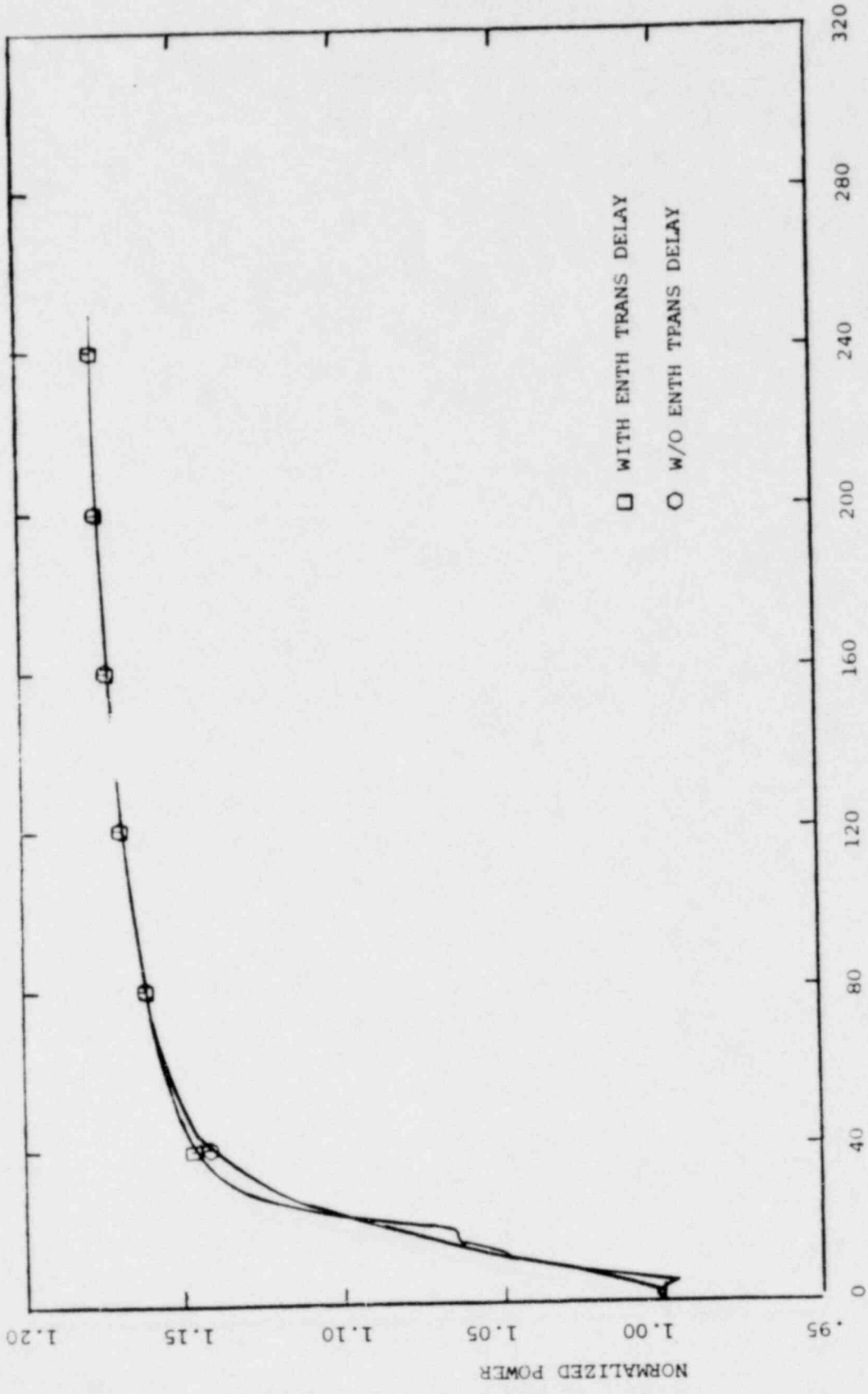

Figure A.5.2
LOFWH, Core Power Vs. Time

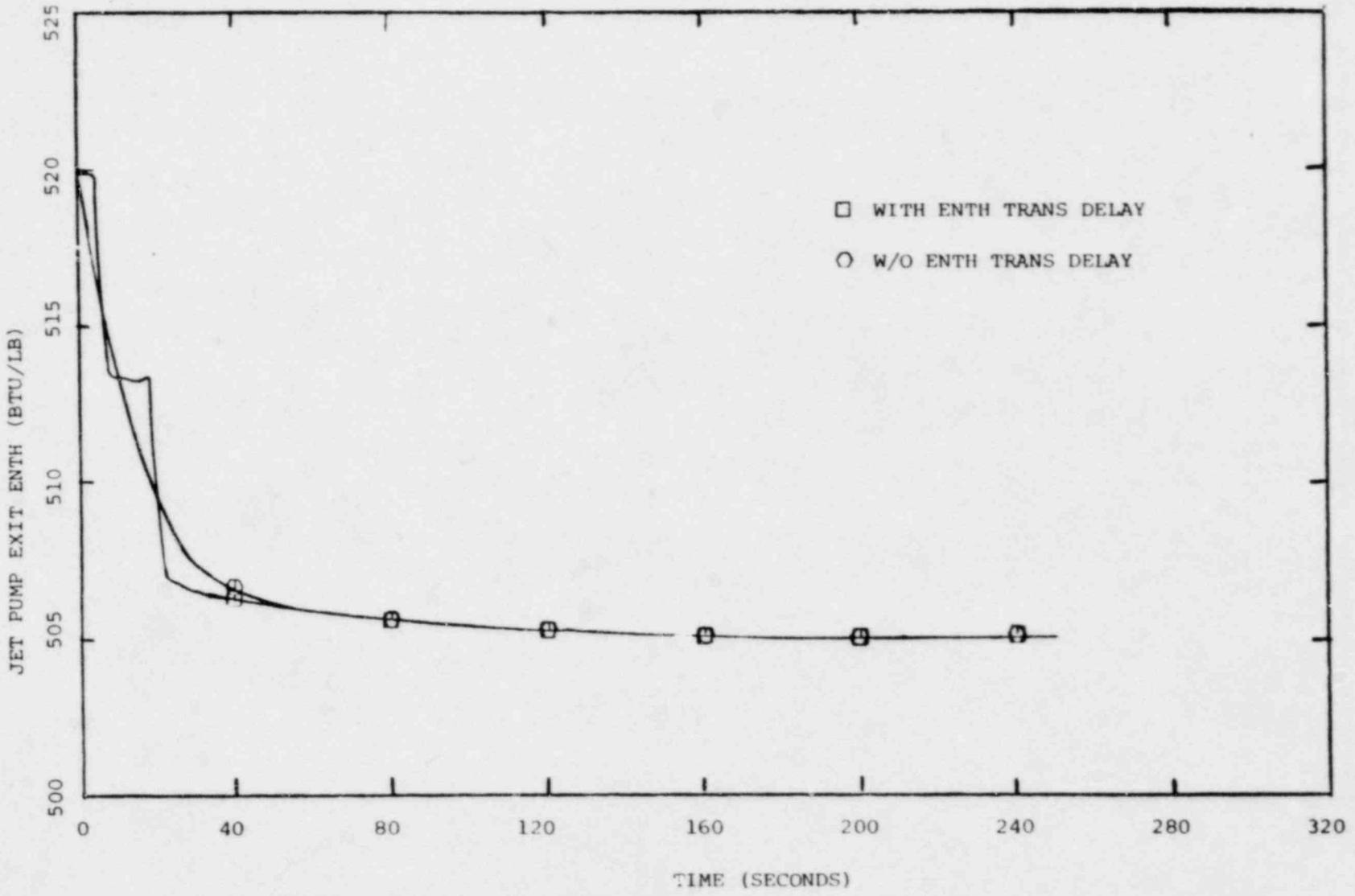

Figure A.5.3
LOFWH, Jet Pump Exit Enthalpy
Vs. Time

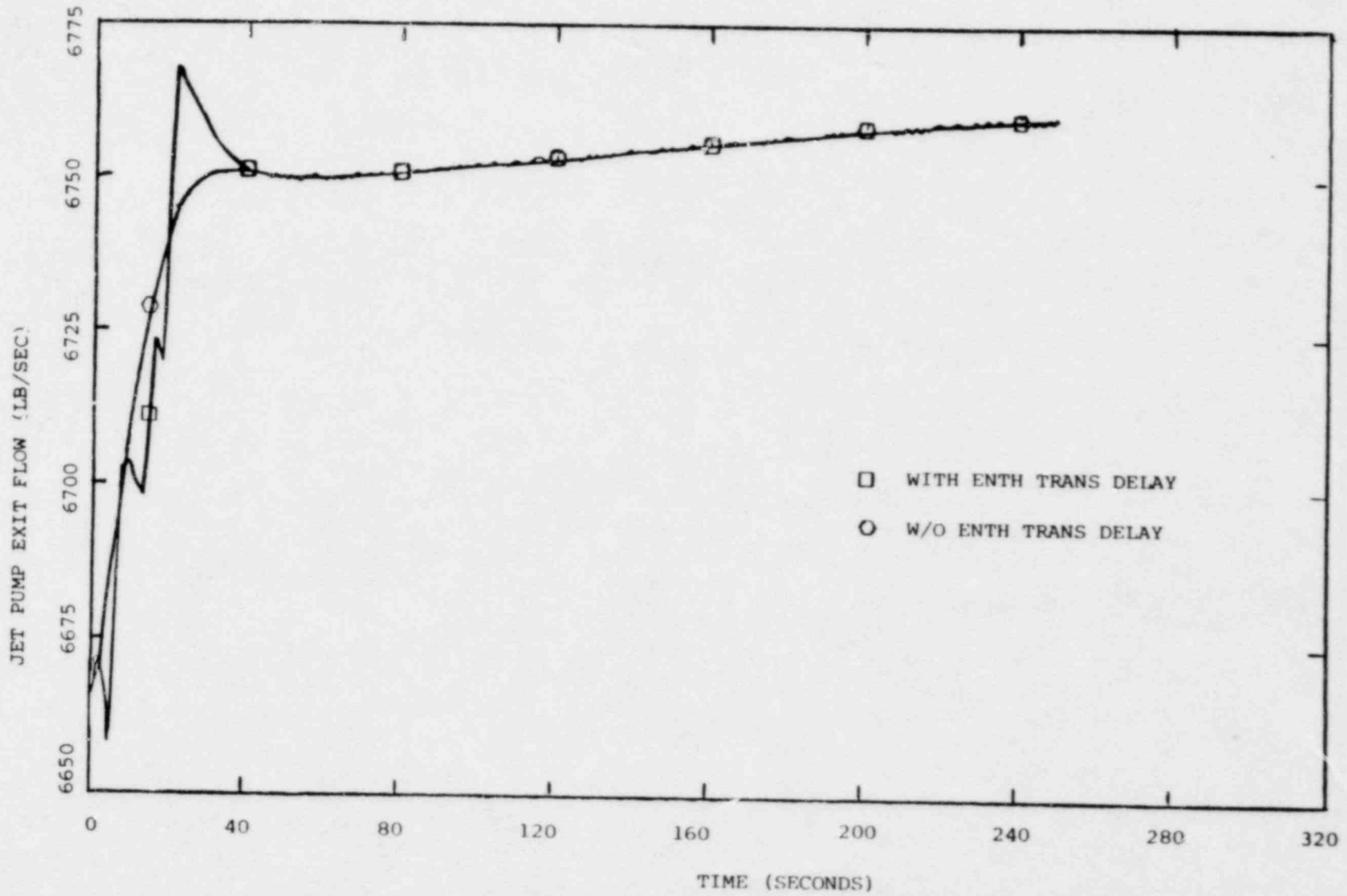

Figure A.5.4
LOFWH, Jet Pump Exit Flow
Vs. Time

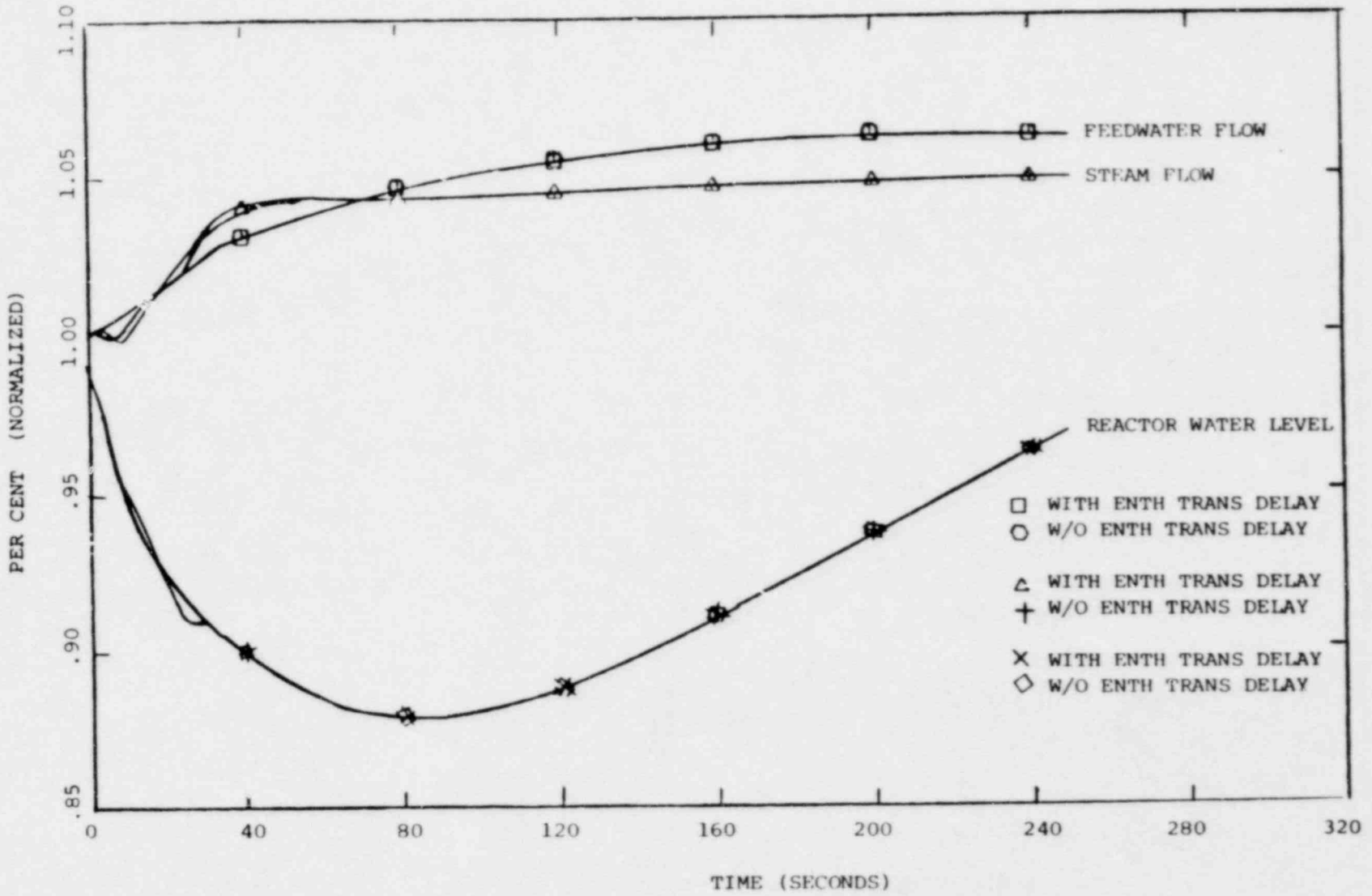

Figure A.5.5
LOFWH, FW Flow, Steam Flow,
and Water Level Vs. Time

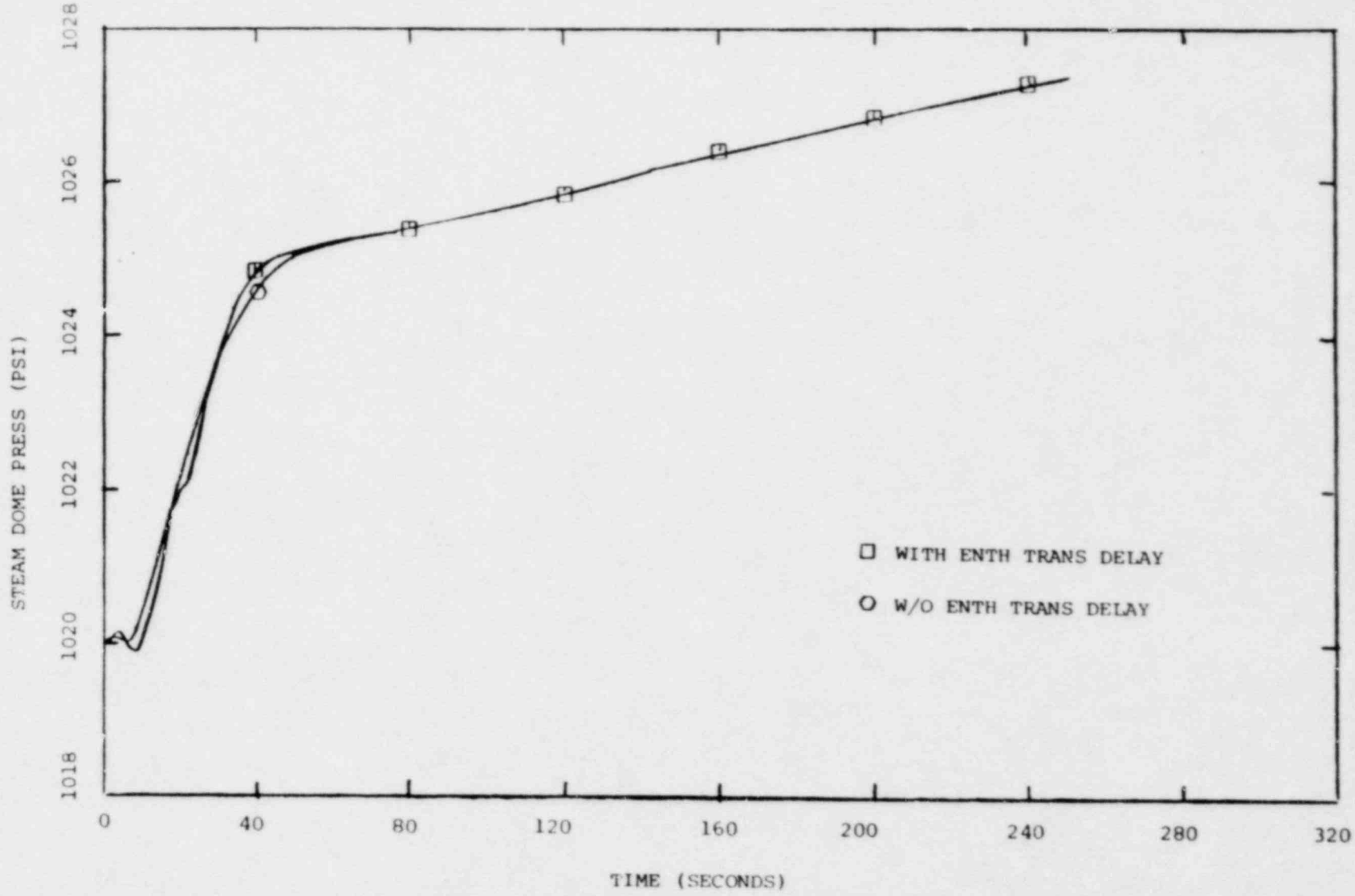

Figure A.5.6
LOFWH, Steam Dome Pressure
Vs. Time

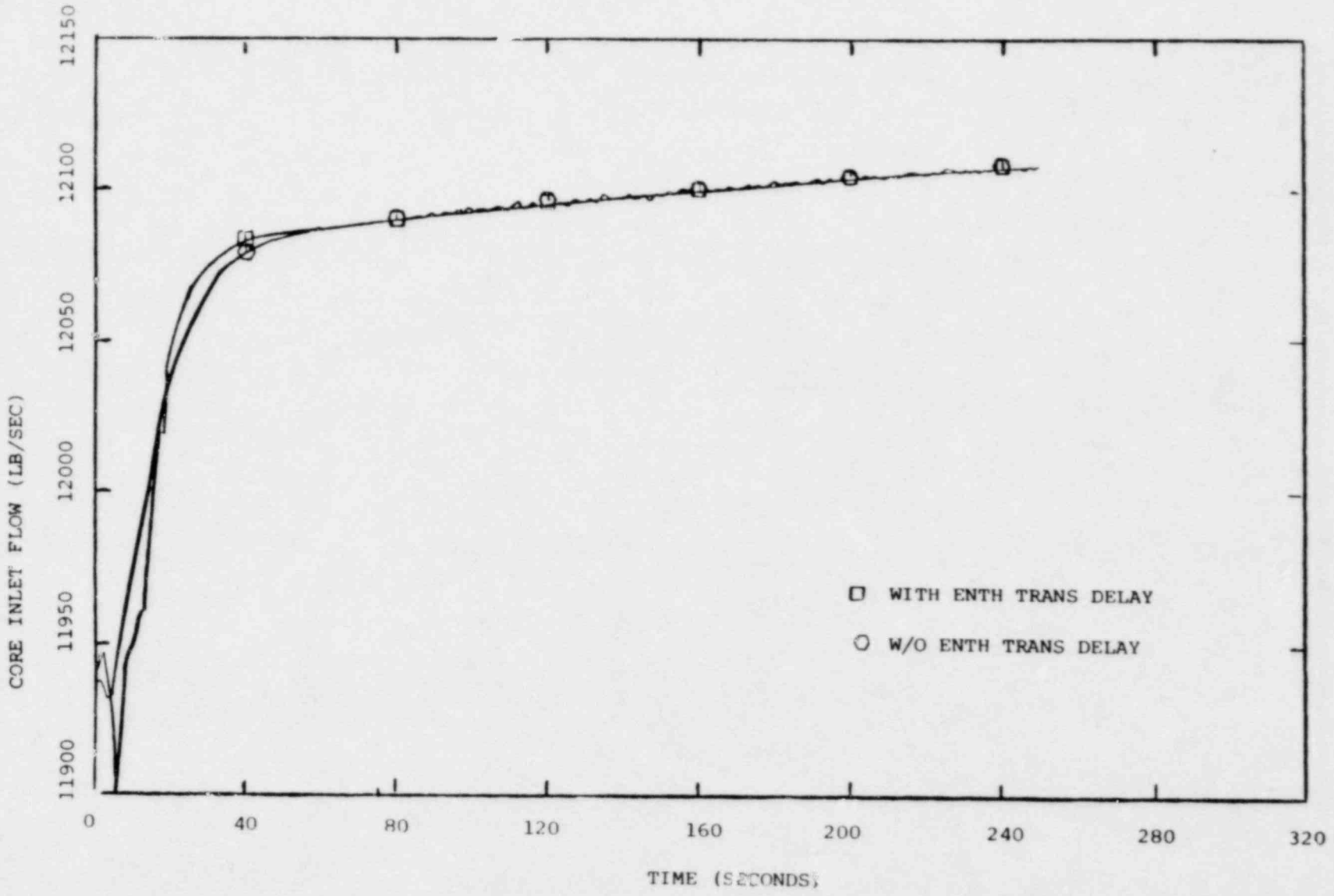

Figure A.5.7
LOFWH, Core Inlet Flow
Vs. Time

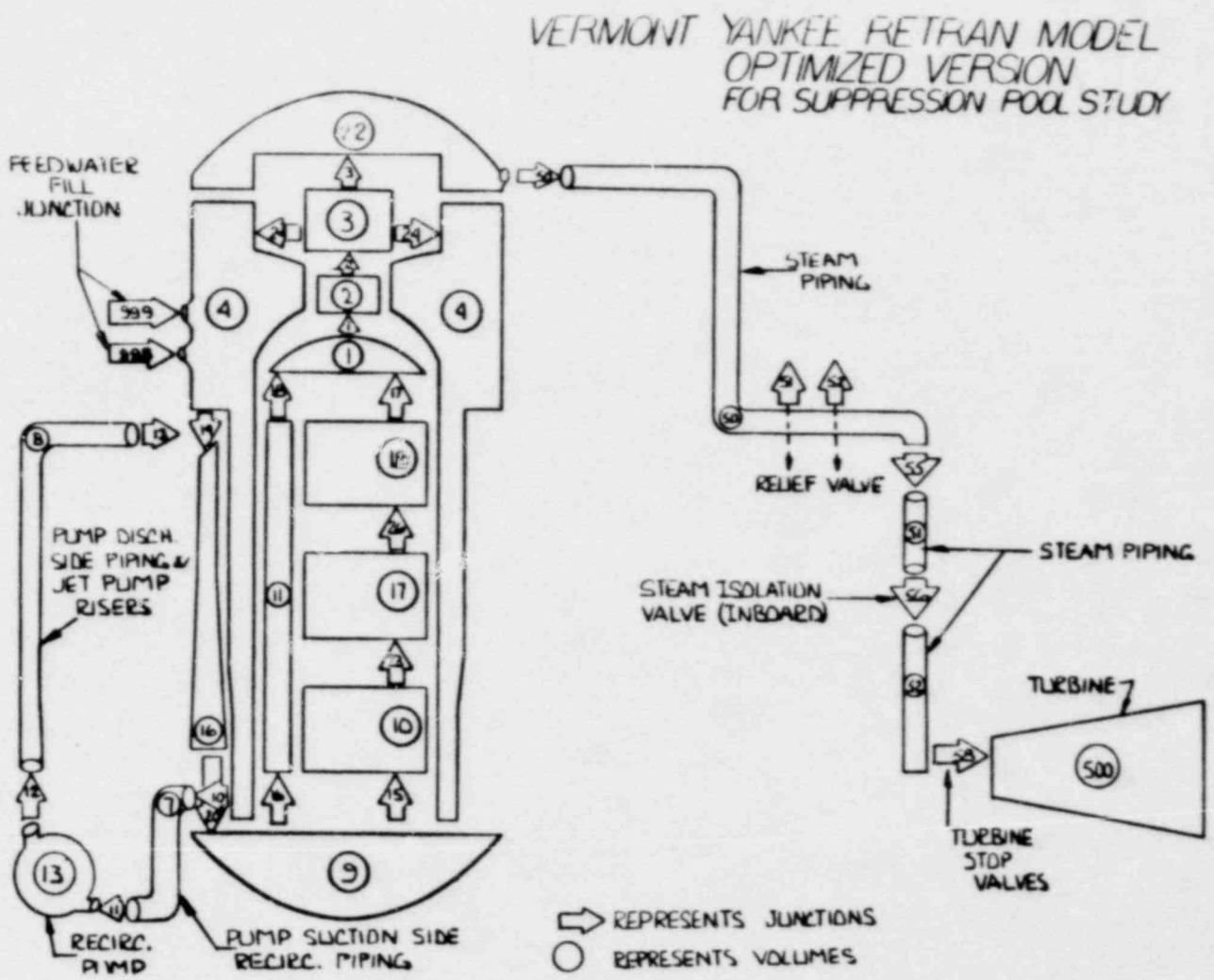

Figure A.6.1
Nodalization Scheme for
SORV Transient

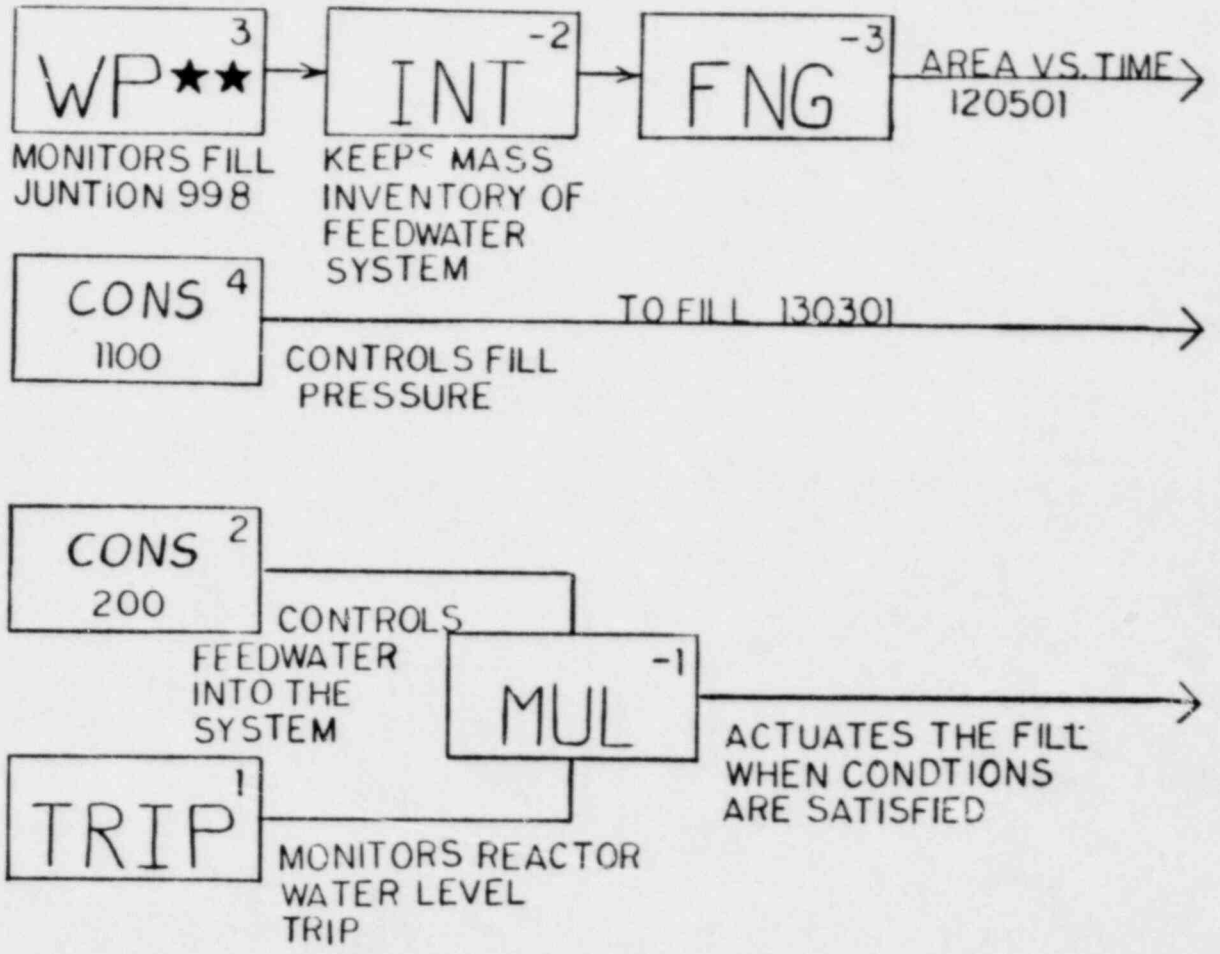

Figure A.6.2
Feedwater Control Scheme for
SORV Transient

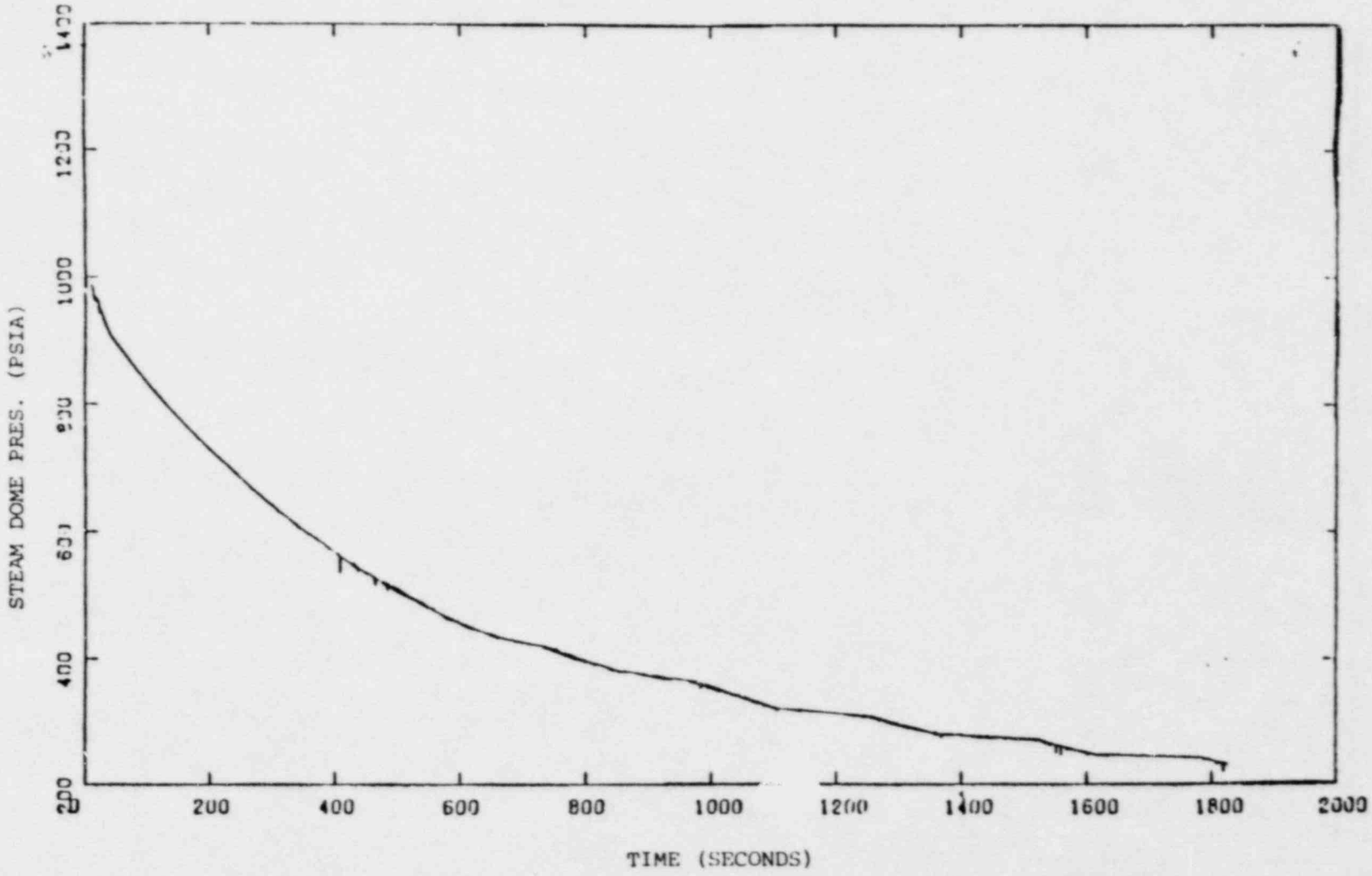

Figure A.6.3
SORV Transient, Steam Dome
Pressure Vs. Time

Figure A.6.4
SORV Transient, Steam Flow
Vs. Time

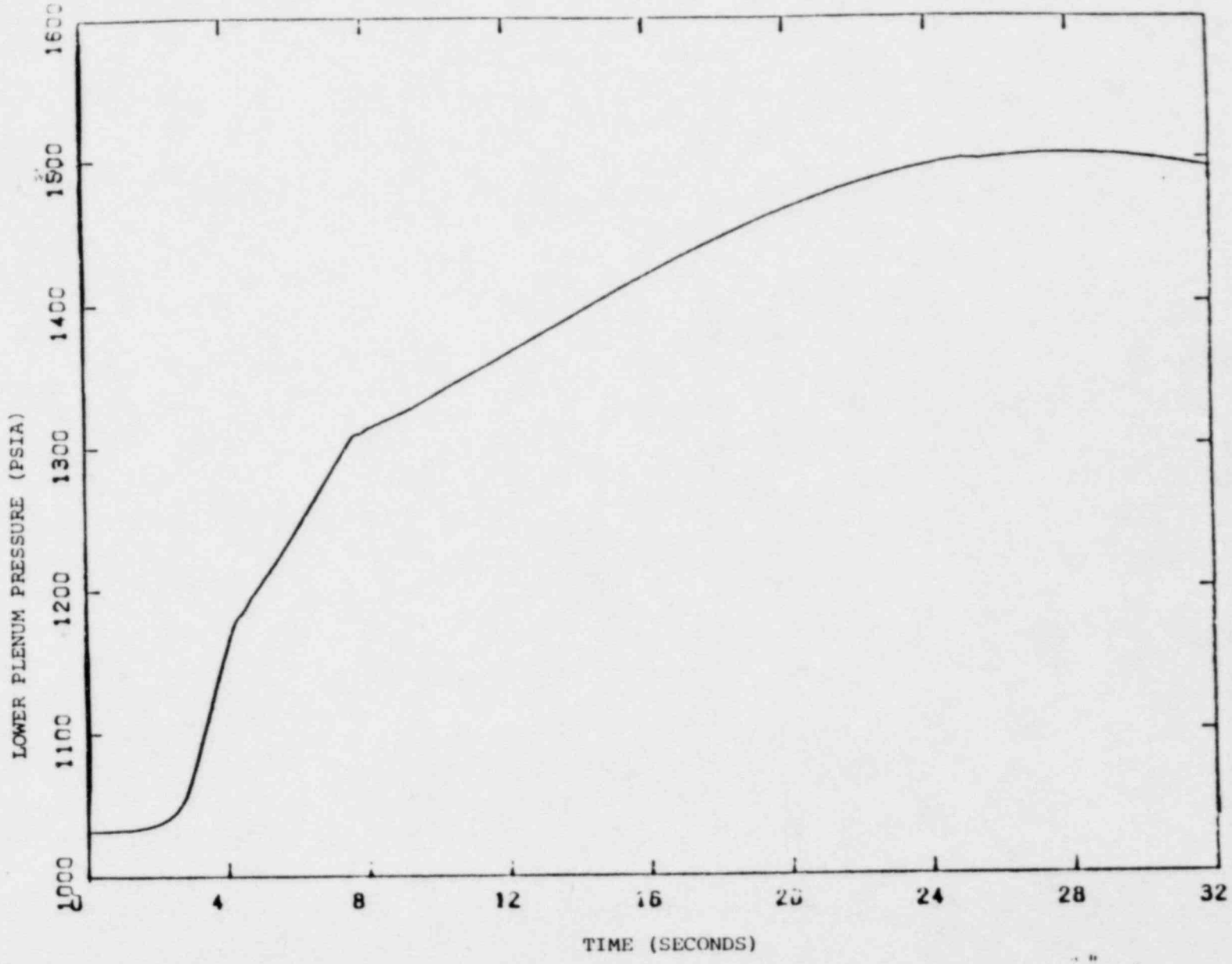

Figure A.7.1
MSIV ATWS, Lower Plenum
Pressure Vs. Time

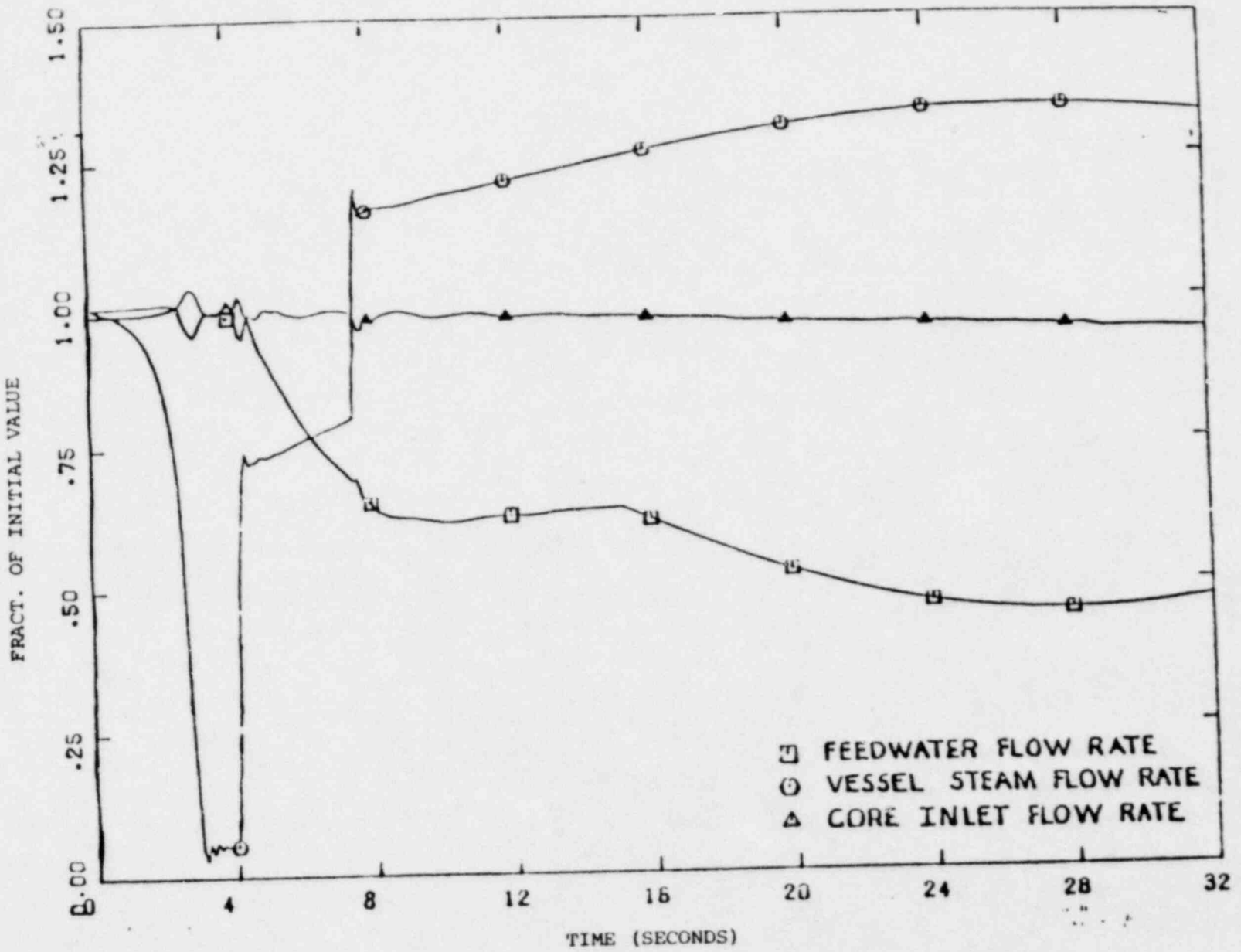

Figure A.7.2
MSIV ATWS, FW, Steam,
and Core Flow Rates Vs. Time

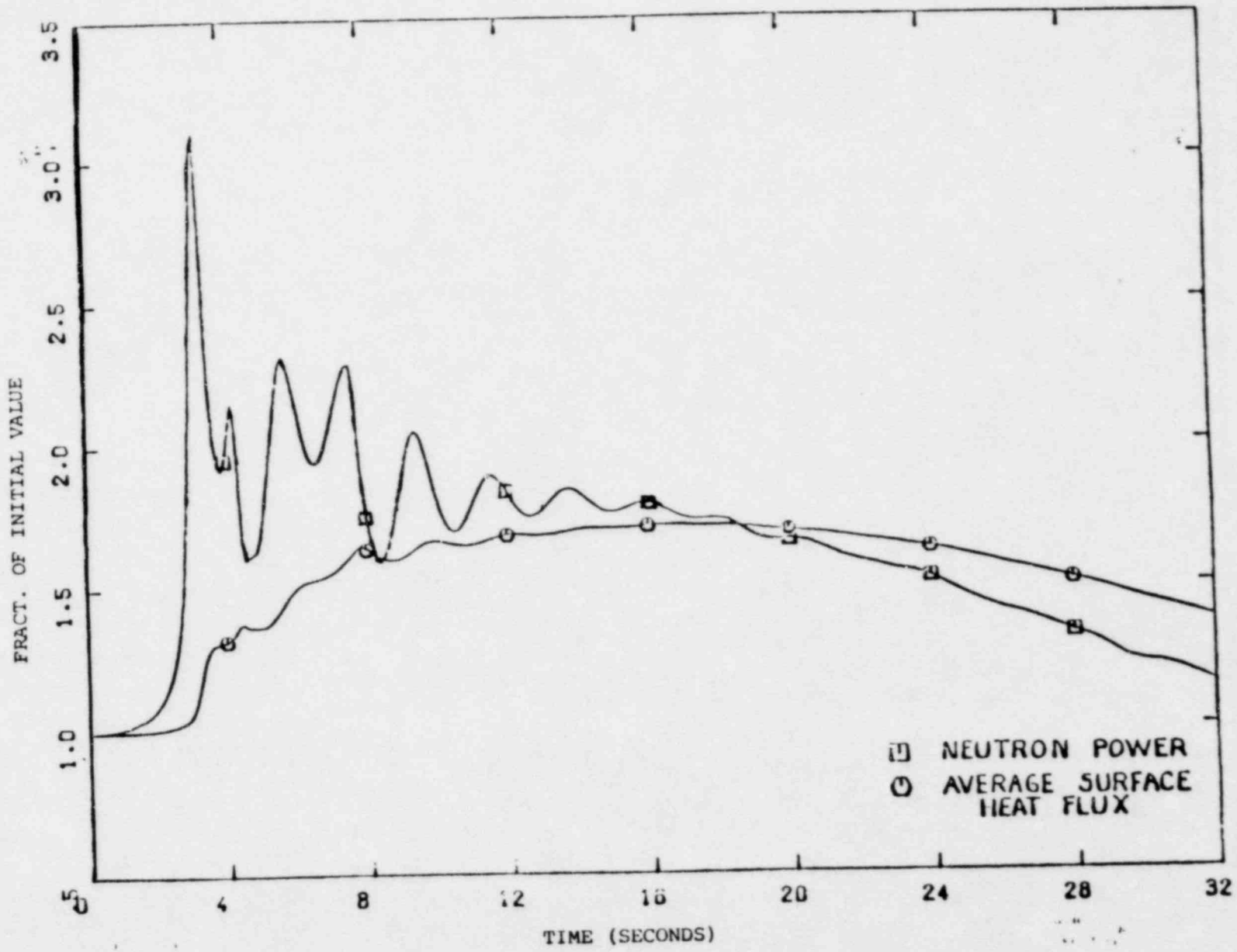

Figure A.7.3
MSIV ATWS, Neutron Power and
Surface Heat Flux Vs. Time

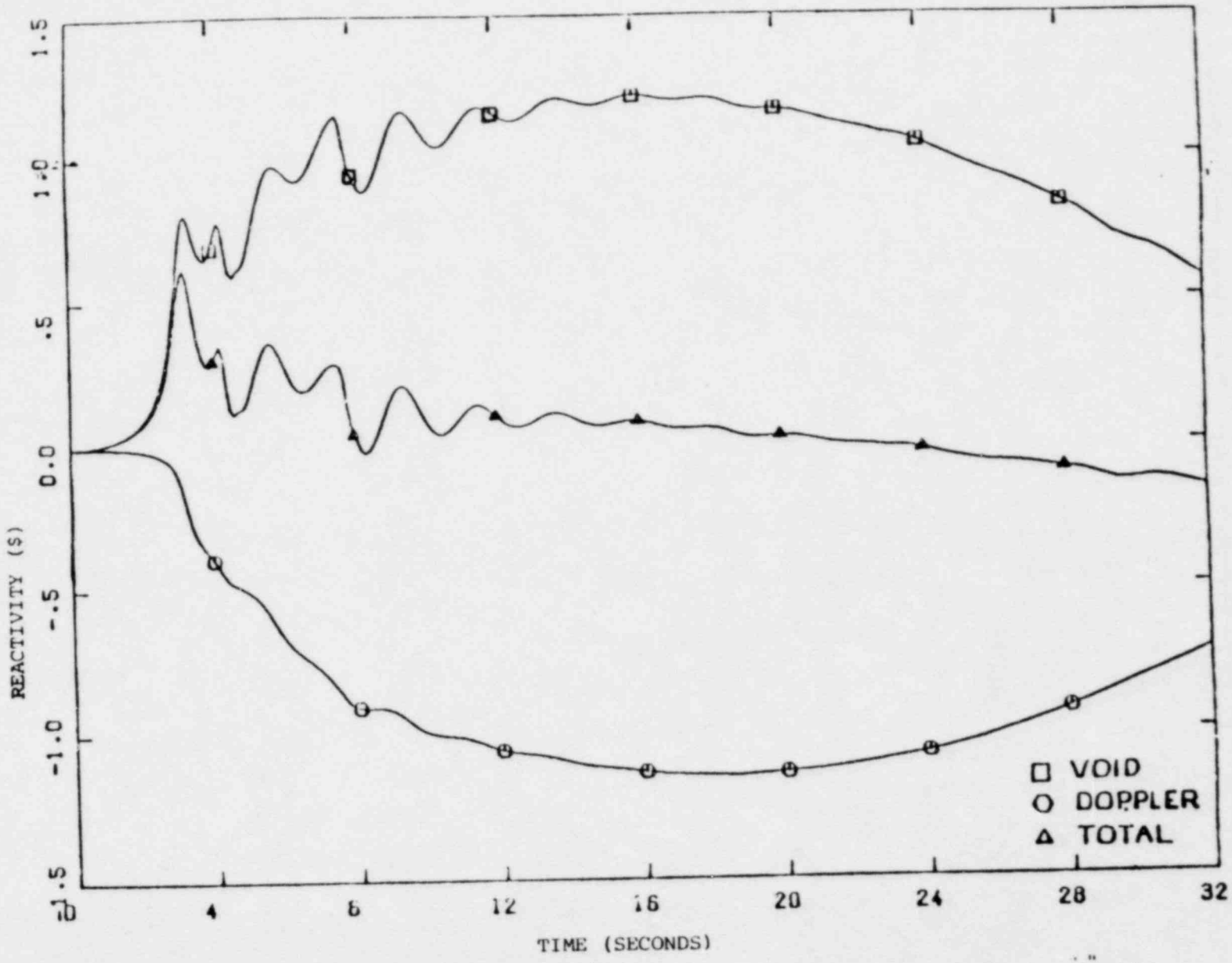

Figure A.7.4
MSIV ATWS, Reactivity
Vs. Time

REFERENCES

1. Vermont Yankee Nuclear Power Corporation, Final Safety Analysis Report, Vermont Yankee Nuclear Power Station.

2. EPRI, RETRAN - A Program for One-Dimensional Transient Thermal-Hydraulic Analysis of Complex Fluid Flow Systems, CCM-5, December 1978.

3. General Electric, Axial-Flow Steam Separator and Dryer Development, 65GL11 (Proprietary), January 15, 1965, General Electric Co., Schenectady, NY.

4. General Electric, Qualification of the One-Dimensional Core Transient Model for Boiling Water Reactors, NEDO-24154, October 1978, General Electric Co., San Jose, CA.

5. Vermont Yankee Nuclear Power Corporation, Appendix A to Operating License DPR-28, Technical Specifications.

6. General Electric, Operations and Maintenance Instructions - Reactor Recirculation System, GEK-9609, June 1971, General Electric Co., San Jose, CA.

7. Vermont Yankee Nuclear Power Corporation, Vermont Yankee Nuclear Power Station Startup Test Report.

8. A. F. Ansari, Methods for the Analysis of Boiling Water Reactors, Steady-State Core Flow Distribution Code (FIBWR), YAEC-1234, December 1980.

9. D. M. VerPlanck, Manual for the Reactor Analysis Program SIMULATE, YAEC-1158, (August 1, 1978).

10. J. M. Holzer, Methods for the Analysis of Boiling Water Reactors, Transient Core Physics, YAEC-1239, April 1981.

11. General Electric, Vermont Yankee Nuclear Power Station Transient Design Analysis, NEDC-10265 (Proprietary), November 1970, General Electric Co., San Jose, CA.

12. General Electric, Vermont Yankee Reload 1 Nuclear Design Report, NEDE-11000 (Proprietary), August 1973, General Electric Co., San Jose, CA.

13. Letter, R. H. Groce (VYNPC) to G. E. Lear (USNRC), "Vermont Yankee Suppression Pool Temperature Transients", WVY 78-53 (June 7, 1978).

14. EPRI, Transient and Stability Tests at Peach Bottom Atomic Power Station Unit 2 at End of Cycle 2, NP-564, June 1978.

15. EPRI, RETRAN Analysis of Turbine Trip Tests at PB2, NP-1076-SR, April 1979.

16. E. E. Pilat, Methods for the Analysis of Boiling Water Reactors, Lattice Physics, YAEC-1232, December 1980.

17. S. P. Schultz and K. E. St. John, Methods for the Analysis of Oxide Fuel Rod Steady-State Thermal Effects (FROSSTEY): Code/Model Description Manual, YAEC-1249, April 1981.